SPECTROSCOPY, PHOTOCHEMISTRY, AND PHOTOINITIATION BEHAVIOR OF GROUP 8 METALLOCENES

by

MATTHEW JAMES MORGAN

(Under the Direction of Charles Kutal)

ABSTRACT

The electronic properties of benzoyl-substituted ferrocenes are influenced by the mixing of appreciable metal-to-ligand charge transfer (MLCT) character into the low-energy excited states of these complexes. Visible light irradiation of benzoyl-substituted ferrocenes in a strongly coordinating solvent causes metal-ring cleavage that produces the benzoylcyclopentadienide anion and a half-sandwich iron (II) cationic complex. The quantum efficiency of photoinduced metal-ring bond cleavage in 1,1'-dibenzoylferrocene (DFc) remains reasonably constant over a range of excitation wavelengths that encompass the two low-energy absorption bands of the complex. This behavior suggests that the initially populated Franck-Condon excited state undergoes very rapid electronic and vibrational relaxation to yield a common thermally equilibrated excited (thexi) state of DFc, from which reaction occurs. Increasing solution temperature does not influence the excited state reactivity. Spectral similarities exist between the benzoyl-substituted ferrocenes and the silicon-bridged [1]ferrocenophanes. Spectroscopic, photochemical, and photoinitiation studies are reported for $Fe(\eta\text{-}C_5H_4)_2(SiR_2)$ ($FcSiR_2$, where R = Me or Ph). The spectral behavior of a $FcSiR_2$ is mainly caused by the ring tilt

and bond angle distortions inherent in the complex rather than the presence of significant MLCT character in the low-energy excited states of the complex. The silicon-bridged [1]ferrocenophanes are very photoreactive in room-temperature methanol with disappearance quantum yields that approach unity. This photochemistry is wavelength dependent as evidenced by the almost 50% decrease in the quantum yield upon irradiation of a $FcSiR_2$ in methanol at 313 nm. Lowering the temperature of solutions of $FcSiR_2$ to 5^oC increases the photoreaction rate. Solvent also influences the photoreaction rate as evidenced by the sharp decrease in the quantum yield upon switching to hexane. Mechanistic studies reveal that the photochemical process occurs via metal-ring cleavage, substantiated by the identification of the free ligand species, $R_2(\eta\text{-}C_5H_4)_2Si$ (R_2SiCp_2, where R = Me or Ph).

INDEX WORDS: Metallocene, ferrocene, 1,1'-dibenzoylferrocene, ferrocenophane, quantum yield, mass spectrometry, photoinitiated polymerization, group transfer polymerization, living ring-opening polymerization

SPECTROSCOPY, PHOTOCHEMISTRY, AND PHOTOINITIATION BEHAVIOR OF GROUP 8 METALLOCENES

by

MATTHEW J. MORGAN

B.S., North Carolina State University, 1997

M.S., Georgia Institute of Technology, 2002

A Dissertation Submitted to the Graduate Faculty of The University of Georgia in Partial Fulfillment of the Requirements for the Degree

DOCTOR OF PHILOSOPHY

ATHENS, GEORGIA

2008

© 2008

Matthew J. Morgan

All Rights Reserved

SPECTROSCOPY, PHOTOCHEMISTRY, AND PHOTOINITIATION BEHAVIOR OF GROUP 8 METALLOCENES

by

MATTHEW J. MORGAN

Major Professor: Charles Kutal

Committee: Michael K. Johnson
Richard A. Dluhy

Electronic Version Approved:

Maureen Grasso
Dean of the Graduate School
The University of Georgia
December 2008

ACKNOWLEDGEMENTS

Many thanks go out to my adviser, Dr. Charles Kutal. Not only was Dr. Kutal a source of financial support, but he also wrote me letters of recommendation that helped me win an American Chemical Society travel award and a Graduate School Teaching Portfolio Certificate. I also benefited greatly from his teaching style and his professionalism.

Many people in the University of Georgia Chemistry Department helped me with my research and my professional career. Dr. Bobby Stanton, while being an excellent lab coordinator to work for, also wrote me letters of recommendation. Dr. Gregory Robinson and his group (especially Dr. Brandon Quillian and Dr. Yuzhong Wang) taught me synthesis techniques and gave me some distilled solvents for use in my experiments. Dr. Dennis Phillips and Dr. Tracy Andacht ran numerous mass spectrometry samples for me. Dr. Greg Wylie ran numerous NMR samples for me, taught me how to use the Varian 500 MHz NMR instrument, and helped me to clarify some data. Dr. Robbie Phillips also helped me to clarify some NMR data. Dr. Richard Dluhy and his group loaned me parts and let me use their computer software. Dr. James de Haseth and his group (Dr. Brian Loudermilk) also let me use their computer software. Yebin Zhao taught me to use MestReC. Dr. Todd Harrop and his group allowed me to use the Cary 50 Bio spectrophotometer, loaned me glassware, and gave me distilled solvents for use in my experiments. Dr. Jon Amster and his group helped

me to interpret mass spectrometry data and to troubleshoot faulty equipment. Ronnie Claxton helped me to prepare for experiments.

Also, thanks to Dr. Cindy Sanderson, Michelle Borden, Jessica Quinlan, and Jennifer Sinclair for nice friendships. Cecilia Ieong, a doctoral student in Professor Ian Manners' group at the University of Bristol (UK), synthesized and prepared 2.5 g of diphenylsila[1]ferrocenophane for me to use in my experiments. Cecilia also helped me to clarify some of my data through email correspondence.

Thank you.

TABLE OF CONTENTS

Page

ACKNOWLEDGEMENTS iv

LIST OF TABLES viii

LIST OF FIGURES ix

CHAPTER

1 INTRODUCTION 1

Unsubstituted group 8 metallocenes 1

Benzoyl-substituted ferrocenes 10

[1]ferrocenophanes 18

Anionic polymerization using group 8 metallocene photoinitiators 22

Group transfer polymerization of methyl methacrylate 24

Project goals 29

2 EXPERIMENTAL 32

Materials 32

Synthesis of dimethylsila[1]ferrocenophane 33

Instrumentation 36

Group transfer polymerization procedures 38

Photochemical procedures 38

NMR procedures 39

3 SPECTROSCOPY AND PHOTOCHEMISTRY OF 1,1'-DIBENZOYL-FERROCENE 41
4 SPECTROSCOPY AND PHOTOCHEMISTRY OF DIMETHYLSILA[1]-FERROCENOPHANE 51
Electronic structure 51
Thermal chemistry of dimethylsila[1]ferrocenophane in methanol 58
Photochemistry of dimethylsila[1]ferrocenophane 66
Photochemical mechanism of dimethylsila[1]ferrocenophane 73
5 SPECTROSCOPY AND PHOTOCHEMISTRY OF DIPHENYLSILA[1]-FERROCENOPHANE 84
Electronic structure 84
Thermal chemistry of diphenylsila[1]ferrocenophane 87
Photochemistry of diphenylsila[1]ferrocenophane 95
Photochemical mechanism of diphenylsila[1]ferrocenophane 106
6 GROUP TRANSFER POLYMERIZATION OF METHYL METHACRYLATE 117
7 CONCLUSIONS 123
REFERENCES 129

LIST OF TABLES

Page

Table 1: Disappearance quantum yield data 49

Table 2: Electronic absorption spectral data for $FcSiMe_2$ 59

Table 3: Thermal proton NMR spectral data for $FcSiMe_2$ in methanol-d_4 60

Table 4: Disappearance quantum yield data for $FcSiMe_2$ 69

Table 5: Chemical shifts in proton NMR spectra of Me_2SiCp_2 77

Table 6: Electronic absorption spectral data for $FcSiPh_2$ 88

Table 7: Thermal proton NMR spectral data for $FcSiPh_2$ in methanol-d_4 89

Table 8: Disappearance quantum yield data for $FcSiPh_2$ 102

Table 9: Chemical shifts in proton NMR spectra of irradiated solutions of $FcSiPh_2$ in methanol-d_4 and acetonitrile-d_3 113

LIST OF FIGURES

Page

Figure 1: Structures of group 8 metallocenes 3

Figure 2: A qualitative molecular orbital diagram for Fc 5

Figure 3: Electronic absorption spectrum of Fc and Rc in room-temperature methanol 8

Figure 4: Electronic absorption spectra of Fc, BFc, and DFc in room-temperature methanol 12

Figure 5: A resonance structure showing the MLCT character of the low-energy excited states of DFc 14

Figure 6: Solid state, low-temperature (17K) Raman spectra of BFc using 488-, 568-, and 647-nm excitation 16

Figure 7: The two main mechanistic pathways for group transfer polymerization 27

Figure 8: Electrospray ionization mass spectrum of a photolyzed solution of DFc in acetonitrile 43

Figure 9: UV-vis spectral changes arising from the 488-nm irradiation of DFc in deoxygenated methanol 46

Figure 10: UV-vis spectral changes arising from the 488-nm irradiation of DFc in deoxygenated cyclohexane 48

Figure 11: Distortions in [1]ferrocenophanes defining angles α, β, δ, and θ 53

Figure 12: Electronic absorption spectrum of Fc and $FcSiMe_2$ in room-temperature methanol 55
Figure 13: Extended Hückel molecular orbital diagram comparison of eclipsed Fc and $FcSiH_2$ 57
Figure 14: Thermal proton NMR spectral data for $FcSiMe_2$ in methanol-d_4 63
Figure 15: UV-vis spectral changes arising from the thermal reaction of $FcSiMe_2$ in room-temperature methanol 65
Figure 16: UV-vis spectral changes arising from the 488-nm irradiation of $FcSiMe_2$ in room-temperature methanol 68
Figure 17: UV-vis spectral changes arising from the room- and low-temperature 488-nm irradiation of $FcSiMe_2$ in acetonitrile 71
Figure 18: UV-vis spectral changes arising from the 488-nm irradiation of $FcSiMe_2$ in THF and hexane 75
Figure 19: Proton NMR spectra resulting from the irradiation of $FcSiMe_2$ in methanol-d_4 and acetonitrile-d_3 79
Figure 20: Tautomers of Me_2SiCp_2 generated photochemically via Fe-Cp bond cleavage of $FcSiMe_2$ 82
Figure 21: Electronic absorption spectrum of Fc and $FcSiPh_2$ in room-temperature methanol 86
Figure 22: Thermal proton NMR spectral data for $FcSiPh_2$ in methanol-d_4 92
Figure 23: UV-vis spectral changes arising from the thermal reaction of $FcSiPh_2$ in room-temperature methanol 94

Figure 24: Mass spectrum of a solution of $FcSiPh_2$ and the ring-opened, thermal product in room-temperature methanol 97

Figure 25: UV-vis spectral changes arising from the thermal reaction of $FcSiPh_2$ in acetonitrile and THF 99

Figure 26: UV-vis spectral changes arising from the 488- and 313-nm irradiation of $FcSiPh_2$ in room-temperature methanol 101

Figure 27: UV-vis spectral changes arising from the room- and low-temperature 488-nm irradiation of $FcSiPh_2$ in THF 105

Figure 28: Proton NMR spectral data for $FcSiPh_2$ in benzene-d_6 108

Figure 29: Proton NMR spectra resulting from the irradiation of $FcSiPh_2$ in methanol-d_4 and acetonitrile-d_3 110

Figure 30: A portion of the mass spectrum of a filtered solution of $FcSiPh_2$ irradiated at 488 nm in room-temperature methanol and acetonitrile 115

Figure 31: The thermal GTP of MMA in pure THF and in THF/acetonitrile mixtures ... 119

Figure 32: The photochemical GTP of MMA in glyme versus a dark, control reaction 122

Figure 33: Two possible scenarios to explain the wavelength dependence of solutions of silicon-bridged [1]ferrocenophanes 126

CHAPTER 1

INTRODUCTION

Unsubstituted group 8 metallocenes

Ferrocene

Ferrocene (Fc in Figure 1) is a “sandwich” compound with D_{5d} symmetry at its energy minimum, in which the two cyclopentadienyl (Cp) rings are staggered with respect to each other. The energy difference[1] between the staggered and eclipsed rotational conformations in ferrocene is about 2 kcal/mol, with an energy barrier[2] of only 2-5 kcal/mol. For the molecular orbital description of the Fc molecule, there are three sets of ligand π orbitals: a low-lying filled pair of a_{1g} and a_{2u} symmetry; a filled set of e_{1g} and e_{1u} symmetry; and an unfilled set of anti-bonding orbitals of e_{2g} and e_{2u} symmetry at higher energy.[3] Figure 2 shows a qualitative molecular orbital diagram for Fc with D_{5d} symmetry.[3,4] The best orbital interaction occurs between the ligand e_{1g} orbitals and the iron (Fe) $3d_{xz}$ and $3d_{yz}$ orbitals, creating two strong π bonds. The corresponding $2e^*_{1g}$ antibonding molecular orbitals are unoccupied and mainly metal in character. The remaining Fe *d* orbitals (d_z^2, $d_{x^2-y^2}$, d_{xy}) are essentially nonbonding: the ligand a_{1g} orbitals point toward the nodal cone of the metal $3d_z^2$ orbital, while poor δ-type overlap exists between the ligand e_{2g} orbitals and the metal e_{2g} set.[3] The resulting molecular orbitals ($2a_{1g}$ and $1e_{2g}$, respectively) are mainly metal in character. Because the $2e^*_{1g}$, $2a_{1g}$, and $1e_{2g}$ molecular orbitals are mainly metal in character, ligand field theory can be used to model the low-lying electronic transitions of Fc.[5,6] Referring to Figure 2, the

Figure 1

Structures of group 8 metallocenes.

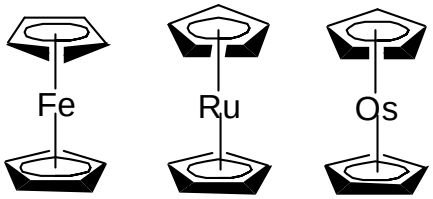

Fc Rc Oc

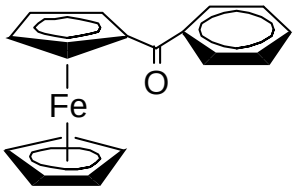

BFc

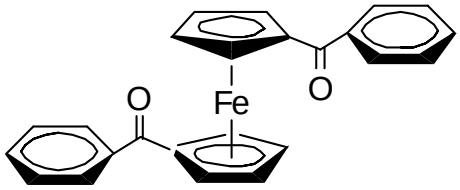

DFc

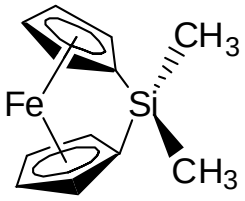

$FcSiMe_2$

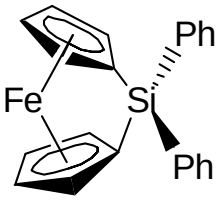

$FcSiPh_2$

FcS

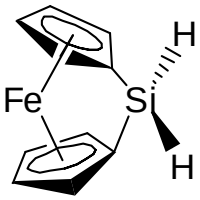

$FcSiH_2$

Ph = C_6H_5

Figure 2

A qualitative molecular orbital diagram for Fc. Reproduced from Ref. (3) and Ref. (4). Copyright 1998 Blackwell Science and copyright 1997 American Chemical Society, respectively.

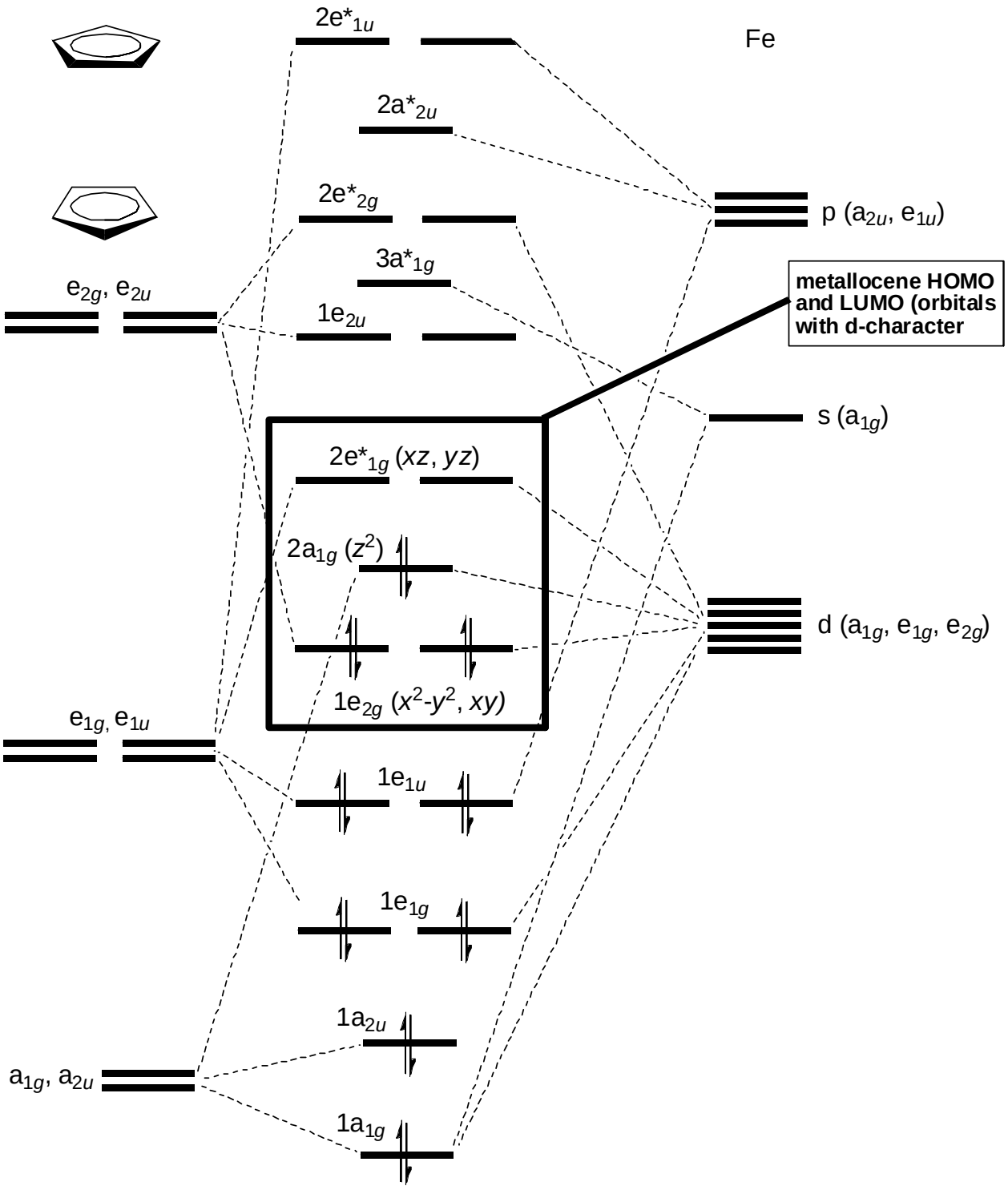
2e*1u
Fe
2a*2u
2e*2g
p (a2u, e1u)
3a*1g
e2g, e2u
1e2u
metallocene HOMO and LUMO (orbitals with d-character
s (a1g)
2e*1g (xz, yz)
2a1g (z2)
d (a1g, e1g, e2g)
1e2g (x2-y2, xy)
e1g, e1u
1e1u
1e1g
1a2u
a1g, a2u
1a1g

d-orbital electronic configuration of Fc is $(1e_{2g})^4(2a_{1g})^2(2e^*_{1g})^0$, from which the $^1A_{1g}$ ground state arises. Photoexcitation of a $2a_{1g}$ electron to the empty $2e^*_{1g}$ orbitals produces an E_{1g} excited state, while E_{2g} and E_{1g} excited states result from the photoexcitation of a $1e_{2g}$ electron to the $2e^*_{1g}$ orbitals. The $^1A_{1g} \longrightarrow a^1E_{1g}$ and the $^1A_{1g} \longrightarrow {}^1E_{2g}$ spin-allowed transitions are unresolved and are responsible for the broad band at 442 nm in the electronic absorption band of Fc in room-temperature methanol (Fc in Figure 3). The $^1A_{1g} \longrightarrow b^1E_{1g}$ spin-allowed transition is responsible for the band at 326 nm. Since these *d*-*d* transitions are Laporte forbidden, the extinction coefficients are relatively low. Also, these transitions involve an angular redistribution of electron density centered on the metal rather than a vectorial displacement of charge between the metal and ligands, so the bands undergo only minor shifts in energy as a function of solvent polarity.[7] Although there are several potentially reactive ligand field and other charge transfer excited states in Fc, it undergoes no photoinduced metal-ring bond cleavage or redox processes in non-halogenated solvents such as cyclohexane, acetone, and methanol.[8] However, Fc can form a photoreactive ground-state donor-acceptor complex with a good electron-accepting solvent such as a halogenated hydrocarbon[9] or ethyl 2-cyanoacrylate[10] (CA). Irradiating the complex causes the one-electron oxidation of Fc to the ferricinium cation and reduction of the solvent to its corresponding radical anion (Equation 1).[10]

$$\mathrm{Fc} + \mathrm{CA} \rightleftharpoons \underset{\text{donor-acceptor complex}}{[\mathrm{Fc, CA}]} \xrightarrow{h\nu} \mathrm{Fc}^+ + \mathrm{CA}^{\bullet -} \qquad (1)$$

Figure 3

Electronic absorption spectra of Fc and Rc in room-temperature methanol.

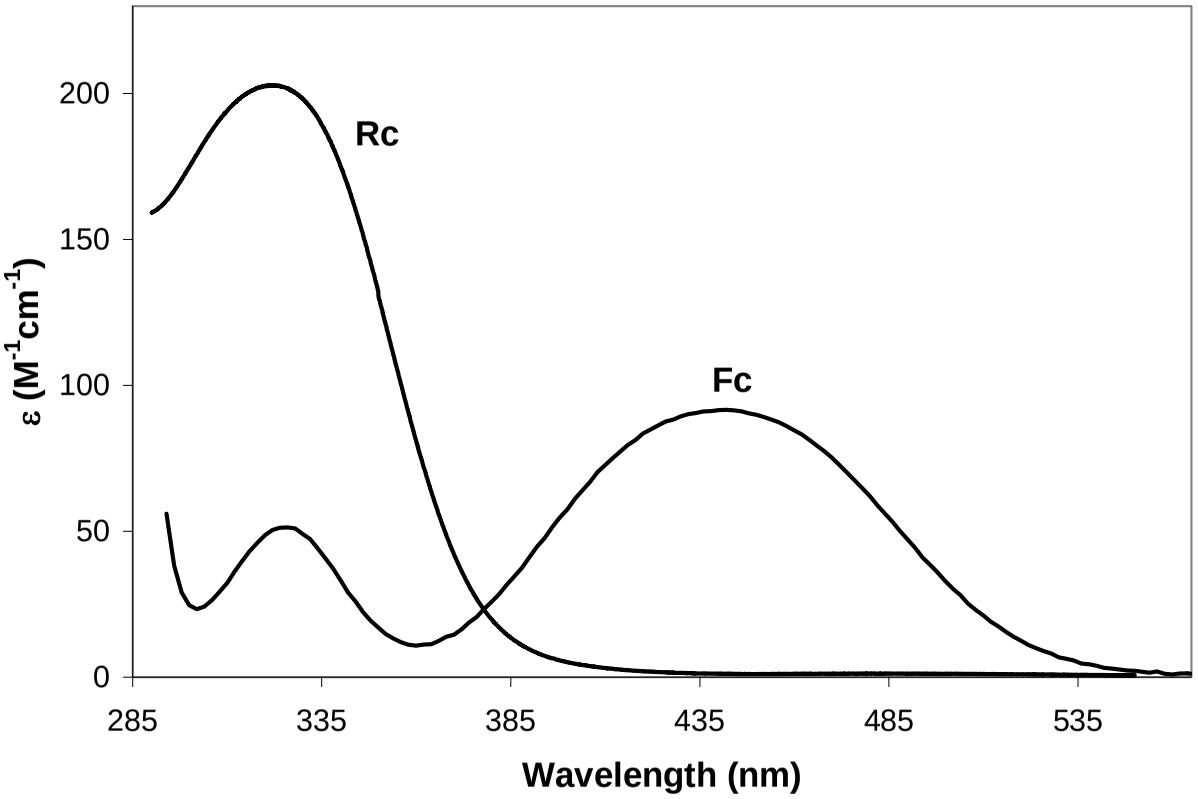
200
150
100
50
0
ε (M-1cm-1)
Rc
Fc
285
335
385
435
485
535
Wavelength (nm)

Ruthenocene and Osmocene

Ruthenocene (Rc in Figure 1) is a “sandwich” compound with D_{5h} symmetry, in which the two Cp rings are eclipsed with respect to each other. Referring to Figure 2 and applying the same analysis to Rc, the *d*-orbital electronic configuration of Rc is $(1e_2')^4(2a_1')^2(2e^*_1')^0$, from which the $^1A_1'$ ground state arises. Photoexcitation of a $2a_1'$ electron to the empty $2e^*_1'$ orbitals produces an E_1' excited state, while E_2' and E_1' excited states result from the photoexcitation of a $1e_2'$ electron to the $2e^*_1'$ orbitals. The $^1A_1' \longrightarrow a^1E_1'$ and the $^1A_1' \longrightarrow {}^1E_2'$ ligand field, spin-allowed transitions overlap and are responsible for the band at 321 nm in the electronic absorption band of Rc in room-temperature methanol (Rc in Figure 3). Like Fc, Rc undergoes no photoinduced metal-ring bond cleavage or redox processes in non-halogenated solvents, but it can form a photoreactive ground-state donor-acceptor complex with CA.[10] Irradiation of the complex causes the one-electron oxidation of Rc to the ruthenicinium cation and reduction of the solvent to its corresponding radical anion.

Osmocene (Oc in Figure 1) has a similar crystal structure to Rc. In the electronic absorption spectrum of Oc, ligand field, spin-allowed electronic transitions are responsible for two shoulders at 310 nm and 280 nm. Another *d-d* transition, appearing as a shoulder at 251 nm, is overlapped by a charge-transfer band at 243 nm. Like Fc and Rc, Oc undergoes no photoinduced metal-ring bond cleavage or redox processes in non-halogenated solvents. However, recent work has demonstrated that it can form a photoreactive ground-state donor-acceptor complex with carbon tetrachloride (CCl_4).[11] Irradiation of the complex causes the one-electron oxidation of Oc to the osmocinium cation and reduction of the solvent to its corresponding radical anion.

Benzoyl-substituted ferrocenes

The addition of electron-withdrawing benzoyl groups to one or both rings of Fc causes a significant perturbation of electronic properties.[4,8,12] Figure 4 shows the effects of this perturbation in the electronic absorption spectra of Fc vs. benzoylferrocene (BFc in Figure 1) vs. 1,1'-dibenzoylferrocene (DFc in Figure 1). Placing a benzoyl group onto one or both rings of Fc induces a sharp increase in intensity of both the high- and low-energy absorption bands of the benzoyl complexes. These bands also shift to lower energy and become solvent sensitive. As the polarity of the solvent increases, the bands become more red-shifted. This spectral behavior has been attributed to the mixing of appreciable metal-to-ligand charge transfer (MLCT) character into the low-energy excited states of the benzoyl complexes.[7] Figure 5 shows a resonance structure which depicts the MLCT in DFc. The formal charges on the iron and oxygen indicate the vectorial movement of electron density from the metal to the ligand. Conjugation between the π orbitals of the cyclopentadienyl and phenyl rings and the adjacent carbonyl group allows the transferred charge to be delocalized over several atoms, thus stabilizing the MLCT excited state relative to the ground state and lowering the transition energy.[13] The charge transfer results in a more dipolar complex that is stabilized in polar solvents, additionally lowering the transition energy. Resonance Raman spectroscopy data also confirm the presence of MLCT character in the benzoyl complexes, as shown in the low-temperature solid-state Raman spectra of BFc in Figure 6 (similar results are obtained for DFc).[12] The band intensities measured at each excitation have been normalized relative to the non-resonantly enhanced band of the sulfate ion at 985 cm^{-1}. The resonant enhancement is most pronounced for vibrations

Figure 4

Electronic absorption spectra of Fc, BFc, and DFc in room-temperature methanol.

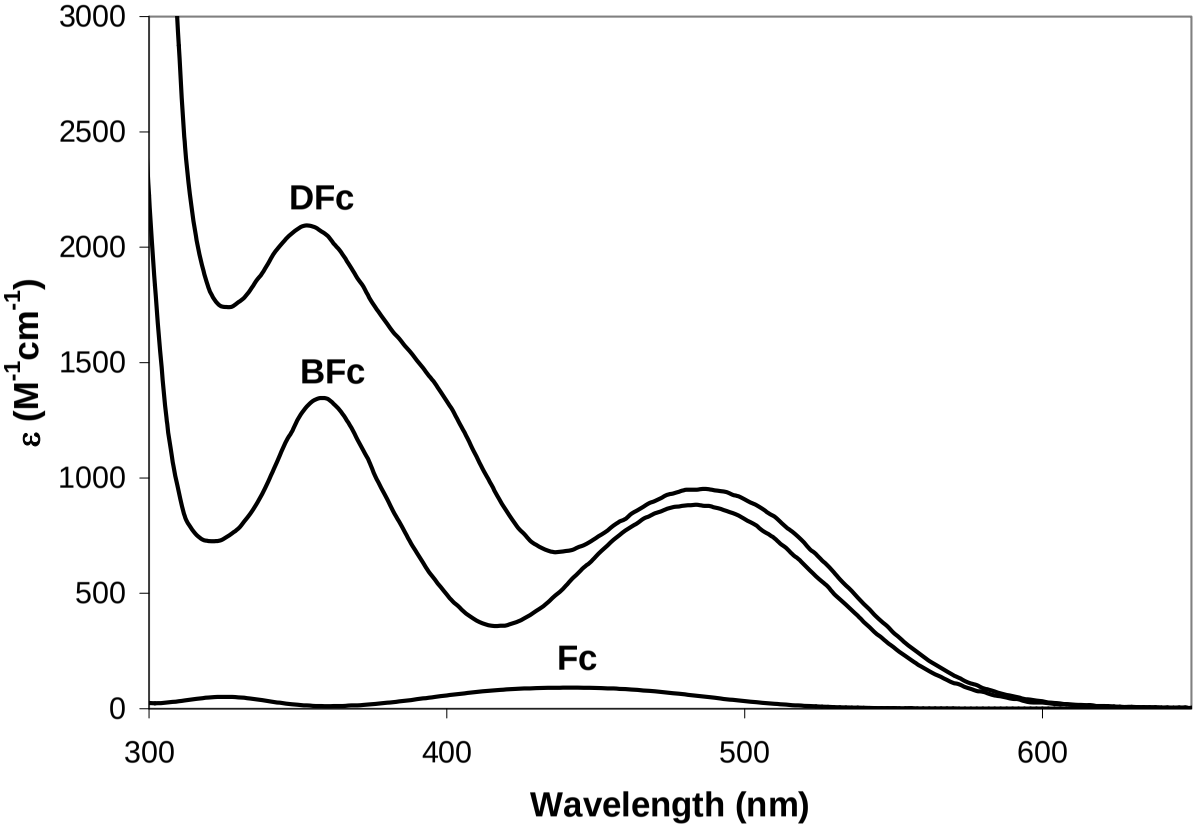
3000
2500
2000
1500
1000
500
0
ε (M-1cm-1)
DFc
BFc
Fc
300
400
500
600
Wavelength (nm)

Figure 5

A resonance structure showing the MLCT character of the low-energy excited states of DFc.

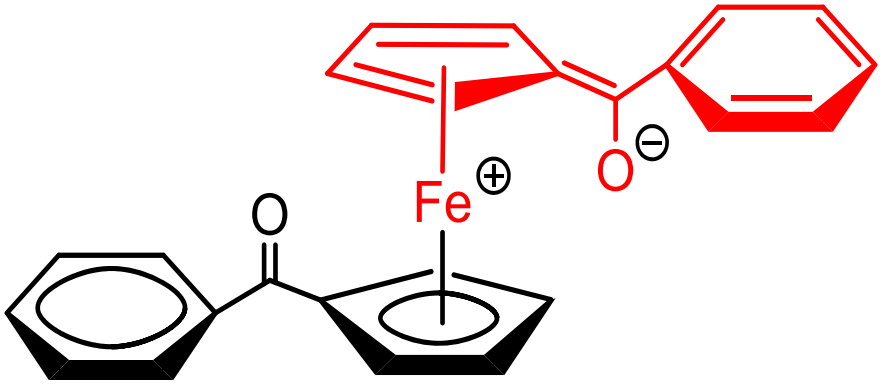
O
Fe
O

Figure 6

Solid state, low-temperature (17K) Raman spectra of BFc using 488-, 568-, and 647-nm excitation. The Raman intensities at each excitation wavelength have been normalized to the intensity of the sulfate band at 985 cm^{-1} (marked with an asterisk). Reproduced from Ref. (12). Copyright 2003 American Chemical Society.

Raman Intensity
Raman Shift (cm-1)
1000
1200
1400
1600
1800
647 nm
568 nm
488 nm
985*
1000
1028
1059
1105
1167
1176
1440
1579
1598
1624

that mimic the distortion in the electronic excited state populated.[14] Preresonance excitation at 647 nm produces two dominant bands. The 1624 cm^{-1} band corresponds to the υ(C-O) stretching mode of the benzoyl- cyclopentadienyl ligand, and the 1105 cm-1 band corresponds to the υ(C-C) symmetric breathing mode of the unsubstituted cyclopentadienyl ring.[7] Excitation at 568 nm into the tail of the low-energy absorption band of BFc and DFc selectively enhances the Raman band at 1624 cm^{-1}, while no resonant enhancement occurs for the Raman band at 1105 cm^{-1}.[7] The evidence indicates that the C-O bond becomes longer and weaker, and then the υ(C-O) stretching mode becomes more intense in the Resonance Raman spectrum, as expected upon populating an excited state containing appreciable MLCT character. Excitation at 488 nm into the low-energy band maximum of BFc or DFc causes extensive sample decomposition as evidenced by the substantially lower intensities of all Raman bands relative to the standard.[7] The evidence here of photoreactivity was another consequence of mixing MLCT character into the low-energy excited states of benzoyl-substituted ferrocenes.[4,12] Figure 5 shows that upon irradiation, the iron-cyclopentadienide (Fe-Cp) bond weakens and the iron atom becomes more electrophilic. This renders the iron atom more subject to attack by a solvent ligand as the hapticity of a Cp ring decreases from η^5 to η^4.

The solution photochemistry of benzoyl-substituted ferrocenes has been investigated in considerable detail.[4,12] Irradiation of DFc in strongly coordinating solvents weakens the metal-ring bond, and the solvent coordinates to the electrophilic iron atom to produce a solvated half-sandwich complex (Equation 2). In the process, a

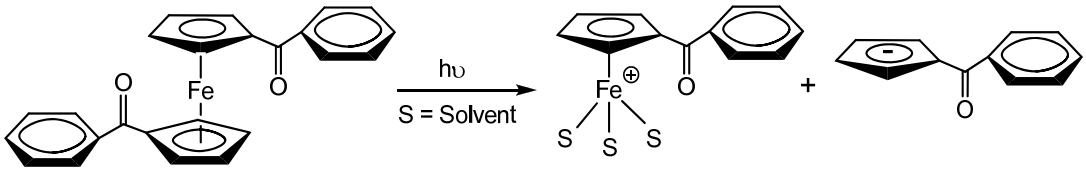

reactive benzoylcyclopentadienide anion is released. Yamaguchi and Kutal, as well as Ding, Sanderson et al. suggested that the photoinduced loss of this reactive anion proceeds via a succession of ring-slipped intermediates such as the η^5, η^3 complex shown in Equation 3.[4,12] Upon irradiation, the solvent attacks the electrophilic metal

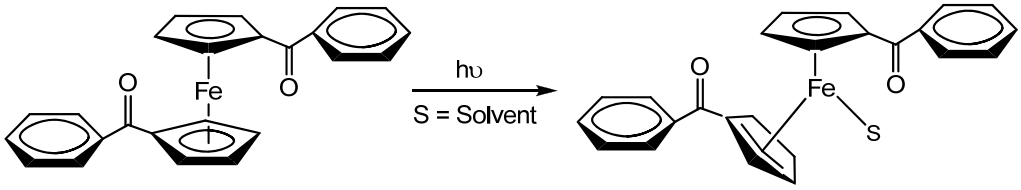

center in the excited state and partially displaces a Cp ring. The η^5, η^3 intermediate can then either react further with solvent to produce the half-sandwich product, or it can expel the coordinated solvent to regenerate the parent complex.

[1]Ferrocenophanes

Osborne and Whiteley prepared the first examples of [1]ferrocenophanes in 1975.[15] These [1]ferrocenophanes contain silicon as the bridging atom (refer to $FcSiMe_2$ and $FcSiPh_2$ in Figure 1), and the ^1H NMR spectra of the Fc groups consist of two well-separated unsymmetrical triplets and are solvent dependent. This spectral feature has been shown to be characteristic of ring-tilted ferrocenes.[16] The tilt angle (α) created by the planes of the two Cp rings in a ferrocenophane represents a convenient qualitative measure of the degree of strain present.[17] One of the most important factors that govern

α, and hence the reactivity of [1]ferrocenophanes, is the identity of the bridging atom E.[18] Upon reduction of the covalent radius of the bridging element, [1]ferrocenophanes exhibit increased strain, with larger tilt-angles and an increased bathochromic shift and intensity for the longest wavelength electronic transition in the electronic absorption spectrum.[17] These spectral features are caused by a decreased HOMO-LUMO gap and to some extent by increased ligand character in the LUMO as α increases.[17,19-21] The inherent ring strain in [1]ferrocenophanes allows them to undergo ring opening reactions. Sila[1]ferrocenophanes ($FcSiR_2$, where R = Me or Ph) undergo thermal[22,23], anionic[24], or transition metal catalyzed[25,26] ring-opening polymerization (ROP) to give polyferrocenylsilanes (PFS) through cleavage of the *ipso*-Cp-Si bond.[18]

Most of the previous studies on [1]ferrocenophanes have shown that they undergo ROP at the bridging atom E-Cp bond.[18] However, more recent reports on [1]ferrocenophanes have shown that they may also undergo ROP at the Fe-Cp bond upon photolysis. For example, Tanabe and Manners first reported the photolytic living anionic ROP of dimethylsila[1]ferrocenophane ($FcSiMe_2$ in Figure 1), wherein initiation occurs by irradiation of $FcSiMe_2$ in the presence of an anionic initiator, sodium cyclopentadienide ($Na[C_5H_5]$), in tetrahydrofuran (THF) with ultraviolet and visible (UV-vis) light (Equation 4).[27] These workers proposed that irradiation weakens the Fe-Cp

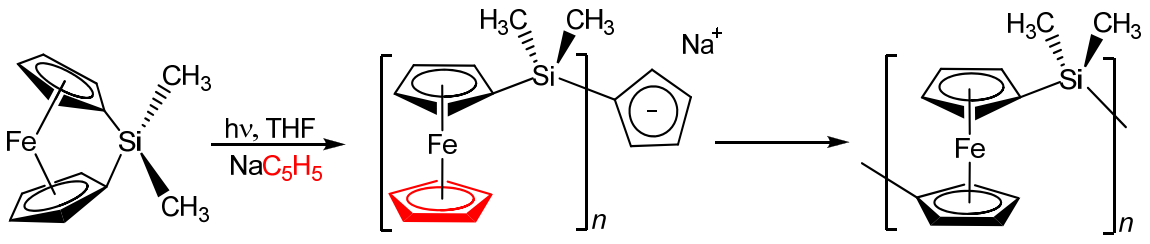

(4)

bond in the monomer, which allows attack on the iron atom by the cyclopentadienide initiator to first form the dangling silyl-substituted cyclopentadienide anion. The dangling anion then undergoes chain propagation in the presence of more photoexcited monomer (M* in Equation 5).[27,28] This method not only provides a new

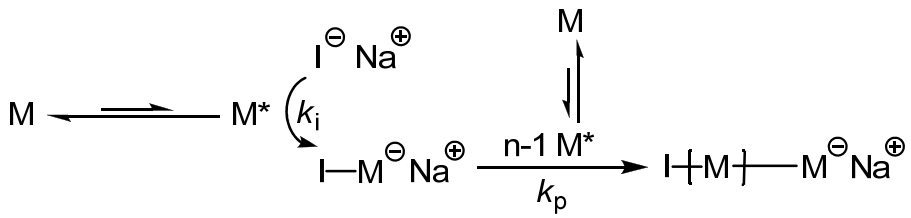

(5)

concept for living provides a new concept for living anionic polymerization but also offers opportunities to synthesize PFS block copolymers under mild conditions.[29]

Recently, Tanabe, Vandermeulen et al. prepared a highly metallized polyferrocenylsilane block copolymer using the photolytic living ROP technique.[28] An acetylide functionalized monomer was successfully polymerized sequentially with $FcSiMe_2$. First, irradiation of a mixture of the acetylide functionalized monomer and $Na[C_5H_5]$ in THF with light formed a dangling silyl-substituted cyclopentadienide anion with acetylide side chains. When the light was switched off, $FcSiMe_2$ was added, and then the solution was irradiated further for approximately 2 hours. When the light was switched off, the living polymerization was capped with methanol. The pendant acetylide groups on the isolated copolymer acetylidePFS-*b*-PFS were then transformed into nickel-based clusters with $[\{NiCp(CO)_{12}\}_2]$ to yield the highly metallized block copolymer NiPFS-*b*-PFS. Preliminary investigations showed that this air stable block copolymer can self-assemble in the bulk solid state into phase separated nanodomains of NiPFS and iron-only PFS.[29] One potential application for block copolymer self-assembly is in

microelectronics. Moore's Law predicts that the number of transistors on integrated circuits will double every two years. Until now, standard photolithography has been sufficient to supply the need for tinier transistors. But it has become more expensive to manufacture sub-30-nm features. Block copolymer lithography has the potential to reduce feature size below 10 nm by taking advantage of spontaneous self-assembly processes to create arrays of molecular-scale features whose size is dictated by the chemistry of block copolymers.[30]

Recently, Ieong, Chan et al. performed a series of photochemical studies on diphenylsila[1]ferrocenophane ($FcSiPh_2$ in Figure 1) and thia[1]ferrocenophane (FcS in Figure 1) in the presence of metal carbonyls ($[Fe(CO)_5]$, $[Fe_2(CO)_9]$, and $[Co_2(CO)_8]$) as co-reactants.[31] In one reaction, $FcSiPh_2$ was reacted with excess $[Fe(CO)_5]$ under UV irradiation ($\lambda > 310$ nm) in THF to give the new dinuclear complex $[Fe_2(CO)_2(\mu\text{-}CO)_2(\eta\text{-}C_5H_4)_2SiPh_2]$ (Equation 6). Control reactions in the dark were also performed and gave

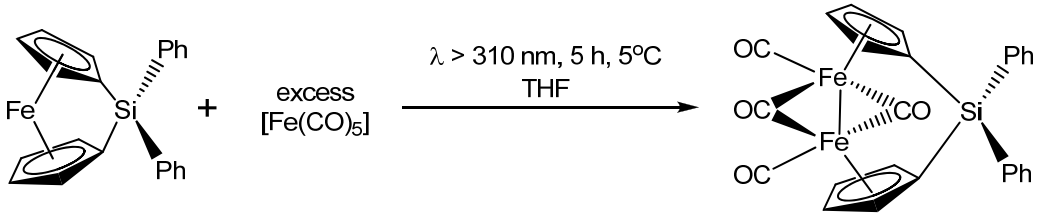

(6)

no detectable reaction after 5 h. This work shows that $FcSiPh_2$ can undergo insertions and cleavage reactions at the Fe-Cp bond upon irradiative weakening.[31] This weakening was sufficient to also cause oligomerization of FcS; however, the less strained $FcSiPh_2$ was resistant to this process. In addition, these workers also reported that FcS underwent insertion reactions with $[Fe_2(CO)_9]$ and $[Co_2(CO)_8]$ in the absence of light, but at a significantly slower rate. $FcSiPh_2$ did not undergo reaction in the absence

of light. Therefore, while photochemical activation of the Fe-Cp bond is observed for both $FcSiPh_2$ and FcS, the inherent ring strain in FcS alone is sufficient for reactions to occur, although at a significantly slower rate. These workers also reported that the photochemical rate is solvent dependent.

Anionic polymerization using group 8 metallocene photoinitiators

Our research group has studied the spectroscopy and photochemistry of Fc, Rc, and their benzoyl-substituted derivatives not only because of their interesting physical properties, but also because of their potential role as anionic photoinitiators.[32,33] Group 8 metallocenes have several attractive properties that make them suitable photoinitiators such as excellent thermal stability, absorption in the UV-vis region, and solubility in a broad range of nonaqueous solvents. Also, earlier studies indicated that these compounds undergo photochemical reactions that release anionic species.[34]

Kutal, Grutsch et al. demonstrated the first example of photoinitiated anionic polymerization in 1991.[35] They showed that a photogenerated thiocyanate anion originating from the transition metal compound Reinecke's salt will react with CA to initiate anionic polymerization. This work led to the expanded use of other transition-metal compounds as sources for the controlled release of anionic initiators for polymerization reactions. Sanderson, Palmer et al. demonstrated that the CA radical anion (Equation 6) formed upon irradiation of either the ferrocene or the ruthenocene donor-acceptor complex initiates the anionic polymerization of CA (Equation 7).[10]

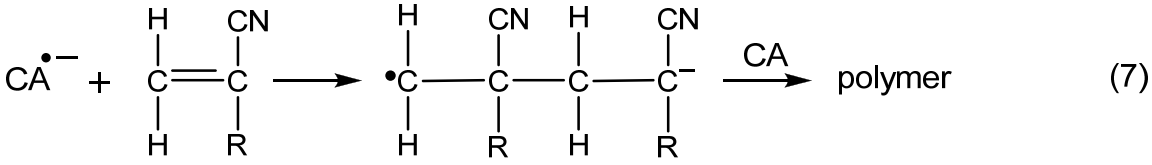

(7)

Yamaguchi and Kutal demonstrated that the release of the benzoylcyclopentadienide anion upon irradiation of DFc also initiates the anionic polymerization of CA.[36] Addition of the benzoylcyclopentadienide anion (represented by X^- in Equation 8) to the carbon-carbon double bond (C=C) of the electrophilic

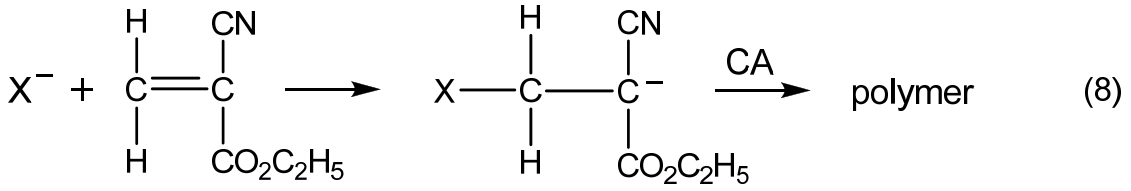

(8)

monomer yields a stabilized carbanion, and then chain-growth polymerization of CA proceeds from the active anionic site. Sanderson, Quinlan et al. also demonstrated that irradiating benzoyl-substituted ruthenocenes in CA initiates the polymerization of CA.[37] In all of these studies, polymerization characterization data were obtained by Fourier transform infrared spectroscopy (FT-IR). The extent of polymerization is directly related to the decrease in the absorbance of the carbon-carbon double bond of CA at 1616 cm^{-1}.[37] This relationship is expressed in Equation 9, where A_o is the initial area of

$$\% \text{ polymerization} = \frac{A_o - A_t}{A_o} \times 100 \qquad (9)$$

the C=C peak before initiation, and A_t is the area of the peak at time t. The rate of photoinitiated polymerization (R_p) at any point in the run can be determined by using Equation 10, where A_{t1} and A_{t2} are the areas of the double bond peak at the

$$R_p = \frac{M(At_1 - At_2)}{A_o(t_2 - t_1)} \quad (10)$$

indicated times, and M is the monomer concentration.[37]

For the Fc compounds, R_p decreases in the order DFc > BFc > Fc, indicating that the presence of a benzoyl group increases R_p.[37] This observation also agrees with prior observations that CA solutions containing DFc or BFc require shorter irradiation times to undergo a visually detectable change in viscosity than solutions containing Fc.[38] R_p occurs at a higher rate for benzoyl-substituted ferrocenes because their bands have higher extinction coefficients and extend over a broader wavelength range than the charge-transfer-to-solvent (CTTS) of the [Fc, CA] donor-acceptor complex (Equation 1).[7] Therefore, the benzoyl-substituted ferrocenes can absorb more of the incident light needed to form the reactive initiator.

<u>Group transfer polymerization of methyl methacrylate</u>

The term “group transfer polymerization” (GTP) was first coined by scientists at DuPont in 1983.[39] The only commercial method for the controlled, living polymerization of MMA is GTP.[40] Initially, we wanted to photochemically generate an initiating species that would polymerize the monomer, methyl methacrylate (MMA), in a controlled manner to form poly (methyl methacrylate) (PMMA). In terms of the photo-polymerization of MMA, it would be the first example of a purely anionic route.

Ideally, the PMMA created photochemically in a GTP system should exhibit similar properties as the PMMA produced in a thermal GTP system, such as high syndiotacticity and low polydispersity.

The two mechanisms under consideration for base catalyzed GTP are the dissociative pathway (Figure 7a) and the associative pathway (Figure 7b). In the dissociative pathway, the nucleophilic catalyst (X^-) complexes with MTS, and in a reversible cleavage step, a reactive enolate end is generated that adds monomer.[40] The enolate end groups are then capped by $(CH_3)_3SiX$ to regenerate silyl ketene acetal ends. Since low molecular weight distribution (MWD) and controlled molecular weight polymer are obtained at low catalyst concentrations, the equilibrium generating the enolate end groups must be much faster than the polymerization rate.[40] In the associative pathway, the nucleophilic catalyst complexes with MTS for addition to monomer. The silyl group transfers to incoming monomer and remains on the same polymer chain during the polymerization step.[40]

However, in work by Quirk that diminishes the role of the associative mechanism, an ester enolate was used as a catalyst for GTP of MMA initiated by MTS at 50^{o}C.[41] The MWD was in the 1.2 range, and the molecular weight was controlled by the ratio of MTS to monomer.[41] In similar experiments without the MTS, conversions were lower, the MWD was broader, and molecular weight control was lost. Quirk postulates that the ester enolate end groups are being stabilized by complexation with MTS (Equation 11).[40,41] He agrees that this complex could be adding monomer by the associative process. However, since all of the chains are growing at the same rate, the equilibrium between the complex and the bare enolate must be faster than the polymerization rate.

Figure 7

The (a) dissociative and (b) associative mechanisms for group transfer polymerization (GTP). X^- denotes the nucleophilic anion. Reproduced from Ref. (40). Copyright 2004 Springer-Verlag Berlin Heidelberg.

(a)

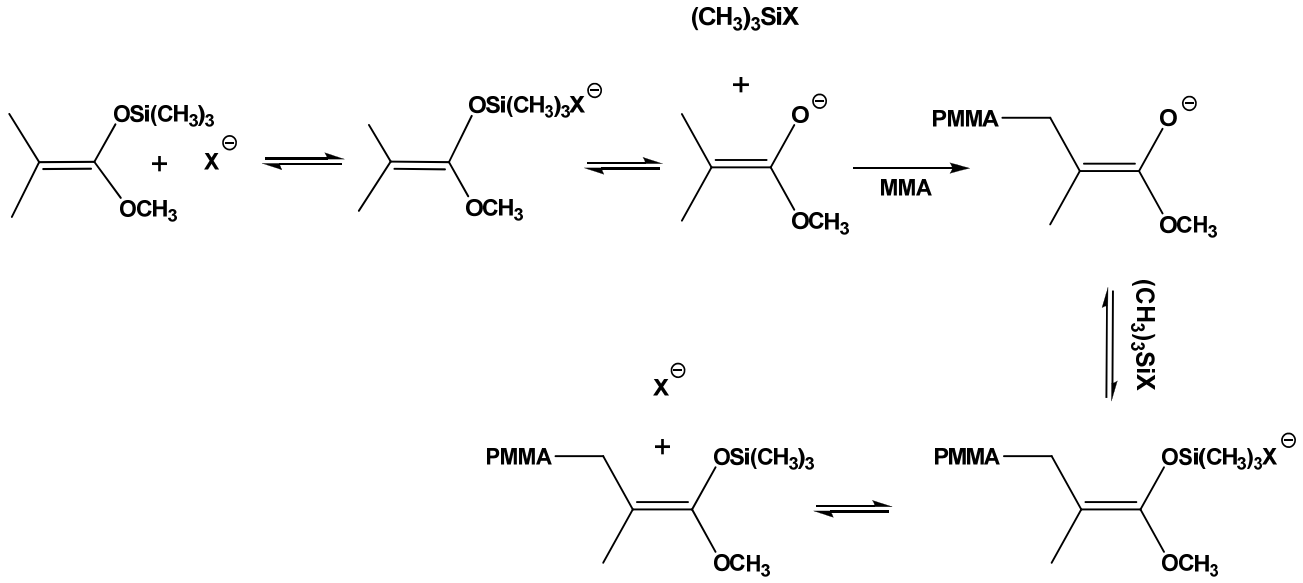
(CH3)3SiX
OSi(CH3)3
X⊖
OCH3
OSi(CH3)3X⊖
O⊖
MMA
PMMA
(CH3)3SiX

(b)

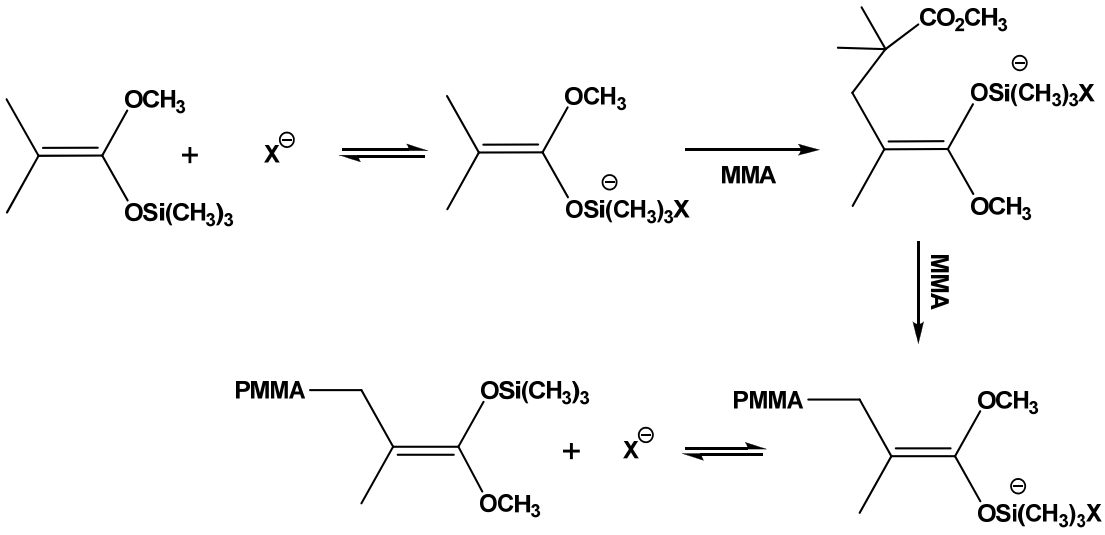
OCH3
X⊖
OSi(CH3)3
OSi(CH3)3X⊖
CO2CH3
MMA
PMMA

Thus, unless the polymerization rates by the complex (associative case) and by the enolate end group (dissociative case) were the same (which is highly unlikely), the MWD and molecular weight control would be lost.[40]

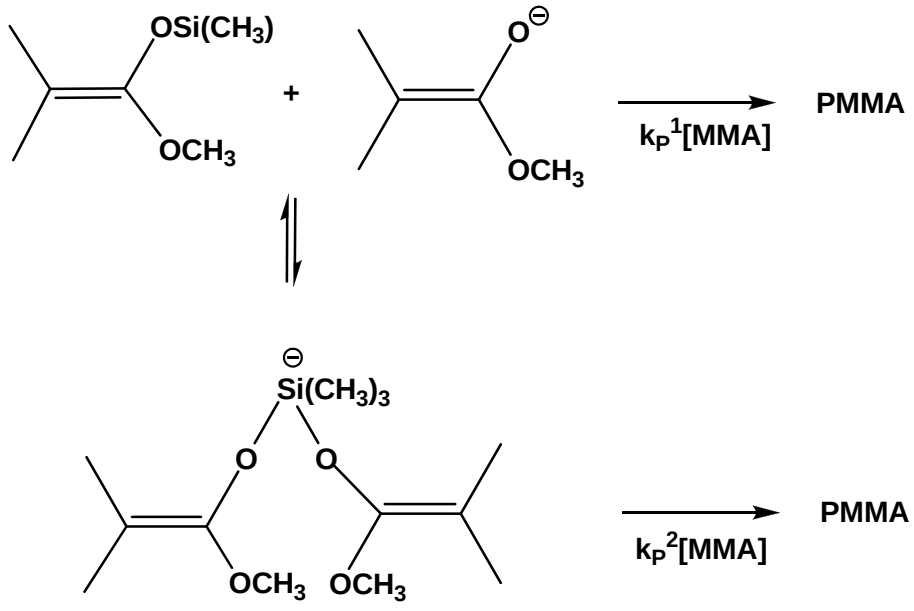

(11)

Further work by Muller confirms the validity of Quirk's finding. Muller found that adding too much MTS decreases the rate of GTP.[42] In Equation 11, an excess amount of MTS would shift the equilibrium between the enolate end group and the complex to the complex side, which would lower the concentration of the enolate and thus, the polymerization rate. Quirk's work may explain why adding too much catalyst (the nucleophilic anion) decreases the rate of polymerization. In the associative pathway, an excess amount of catalyst should increase the polymerization rate. In the dissociative pathway, an excess amount of catalyst may generate more enolate end groups, too much to be stabilized through complexation with MTS, resulting in a decrease in the rate of polymerization.[40] Bandermann also studied the effects of catalyst concentration

on GTP.[43] Other factors such as the reaction of catalyst with initiator, the need for large, unreactive counterions, and the presence of an induction period support the dissociative mechanism.

There are several characteristics of a commercially viable process for controlled polymerization: operating temperatures in the 50-80^{o}C range, low sensitivity to impurities, low cost of reagents, minimal chain termination (living), and a colorless product.[40] GTP is the only process that meets most of these requirements. The disadvantages of GTP are the high cost of initiator and sensitivity to protic species. Other systems have been developed to try and bypass the shortcomings of GTP while replicating its benefits, most notably, different types of controlled free radical polymerization.[40] However, these methods fall short of feasible use in industry.[40]

Project goals

Our research group has studied the spectroscopy and photochemistry of Fc, Rc, and their benzoyl-substituted derivatives and the potential use of these compounds as anionic photoinitiators.[32,33] One of the most attractive photoinitiator candidates is 1,1'-dibenzoylferrocene (DFc), which features good thermal stability, strong light absorption throughout the visible and ultraviolet regions, and high photosensitivity originating from an electronic excited state possessing considerable MLCT character. In this work, we calculated values of the disappearance quantum yield (ϕ_{dis}) over a range of excitation wavelengths that encompass both low-energy absorption bands of DFc in methanol at room temperature to determine the wavelength dependence of the excited-state reaction. We also calculated values of ϕ_{dis} near 50^{o}C to determine if temperature affects the photochemical behavior of DFc. Such studies provide important information about

the excited state reaction mechanism and thereby facilitate the rational design of the next generation of photoinitiators with improved performance characteristics.

Some similarities exist between the electronic properties of benzoyl-substituted ferrocenes and the silicon-bridged [1]ferrocenophanes. Tanabe and Manners discovered that irradiating solutions of $FcSiMe_2$ induces ROP of the monomer in the presence of a cyclopentadienide initiator. We were interested to determine if this photochemical process occurred via a MLCT pathway. Tanabe, Guido, et al. reported that ROP rates were wavelength and temperature dependent.[28] The explanations proposed for this behavior were based upon measurements of the kinetics and product yield of polymerization. Because these measured quantities depend upon both the photochemical/photophysical processes undergone by the metallocenophanes and subsequent thermal polymerization steps, it is difficult to unravel which processes contribute to the wavelength and temperature dependence. Therefore, our goal was to provide quantitative information about the primary processes occurring from the photoexcited metallocenophane. Accordingly, we ran experiments to examine the solvent, wavelength, and temperature dependence of the photochemical process. Each of these variables could significantly influence the performance of the monomer in ROP systems. Listed below is a summary of the project goals:

1. Determine how values of ϕ_{dis} behave over a range of excitation wavelengths that encompass both MLCT bands of DFc in methanol at room temperature.
2. Determine the effects of high temperature on ϕ_{dis} of DFc in methanol.

3. Determine if the presence of MLCT character in the low-energy excited states of $FcSiMe_2$ is responsible for the spectral similarities it shares with DFc.
4. Determine the effects of solvent on the photochemistry of $FcSiMe_2$.
5. Determine if the photochemistry of $FcSiMe_2$ is wavelength and temperature dependent.
6. Determine the mechanism by which $FcSiMe_2$ acts as a photoinitiator in living anionic ROP systems.
7. Expand this work to include the spectroscopy and photochemistry of $FcSiPh_2$.
8. Determine if DFc, $FcSiMe_2$, or $FcSiPh_2$ can function as photoinitiators for the group transfer polymerization of MMA.

CHAPTER 2

EXPERIMENTAL

Materials

Tetrahydrofuran (THF) and diethyl ether were dried and collected with either one of two methods. In one method, these solvents were dried and collected under nitrogen using an MBraun solvent purification system (MB-SPS). In the other method, these solvents were dried by stirring with finely crushed CaH_2 (~ 2 g/L) overnight. They were then distilled, with the initial (~10%) and final (~15%) cuts being discarded. Methanol was dried and collected with either one of two methods. In one method, methanol was dried by stirring with finely crushed CaH_2 (~ 2 g/L) overnight. It was then distilled. In the other method, it was refluxed over magnesium and iodine and then distilled. Hexane was dried and collected with either one of two methods. In the first method, hexane was dried and collected under nitrogen using a MB-SPS. In the second method, it was dried by stirring over sodium. It was then distilled. Acetonitrile was dried by stirring with finely crushed CaH_2 (~ 2 g/L) overnight. It was then distilled. Benzene (Sigma-Aldrich, thiophene-free) was dried by stirring with finely crushed CaH_2 (~ 2 g/L) and then distilled.

Ferrocene (abbreviated Fc, 98%, Sigma-Aldrich) was sublimed at room temperature and atmospheric pressure by a previously reported procedure.[44] 1, 1'-Dibenzoylferrocene (abbreviated DFc, Sigma Chemical Company) was purified by recrystallization from warm hexanes. TMEDA (Fluka, puriss., absolute, $\geq$ 99.0% (GC))

was distilled from metallic sodium. Dichlorodimethylsilane (Fluka, puriss., ≥ 99.5% (GC)) was distilled. Butyllithium (Sigma-Aldrich, 1.6M or 2.5M solution in hexanes) was used as purchased. Methanol-d_4 and acetonitrile-d_3 were used as purchased. Diphenylsila[1]ferrocenophane ($FcSiPh_2$) was synthesized by Cecilia Ieong at the University of Bristol School of Chemistry in Bristol, England. Anal. Calcd for $C_{22}H_{18}SiFe$: C, 72.14; H, 4.95. Found: C, 71.94; H, 4.95.

Tetrabutylammonium thiocyanate was used as purchased. Methyl methacrylate (Fluka, purum; ≥ 99.0% (GC)) was first washed with 5% KOH until the orange color cleared up. It was then washed with distilled water and dried over CaH_2. It was then distilled. Methyl trimethylsilyl dimethylketene acetal (Sigma Aldrich, 95%) was distilled over molecular sieves. 1,2-Dimethoxyethane (anhydrous, 99.5%) was used without further purification.

Synthesis of dimethylsila[1]ferrocenophane

Dimethylsila[1]ferrocenophane (abbreviated $FcSiMe_2$, Batches 6 and 13) was prepared according to a modified literature procedure.[45] The reactions were performed under argon in a glove box. Vacuum-dried Fc (6 grams) was placed in an oven-dried (180^{o}C, at least 30 minutes) 24/40 200-mL Schlenk flask. Hexane (100 mL) was added to the flask with a glass syringe and a metal 20-gauge needle. TMEDA (4.5 mL) was added to the flask with a 10-mL disposable syringe and needle. A stir bar was placed in the flask, and a rubber septum was placed in the 24/40 joint. Butyllithium (1.6M, 2 X 20 mL) was added to the flask through the septum with 20-mL plastic disposable syringes and metal 20-gauge needles. The contents were stirred overnight. On the next day, the septum was removed from the flask and replaced with a 60-mL addition funnel. Hexane

(30 mL) was added to the addition funnel with a glass syringe and a metal 20-gauge needle. Dichlorodimethylsilane (4.2 mL) was added to the addition funnel with a 5-mL glass syringe and a 20-gauge metal needle. A rubber septum was placed in the 24/40 joint of the addition funnel, and the system was transferred out of the glove box to a fume hood. The flask was cooled to -10^{o}C in an ice/salt bath, and then the dichlorodimethylsilane solution was added dropwise to the flask over 20 minutes. The contents in the flask were stirred for another hour in the ice/salt bath. The flask was then removed from the ice/salt bath. After reaching room temperature, the contents in the flask were stirred for another hour. After letting the lithium chloride settle, the addition funnel was replaced with a rubber septum, and then the solution was filtered via cannula to an oven-dried 24/40 200-mL Schlenk flask. The solvent was removed by vacuum distillation to yield a crude red product in the flask. The red product was purified via sublimation with a water-cooled sublimation apparatus. First, three sublimations were performed onto the cold finger under vacuum at 65^{o}C to remove unreacted Fc. The cold finger was placed back into the flask where red crystals of $FcSiMe_2$ formed on the cold finger under vacuum at 65^{o}C (not exceeding 80^{o}C) for 1 hour. The flask (fitted with the cold finger) was transferred to the glove box where the red crystals were scraped from the cold finger into a 24/40 oven-dried 100-mL Schlenk flask containing 40 mL of hexane. This step was repeated two times, and the resulting red solution was then filtered with a 0.2 μm nylon membrane (in a 25 mm syringe filter attached to a disposable plastic 20 mL syringe) and transferred to a 24/40 oven-dried 100-mL Schlenk flask. The solvent was removed by vacuum distillation to yield red crystals in the flask. The cold finger was placed back into the flask where red crystals of $FcSiMe_2$

formed on the cold finger under vacuum at 65°C (not exceeding 80°C) for 1 hour. The flask (fitted with the cold finger) was transferred to the glove box where the red crystals were scraped into a glass vial. The vial and its contents were wrapped in aluminum foil and stored in a freezer. Anal. Calcd for $C_{12}H_{14}SiFe$: C, 59.52; H, 5.83. Found (Batch 6): C, 58.66; H, 5.91. mp 66-72°C. Found (Batch 13): C, 59.01; H, 5.84.

$FcSiMe_2$ (Batch 2a) was prepared according to published procedures.[24,46] The reactions were performed under argon in a glove box. Vacuum-dried Fc (6.623 grams) was placed in an oven-dried (180°C, at least 30 minutes) 24/40 200-mL Schlenk flask. Hexane (50 mL) was added to the flask with a glass syringe and a metal 20-gauge needle. A stir bar was placed in the flask, and a rubber septum was placed in the 24/40 joint. Butyllithium (2.5M, 2 X 16.4 mL) was added to the flask through the septum with a glass syringe and a metal 20-gauge needle. TMEDA (6.7 mL) was added to the flask with a 10-mL glass syringe and a metal 20-gauge needle. The contents were stirred overnight. On the next day, the septum was removed from the flask. Hexane was decanted from the flask, and approximately 250 mL of diethyl ether were added to the flask. The contents were stirred overnight. On the next day, the septum was removed from the flask and replaced with a 60-mL addition funnel. Dichlorodimethylsilane (4.6 mL) was added to the addition funnel with a 5-mL glass syringe and a 20-gauge metal needle. A rubber septum was placed in the 24/40 joint of the addition funnel, and the system was transferred out of the glove box to a fume hood. The flask was cooled to -10-15°C in an ice/salt bath, and then the dichlorodimethylsilane solution was added dropwise to the flask over 5 minutes. The contents in the flask were left to stir for approximately 2-3 hours to achieve room temperature. After letting the lithium chloride

settle, the addition funnel was replaced with a rubber septum, and then the solution was filtered via cannula to an oven-dried 24/40 300-mL Schlenk flask. The solvent was removed by vacuum distillation to yield a crude red product in the flask. The red product was purified via sublimation with a water-cooled sublimation apparatus. First, one sublimation was performed onto the cold finger under vacuum at 40^{o}C to remove unreacted Fc. The cold finger was placed back into the flask where red crystals of $FcSiMe_2$ formed on the cold finger under vacuum at 40^{o}C (not exceeding 50^{o}C) for 2 hours. The flask (fitted with the cold finger) was transferred to the glove box where the red crystals were scraped from the cold finger into a 24/40 oven-dried 100-mL Schlenk flask containing 35-40 mL of hexane. This step was repeated two times, and the resulting red solution was then filtered with a 0.2 μm nylon membrane (in a 25 mm syringe filter attached to a glass 20 mL syringe) and transferred to a 24/40 oven-dried 100-mL Schlenk flask. The solvent was removed by vacuum distillation to yield red crystals in the flask. The cold finger was placed back into the flask where red crystals of $FcSiMe_2$ formed on the cold finger under vacuum at 40^{o}C (not exceeding 50^{o}C). The flask (fitted with the cold finger) was transferred to the glove box where the red crystals were scraped into a glass vial. The vial and its contents were wrapped in aluminum foil and stored in a freezer. Anal. Calcd for $C_{12}H_{14}SiFe$: C, 59.52; H, 5.83. Found (Batch 2a): C, 59.69; H, 5.87. mp 83^{o}C.

Instrumentation

Melting points were determined with a Thomas-Hoover Unimelt apparatus and are uncorrected. Electronic absorption spectra were recorded at 22 ± 2 ^{o}C on a Cary 300 spectrophotometer or on a Cary 50 spectrophotometer. Electrospray ionization

mass spectrometry (ESI-MS) experiments were performed on a Perkin-Elmer Sciex API 1 Plus single-quadrupole mass spectrometer. Analyte solutions (5 μL) were introduced directly into the spectrometer via an injection loop. Fourier transform mass spectrometry (FT-MS) experiments were performed on a Bruker Apex II mass spectrometer with a 4.7 Tesla magnet and an electron ionization source. Samples were placed in a silica tube and dried down, then placed inside the ion source. It was then exposed to a temperature ramp, where the temperature increased from ambient conditions to 300°C at a rate of 1°C/second. Matrix-assisted laser desorption/ionization time-of-flight (MALDI-TOF) mass spectrometry experiments were performed on a Bruker Autoflex mass spectrometer. Samples were analyzed using laser desorption (LD).

An Illuminations Industries 200-W high-pressure mercury arc lamp was used to perform continuous photolysis experiments at λ_{excit}'s of 313, 365, 406, 436, and 546 nm. Light intensities at 313, 365, and 406 nm were measured with the ferrioxalate actinometer.[47,48] The light intensity at 436 nm was measured with both the ferrioxalate actinometer and the Reineckate actinometer.[49] The light intensity at 546 nm was measured with the Reineckate actinometer. Polychromatic light of wavelengths > 290 nm was obtained by passing the full output of the lamp through Pyrex glass.

A Coherent Innova 70 Series argon-ion laser was used to perform continuous photolysis experiments at λ_{excit}'s of 458, 488, 515, and 577 nm. A JDS Uniphase helium-neon laser was used to perform continuous photolysis experiments at an λ_{excit} of 632 nm. Light intensities at 458, 488, 515, 577, and 632 nm were measured with the Reineckate actinometer.

Group transfer polymerization procedures

All glassware was oven-dried prior to use. All reagents were added to a round bottom flask in a glove box. The reaction was left to stir at a set temperature under a hood. Samples were periodically retrieved from the reaction flask and placed in an Omni-Cell KBr permanently sealed window unit (0.025 mm) for measurement in a Bruker Vector 22 Fourier transform infrared spectrometer. The reaction was stopped with the addition of methanol, and the polymer was crashed out of solution with hexane.

Photochemical procedures

For room temperature experiments encompassing all λ_{excit}'s except 632 nm, solutions of DFc, $FcSiMe_2$, and $FcSiPh_2$ were irradiated with stirring in either 1-cm pathlength rectangular quartz cells or in 10-cm pathlength cylindrical quartz cells that were placed in a cell holder. At 632 nm, solutions of DFc were irradiated in a 20-cm pathlength cylindrical cell. Typical complex concentrations of DFc were in the range (2.4-3) x 10^{-3} M. Typical complex concentrations of $FcSiMe_2$ were in the range (4-12) x 10^{-3} M. Typical complex concentrations of $FcSiPh_2$ in methanol, acetonitrile, hexane, and benzene were in the range (3-8) x 10^{-4} M. Typical complex concentrations of $FcSiPh_2$ in THF were in the range (2-5) x 10^{-3} M. For high- and low-temperature experiments, solution temperature was maintained in a thermostated cell holder with a Thermo Electron NESLAB RTE 10 Refrigerated Bath/Circulator. For high temperature experiments, solutions of DFc were irradiated with stirring in 1-cm rectangular quartz cells maintained at 46 ± 1^{o}C in a thermostated cell holder. For low temperature experiments, solutions of $FcSiMe_2$ and $FcSiPh_2$ were irradiated with stirring in 1-cm rectangular quartz cells maintained at 4 ± 1^{o}C in a thermostated cell holder. For all

compounds, the extent of photoreaction was determined spectrophotometrically by monitoring the decrease in intensity of the lowest energy band in the electronic absorption spectrum. The mathematical relationship is given by Equation 12, where A_o is the initial absorbance at the band maximum, A_t, is the absorbance after irradiation for

$$\%\,\text{reaction} = \frac{A_o - A_t}{A_o - A_f} \times 100\% \qquad (12)$$

time t, and A_f is the final absorbance reached after exhaustive photolysis. Quantum yields were calculated at different extents of reaction and then linearly extrapolated to 0% reaction.

Due to competing absorption by the photoproduct(s) with the starting material at λ_{excit} = 313 nm, the fraction of light absorbed by the starting material was calculated in the following manner. The extent of photoreaction, as measured by the decrease in intensity of the low energy band, was used to calculate the expected absorbance of the high energy band. The fraction of light absorbed by the starting material after irradiation for time t at λ_{excit} = 313 nm (f_{313}) was then calculated by dividing this expected absorbance by the observed absorbance. The average f_{313} over the length of irradiation was used for quantum yield measurements.

NMR Procedures

Filtered irradiated solutions were transferred to screw cap NMR tubes in a glove box. ^{1}H NMR spectra were recorded on a Varian Inova 500 MHz spectrometer at 25 ^{o}C. In methanol-d_4, ^{1}H resonances were referenced internally to the residual protonated solvent resonance at 3.31 ppm. In acetonitrile-d_3, ^{1}H resonances were referenced

internally to the residual protonated solvent resonance at 1.94 ppm. In benzene-d_6, ^{1}H resonances were referenced internally to the residual protonated solvent resonance at 7.16 ppm. Decomposition of the initial $FcSiMe_2$ was calculated by dividing the referenced area of the $Si(CH_3)_2$ peak (0.50 ppm) at time *t* by the referenced area of the same peak initially, and then subtracting this value from 1. Percent decomposition was then calculated by multiplying the result by 100%. Production of the monosubstituted derivative of Fc in methanol-d_4 in all $FcSiMe_2$ samples was observed by monitoring the referenced area of the $Si(CH_3)_2$ peak (0.38 ppm). Decomposition of the initial $FcSiPh_2$ was calculated by dividing the referenced area of the Si(Ph) peak at 7.93 ppm at time *t* by the referenced area of the same peak initially, and then subtracting this value from 1. Percent decomposition was then calculated by multiplying the result by 100%.

CHAPTER 3

SPECTROSCOPY AND PHOTOCHEMISTRY OF 1,1'-DIBENZOYLFERROCENE

As previously mentioned, the solution photochemistry of benzoyl-substituted ferrocenes has been investigated in considerable detail.[4,12] In one study, an acetonitrile solution containing 1,1'-dibenzoylferrocene (DFc) and Na^+ (as the carrier cation) was irradiated in the transparent tip of an electrospray ionization mass spectrometer system. Figure 8 shows that the mass spectrum of the analyte contains three major product series: (1) adducts of benzoylcyclopentadiene and a proton (*m/z* = 171.1) or a sodium ion (*m/z* = 193.0 and 363.1); (2) adducts of half-sandwich iron(II) complexes and a proton (*m/z* = 154.0 and 174.5); (3) fully ring-deligated iron (II) complexes of general formula $[Fe(CH_3CN)_n]^{2+}$ (*m/z* = 89.5, 110.0, and 130.5 for *n* = 3, 4, and 5, respectively).[7] Observation of the first two product series supports heterolytic metal-ring bond cleavage as the primary photochemical reaction of DFc (Equation 2). The benzoylcyclopentadienide anion released in this process is basic enough to abstract a proton from traces of water or other protic impurities to form 1-benzoyl-1,3-cyclopentadiene. The carbonyl oxygen atom of the benzoyl group forms Lewis acid-base adducts with a proton or a sodium ion to yield the ionic products detected.[7] Half-sandwich complexes also contain a carbonyl oxygen atom that form Lewis acid-base adducts with a proton or a sodium ion to yield the dicationic species observed. The completely solvated iron(II) species are likely formed by decomposition of the initially formed half-sandwich complexes.

Figure 8

Electrospray ionization mass spectrum of a photolyzed (488 nm) acetonitrile (AN) solution originally containing 130 μM DFc and 120 μM Na^+. Reproduced from Ref. (12). Copyright 2003 American Chemical Society.

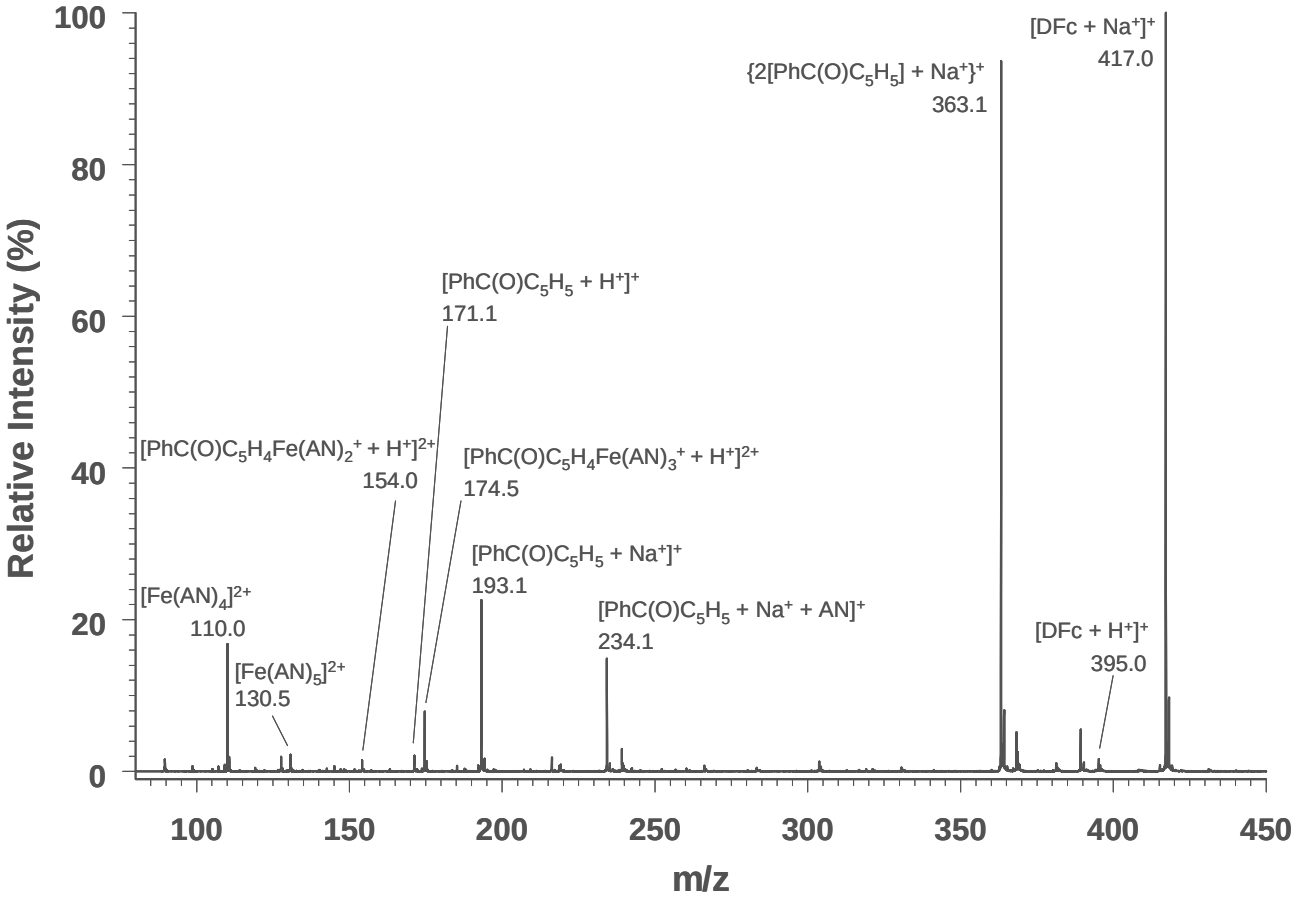
Relative Intensity (%)
100
80
60
40
20
0
100
150
200
250
300
350
400
450
m/z
[DFc + Na+]+
417.0
{2[PhC(O)C5H5] + Na+}+
363.1
[PhC(O)C5H5 + H+]+
171.1
[PhC(O)C5H4Fe(AN)2+ + H+]2+
154.0
[PhC(O)C5H4Fe(AN)3+ + H+]2+
174.5
[PhC(O)C5H5 + Na+]+
193.1
[Fe(AN)4]2+
110.0
[PhC(O)C5H5 + Na+ + AN]+
234.1
[DFc + H+]+
395.0
[Fe(AN)5]2+
130.5

Figure 9 shows representative spectral changes during photolysis in deoxygenated methanol for the purpose of calculating ϕ_{dis}. During the time intervals of excitation with 488-nm light, a steady bleaching of the low-energy band (λ_{max} = 486 nm) of DFc occurs. Equation 12 was applied to determine that approximately 33% of the initial DFc reacts in 20 s. When the solvent is switched from methanol to cyclohexane, the low-energy band (λ_{max} = 471 nm) of DFc undergoes considerably less bleaching during 3100 s of irradiation with 488-nm light (Figure 10).

Table 1 shows ϕ_{dis} data for benzoylferrocene (BFc) and DFc. The data show that the number of benzoyl-substituted rings on ferrocene (Fc) is a key determinant of its excited state reactivity (runs with λ_{excit} = 546 nm). Thus, DFc undergoes loss of a benzoylcyclopentadienide anion much more efficiently than BFc. Earlier work by Yamaguchi showed that substituents present on the phenyl ring of the benzoyl group exert little influence on this ring-loss process.[4] Table 1 also shows that values of ϕ_{dis} remain reasonably constant over a range of λ_{excit}'s that encompass both absorption bands of DFc. This behavior suggests that the initially populated Franck-Condon excited state undergoes very rapid electronic and vibrational relaxation to yield a common thermally equilibrated excited (thexi) state of DFc.[7] Fe-Cp bond cleavage then occurs from this thexi state directly or from a close-lying reactive state reached by thermal upconversion.[50] Increasing solution temperature does not influence the excited state reactivity. Table 1 also reveals the importance of solvent in this photochemical process as evidenced by the sharp decrease of ϕ_{dis} in cyclohexane. As previously mentioned, earlier work suggested that the photoinduced loss of the benzoylcyclopentadienide anion proceeds via a succession of ring-slipped intermediates such as the η^5, η^3

Figure 9

UV-vis spectral changes arising from the 488-nm irradiation of DFc (2.93 mM) in deoxygenated methanol at room temperature. Spectra were acquired in a 1-cm pathlength quartz cell after 0, 5, 10, 15, and 20 seconds of irradiation with an average laser intensity of 3.90×10^{-7} einsteins/s. The arrow indicates the direction of spectral changes as irradiation proceeds.

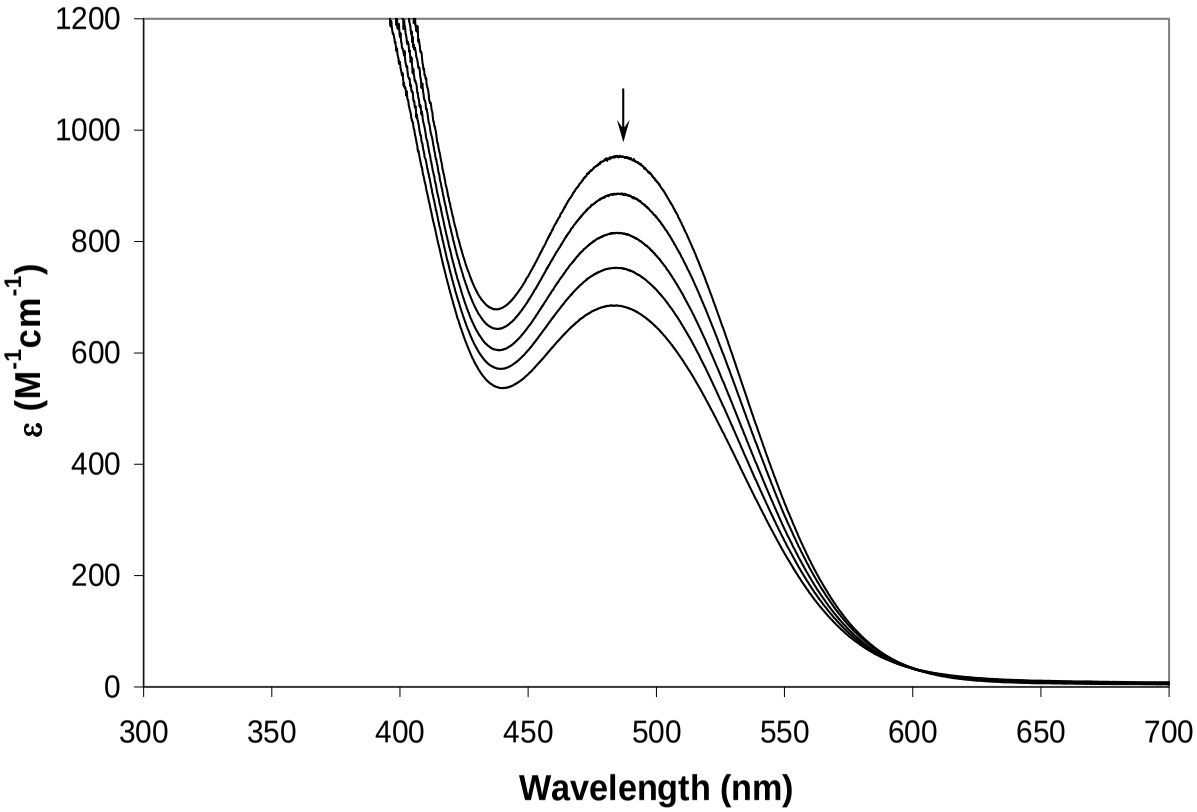
1200
1000
800
600
400
200
0
ε (M-1cm-1)
300
350
400
450
500
550
600
650
700
Wavelength (nm)

Figure 10

UV-vis spectral changes arising from the 488-nm irradiation of DFc (2.51 mM) in deoxygenated cyclohexane at room temperature. Spectra were acquired in a 1-cm pathlength quartz cell after 0, 620, 1240, 1860, 2480, and 3100 seconds of irradiation with an average laser intensity of 3.70×10^{-7} einsteins/s. Only the initial and final spectra are showed. The arrow indicates the direction of spectral changes as irradiation proceeds.

720
620
520
420
ε (M-1cm-1)
400
420
440
460
480
500
520
Wavelength, nm
Initial
t = 3100 s

Table 1. Disappearance Quantum Yield (ϕ_{dis}) Data

Compound (# of Runs)[a]	λ_{excit} (nm)	ϕ_{dis}[b]
DFc (2)	365	0.33 ± 0.00
DFc (2)	406	0.37 ± 0.01
DFc (3)	458	0.38 ± 0.03
DFc (3)	488	0.38 ± 0.05
DFc (1)[c]	488	6.6×10^{-5}
DFc (2)	515	0.36 ± 0.02
DFc (2)[d]	546	0.42 ± 0.06
BFc (1)	546	0.083
DFc (3)	577	0.35 ± 0.03
DFc (1)[e]	577	0.38

a. Performed in deoxygenated methanol; temperature is 22 ± 2°C, unless noted otherwise.

b. Error limit represents mean deviation.

c. Solvent is cyclohexane.

d. Data from Ref (2).

e. Temperature is 46 ± 1 °C.

complex shown in Equation 3. The η^5, η^3 intermediate can then either react further with solvent to produce the half-sandwich product, or it can expel the coordinated solvent to regenerate the parent complex. Strongly coordinating solvents such as methanol favor the former path (high ϕ_{dis}), while poorly coordinating solvents such as cyclohexane favor the latter path (low ϕ_{dis}).

In summary, the results demonstrate that DFc is highly photosensitive in good coordinating solvents over a broad wavelength range in the visible and ultraviolet regions. Reaction occurs from a common thermally equilibrated excited state and is not thermally activated near room temperature.

CHAPTER 4

SPECTROSCOPY AND PHOTOCHEMISTRY OF DIMETHYLSILA[1]FERROCENOPHANE

Electronic Structure

In eclipsed (D_{5h}) Fc, the Cp rings are planar and parallel. In $FcSiMe_2$, the eclipsed Cp rings are inclined towards each other and towards the bridging atom, causing distortions in the complex. A tilt-angle (α) distortion occurs between the Cp ring planes, and bond angle (β) distortions occur between the Cp ring planes and the bridging atom E (Figure 11). Distortions also become apparent with the deviation of the Cp-Fe-Cp angle (δ) from 180° and in the C(Cp)-Si-C(Cp) angle θ. The effects of these distortions appear in the electronic absorption spectrum of $FcSiMe_2$ (α = 20.8°, β = 37.0°, δ = 164.74°, θ = 95.7°)[51] (Figure 12). Compared to Fc, band 3a in the absorption spectrum is more intense and shifted to longer wavelengths while band 1a is more intense.

Rulkens, Gates et al. performed extended Hückel molecular orbital (EHMO) calculations on eclipsed Fc and on dihydrosila[1]ferrocenophane ($FcSiH_2$ in Figure 1). Figure 13 shows a comparison of the primarily metal molecular orbitals in eclipsed Fc and in $FcSiH_2$ (α = 19.1°, β ~ 39.0°, δ = 165.6°, θ = 97.21°)[52]. Because of the metallic nature of these orbitals, ligand field theory can be used to model the electronic transitions between the $6E_2$' and $4A_1$' HOMOs and the $6E_1$" LUMOs.[5,6] Photoexcitation of an E_2' electron to an empty E_1" orbital produces two excited states. These electronic transitions correspond to band 1 and unresolved band 2 in the electronic absorption

Figure 11

Distortions in [1]ferrocenophanes defining angles α, β, δ, and θ. Reproduced from Ref. (51). Copyright 1993 American Chemical Society.

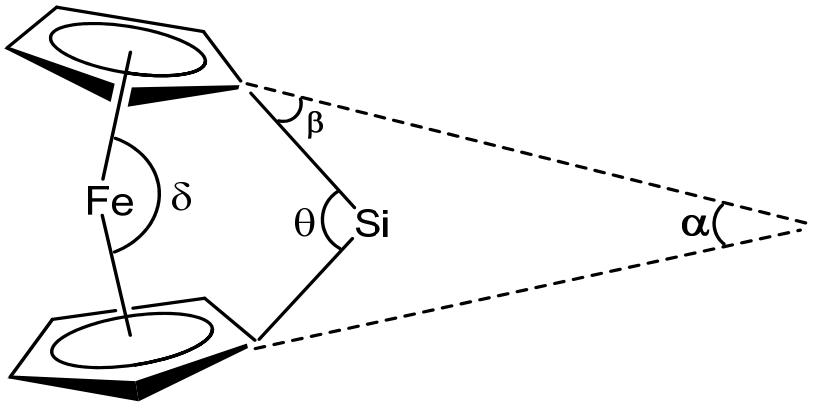
β
Fe
δ
θ
Si
α

Figure 12

Electronic absorption spectrum of Fc and $FcSiMe_2$ in room-temperature methanol.

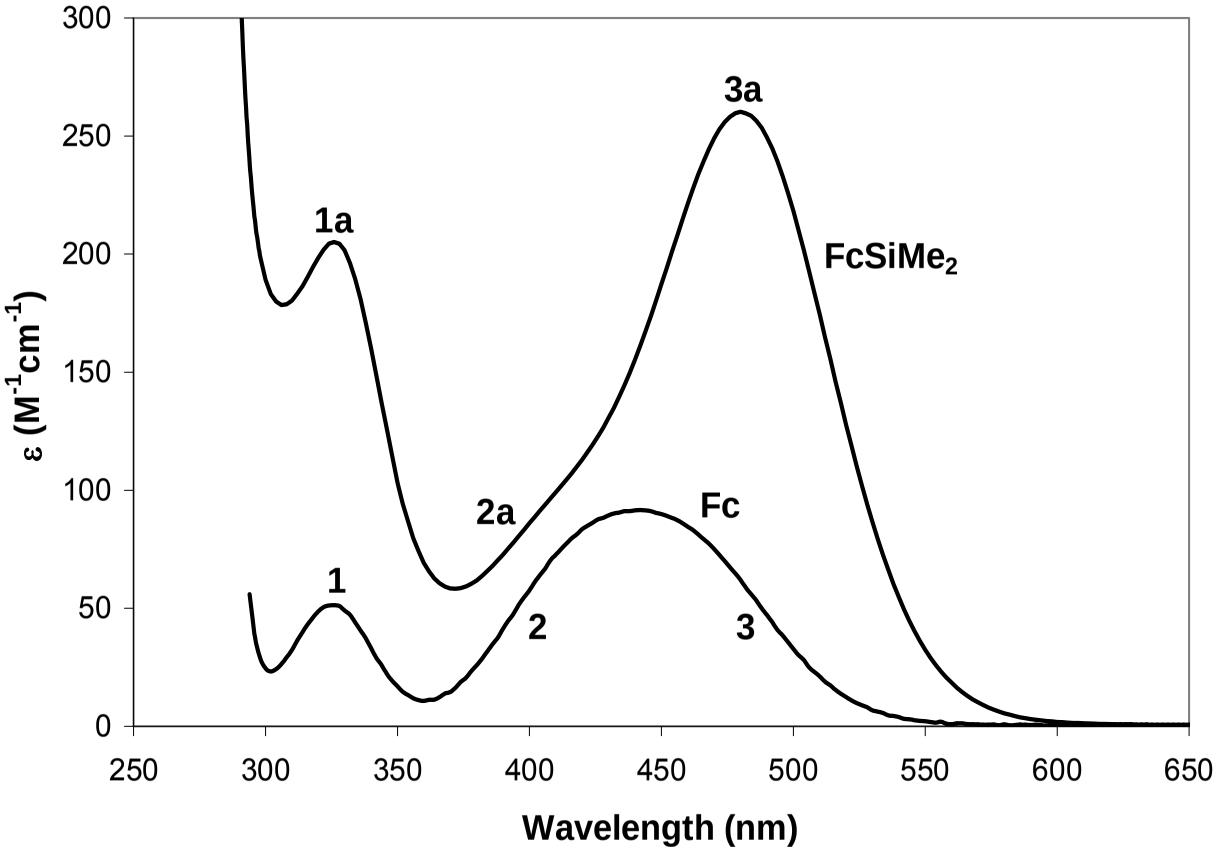
300
250
200
150
100
50
0
ε (M-1cm-1)
250
300
350
400
450
500
550
600
650
Wavelength (nm)
1a
2a
3a
FcSiMe2
1
2
3
Fc

Figure 13

Extended Hückel molecular orbital diagram comparison of eclipsed Fc and $FcSiH_2$. Reproduced from Ref. (21). Copyright 1997 American Chemical Society.

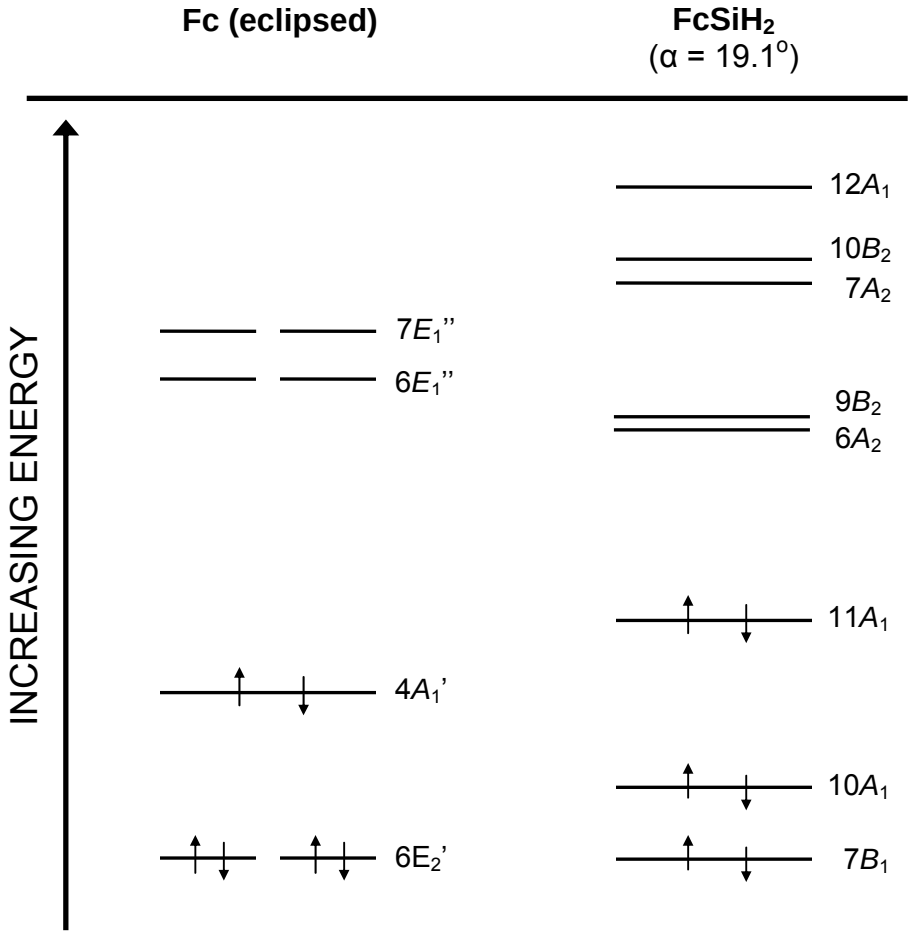
Fc (eclipsed)
FcSiH2
(α = 19.1°)
INCREASING ENERGY
12A1
10B2
7A2
7E1''
6E1''
9B2
6A2
11A1
4A1'
10A1
6E2'
7B1

spectrum of Fc (Figure 12). Photoexcitation of an A_1' electron to an E_1" orbital produces the lowest energy excited state that corresponds to unresolved band 3 in the spectrum of Fc (Figure 12). Figure 13 shows that as an increase in α changes the symmetry of the complex, the energy difference between the HOMOs and the LUMOs decreases significantly. This reduction in energy difference causes band 3 of Fc to shift to longer wavelengths in [1]ferrocenophanes, while the symmetry change relaxes the Laporte rule forbidding ligand field transitions, resulting in the intensification of bands 1 and 3.[21]

To determine if increasing α introduces a degree of MLCT character into the low-energy excited states of $FcSiMe_2$, we recorded electronic absorption spectra of $FcSiMe_2$ (Batch 2a) in different solvents. Earlier work determined that changes in solvent polarity caused significant shifting of the low-energy band in the spectrum of DFc.[4] The largest shifts to longer wavelengths occurred in polar solvents such as methanol. This behavior indicates that the charge-transfer character inherent in DFc stabilizes the low-energy excited states relative to the ground state in polar solvents.[4] Table 2 shows that the wavelength maxima (λ_{max}) for neither band 1a (in Figure 12) nor band 3a (in Figure 12) shift when the solvent polarity is varied. Therefore, we can conclude that the tilting inherent in $FcSiMe_2$ does not produce significant MLCT in the low-energy excited states of $FcSiMe_2$ and that the distortions in the complex are mainly responsible for the behavior observed in the absorption spectrum.

Thermal chemistry of dimethylsila[1]ferrocenophane in methanol

The progress of the thermal reaction of $FcSiMe_2$ with methanol-d_4 was monitored by ^1H NMR. Table 3 summarizes the initial and final ^1H NMR data for $FcSiMe_2$ (Batch

Table 2. Electronic Absorption Spectral Data for $FcSiMe_2$[a]

	λ_{max}, nm (ε, $M^{-1}cm^{-1}$)[b]	
Solvent (ε_r, DN^N)[c]	**Band 1a**	**Band 3a**
Hexane (1.9, 0)	326 (168)	481 (303)
THF (7.6, 0.52)	328 (181)	482 (312)
Methanol (32.7, 0.77)	328 (226)	482 (312)
Acetonitrile (35.9, 0.36)	326 (180)	484 (324)

a. Data recorded at room temperature.

b. ε is extinction coefficient.

c. ε_r is dielectric constant; DN^N is normalized donor number; From Adams, et al., Chemistry in Alternative Reaction Media, 2004, 17.

Table 3. Thermal ^{1}H NMR Spectral Data for $FcSiMe_2$ in CD_3OD[a]

^{1}H NMR[b, c]	
Initial	**Final[d]**
4.47 (t, 4)	4.40 (t, 2)
4.11 (t, 4)	4.17 (t, 2)
0.50 (s, 6)	4.13 (s, 4)
	0.38 (s, 6)

a. Performed under Ar at 25 ± 0.5 °C.
b. ^{1}H NMR are δ ppm units relative to solvent.
c. In parentheses, s = singlet; t = triplet; m = multiplet and numbers are the relative integrations.
d. After approximately 20 h.

13) in methanol-d_4. The ^{1}H NMR spectral changes in methanol-d_4 reveal that reaction occurs thermally according to Equation 13.[53] The data in this study (Figure 14) are

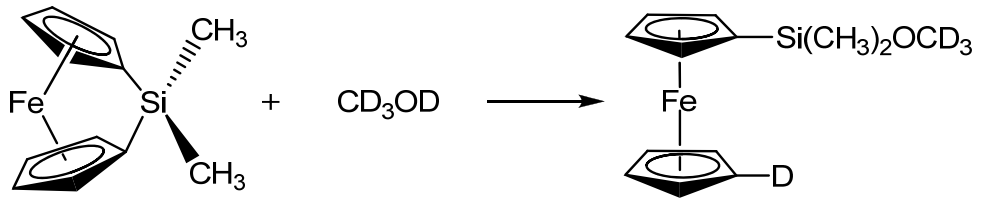

(13)

consistent with data published by Fischer, Kinney et al. that support attack of the –OD group on the strained C-Si$(CH_3)_2$-C bridge to yield a simple, monosubstituted derivative of ferrocene.[53] The peak at 3.43 ppm correlating to the –O(methyl) group does not appear in our spectrum because the solvent is completely deuterated.

Figure 15 shows the spectral changes that occur during a 20 h period when $FcSiMe_2$ (Batch 2a) reacts thermally with methanol at room temperature. As time progresses, the lowest-energy band loses intensity and shifts to higher energy, which indicates the formation of the monosubstituted ferrocene [Fe(η^5-C_5H_4D)(η^5-$C_5H_4Si(OCD_3)(Me_2)$]. As previously discussed, the lowest-energy visible absorption band of $FcSiMe_2$ is redshifted compared to that of Fc. Upon hydrolysis with methanol, the absorption maximum of the lowest-energy band shifts to higher energy compared to the starting spectra. The final spectrum obtained from the hydrolysis of $FcSiMe_2$ shows a new maximum for the lowest-energy band near 440 nm. The redshifted absorption maximum in $FcSiMe_2$ compared to Fc is thus due to the fact that the Cp rings are not parallel owing to the bridging $SiMe_2$ group.[54,55]

Figure 14

(a) Initial ^{1}H NMR spectrum of 50 mM $FcSiMe_2$ in CD_3OD. The * designates the residual protonated solvent resonance at 3.31 ppm.

(b) Final ^{1}H NMR spectrum resulting from the thermal reaction of 50 mM $FcSiMe_2$ in room-temperature (25^{o}C) CD_3OD after approximately 20 h.

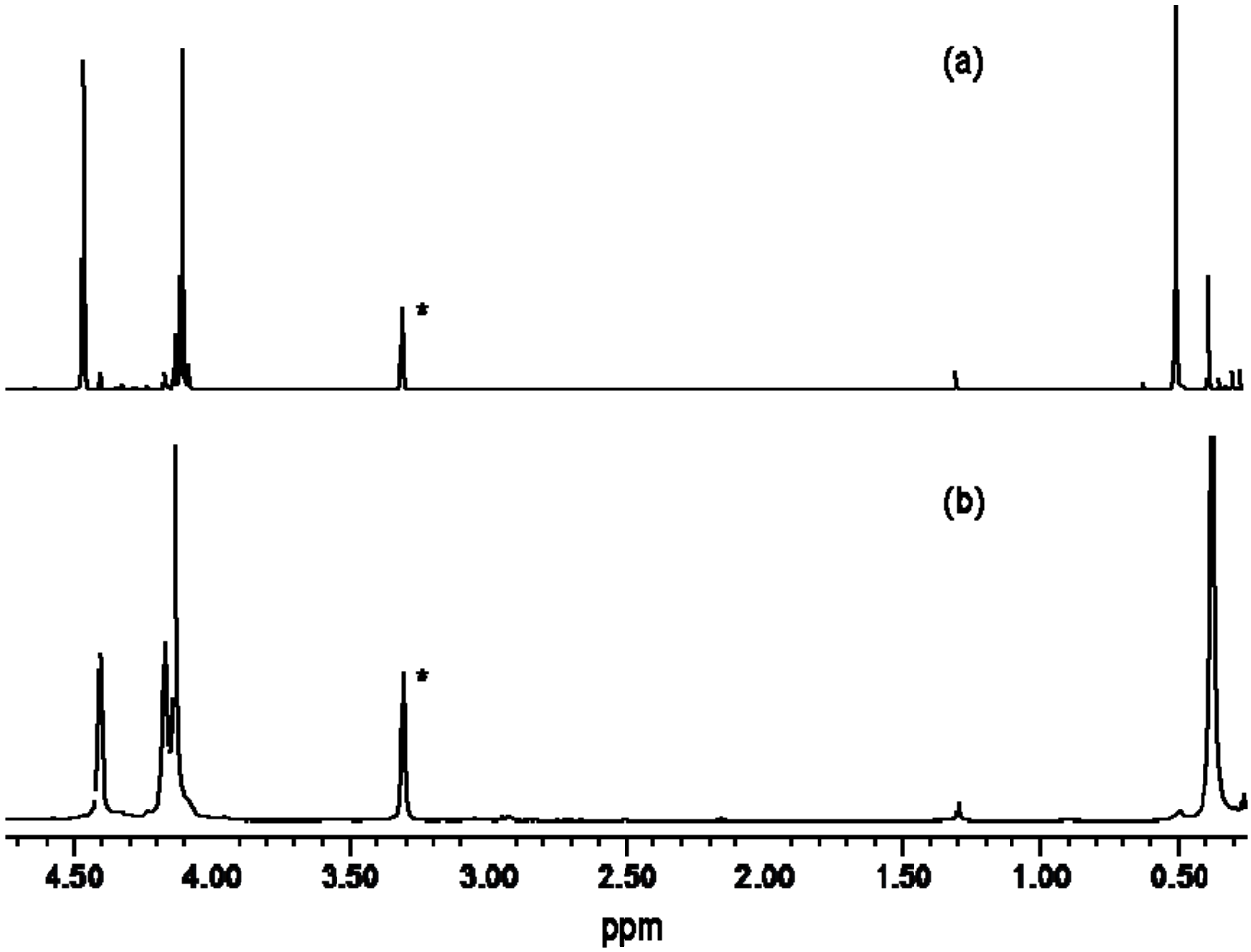
(a)
*
(b)
*
4.50
4.00
3.50
3.00
2.50
2.00
1.50
1.00
0.50
ppm

Figure 15

UV-vis spectral changes arising from the thermal reaction of 4.54 mM $FcSiMe_2$ in room-temperature methanol. The arrows indicate the direction of spectral changes as the reaction proceeds thermally.

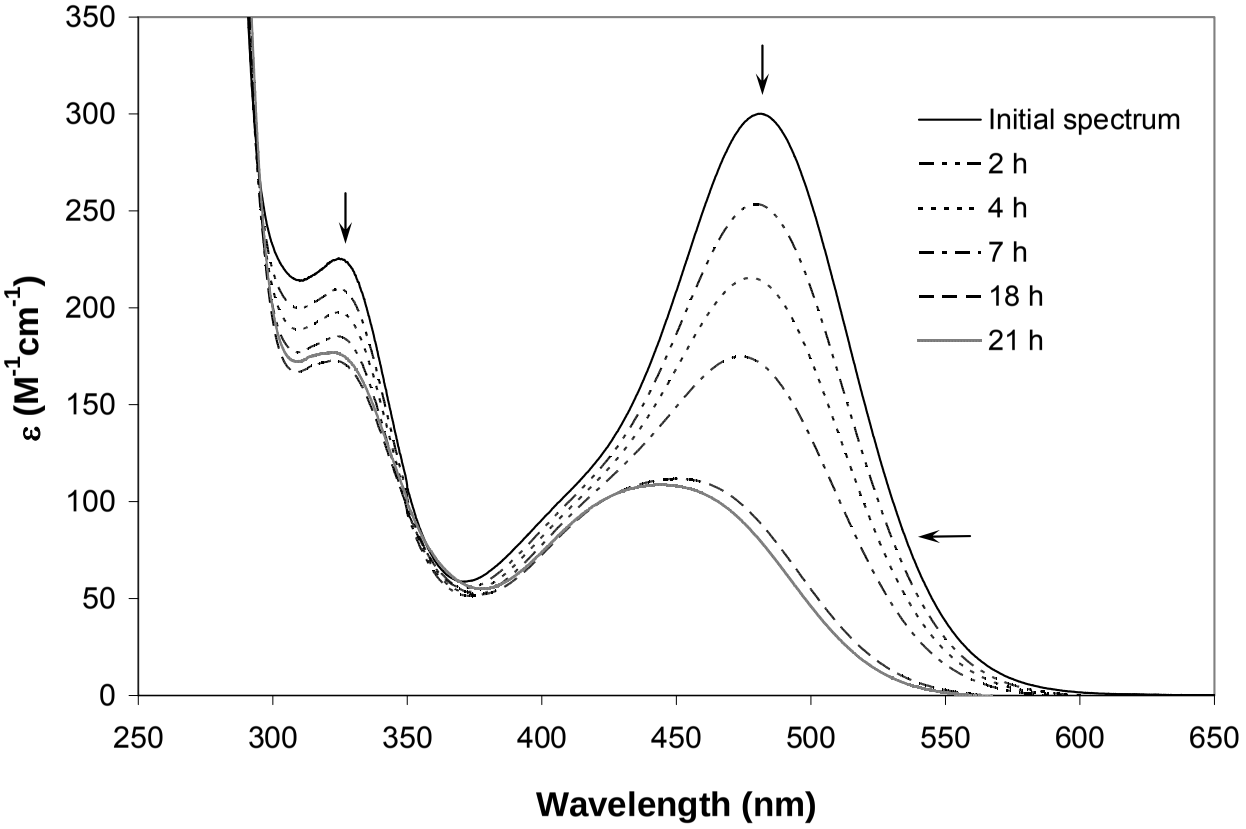
350
300
250
200
150
100
50
0
ε (M-1cm-1)
250
300
350
400
450
500
550
600
650
Wavelength (nm)
Initial spectrum
2 h
4 h
7 h
18 h
21 h

Photochemistry of dimethylsila[1]ferrocenophane

Figure 16 shows representative spectral changes during photolysis of $FcSiMe_2$ (Batch 6) in room-temperature methanol for the purpose of calculating ϕ_{dis}. During the time intervals of excitation with 488-nm light, a steady bleaching of the low-energy band (λ_{max} = 481 nm) of $FcSiMe_2$ is accompanied by a sharp absorbance increase in the ultraviolet region. Equation 12 was applied to determine that approximately 23% of the initial $FcSiMe_2$ reacted in 45 s, at which point the solution lost homogeneity and formed a brown precipitate. A quantum yield within experimental error of unity was determined for the 8.84 mM $FcSiMe_2$ solution in methanol, indicating that photoreaction occurs with very high efficiency. Removing O_2 from the methanol does not influence the efficiency of the photoreaction as indicated in Table 4. Figure 16 also shows an isosbestic point at 432 nm, indicating that secondary photolysis is negligible.

The photoreaction efficiency remains high when room-temperature solutions of $FcSiMe_2$ in methanol are irradiated at 436 nm into the high-energy tail of band 3a (Figure 12). However, the efficiency decreases by 50% upon irradiation near the middle of band 1a with 313-nm light (refer to Table 4). This observation indicates that the photoreaction is wavelength dependent. In earlier work, Tanabe, Vandermeulen et al. observed that irradiation into the lowest-energy absorption band of $FcSiMe_2$ is necessary for polymerization.[28]

Figure 17 shows spectral changes during photolysis of $FcSiMe_2$ (Batch 2a) in room-temperature and low-temperature acetonitrile for the purpose of calculating ϕ_{dis}.

Figure 16

UV-vis spectral changes arising from the 488-nm irradiation of 8.84 mM $FcSiMe_2$ in non-deaerated, room-temperature methanol. Spectra were acquired in a 1-cm pathlength quartz cell after 0, 15, 30, and 45 seconds of irradiation. The arrows indicate the direction of spectral changes as irradiation proceeds.

Wavelength (nm)
250
300
350
400
450
500
550
600
650
ε (M-1cm-1)
0
50
100
150
200
250
300
350

Table 4. Disappearance Quantum Yield (ϕ_{dis}) Data for $FcSiMe_2$

Solvent (# of Runs)[a]	λ_{excit} (nm)	ϕ_{dis}
Hexane (1)	488	$< 10^{-3}$
Methanol (3)	488	1.05 ± 0.11
Methanol (1)[b]	488	0.95
Methanol (3)	436	1.02 ± 0.03
Methanol (2)[c]	313	0.52 ± 0.08
Acetonitrile (4)	488	0.34 ± 0.03
Acetonitrile (3)[d]	488	0.58 ± 0.02
THF (1)	488	0.006

a. Temperature is 22 ± 2 °C, unless noted otherwise.
b. Purged with argon for 30 m prior to irradiation.
c. Fraction of light absorbed at 313 nm is approximate owing to competitive absorption by photoproduct(s).
d. Temperature is 4 ± 1 °C.

Figure 17

UV-vis spectral changes arising from the room- and low-temperature 488-nm irradiation of $FcSiMe_2$ in non-deaerated acetonitrile. Spectra were acquired in a 1-cm pathlength quartz cell initially and after 30 seconds of irradiation. After irradiation, the solution was filtered in a 25 mm syringe filter with a 0.2 μm polypropylene membrane. The arrows indicate the direction of spectral changes as irradiation proceeds.

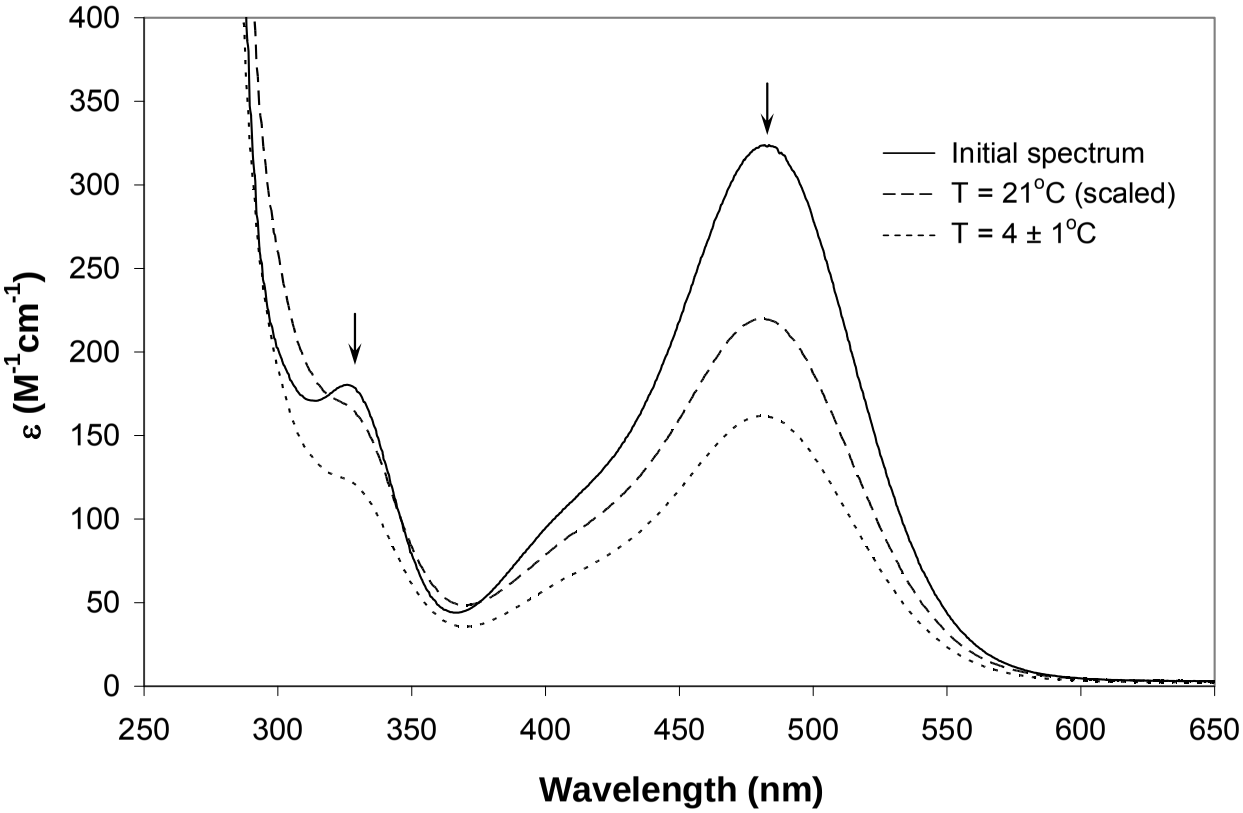
400
350
300
250
200
150
100
50
0
250
300
350
400
450
500
550
600
650
ε (M-1cm-1)
Wavelength (nm)
Initial spectrum
T = 21°C (scaled)
T = 4 ± 1°C

During excitation with 488-nm light in both experiments, an absorbance decrease of the low-energy band (λ_{max} = 481 nm) of $FcSiMe_2$ is accompanied by an absorbance decrease of the high-energy band (λ_{max} = 326 nm). For the low-temperature experiment, Equation 12 was applied to determine that approximately 55% of the initial $FcSiMe_2$ reacted in 30 s as the solution lost homogeneity and formed a brown precipitate. A quantum yield of 0.56 was determined for the 4.29 mM $FcSiMe_2$ solution in acetonitrile. For ease of comparison, the data for the room-temperature experiment were scaled from a different experiment to fit the low-temperature data in Figure 17. In that experiment, approximately 36% of the initial $FcSiMe_2$ reacted in 30 s as the solution lost homogeneity and formed a brown precipitate. A quantum yield of 0.36 was determined for the 4.05 mM $FcSiMe_2$ solution in acetonitrile.

Decreasing solution temperature increases the rate of photoreaction in acetonitrile by almost 71%. Tanabe, Vandermeulen, et al. studied the kinetics of the photocontrolled living ROP of $FcSiMe_2$ at various temperatures (5, 14, and 20^{o}C).[28] They found that the slope of the Penczek plot[56], which is proportional to propagation rate, decreases with increasing temperature. Also, polymerizations at higher temperatures (14 and 20^{o}C) gave slightly broader molecular-weight distributions (polydispersity index (PDI) = 1.2-1.3) compared to those at 5^{o}C (PDI < 1.1). Their explanation is that while photoactivation of the monomer (M in Equation 5) is independent of temperature, the deactivation of the photoexcited monomer (M* in Equation 5) to regenerate the ground state monomer (M) is more favored at higher temperatures.[28] Therefore, at higher temperatures, they would expect the equilibrium between M and M* to lie in favor of the ground-state monomer. This means that less

photoexcited monomer is available for photopolymerization to result in slower initiation, slower propagation, and polymers with a broader molecular-weight distribution. Our results offer quantitative support for this photophysical explanation.

Figure 18a shows spectral changes during photolysis of $FcSiMe_2$ (Batch 2a) in room-temperature THF. During excitation with 488-nm light, an absorbance decrease of the low-energy band (λ_{max} = 482 nm) is accompanied by a slight absorbance increase of the high-energy band (λ_{max} = 328 nm). Approximately 25% of the initial $FcSiMe_2$ reacted in 1320 s as the solution lost homogeneity and formed a brown precipitate. A quantum yield of 0.006 was determined for the 3.63 mM $FcSiMe_2$ solution in THF. Figure 18b shows spectral changes during photolysis of $FcSiMe_2$ (Batch 2a) in room-temperature hexane. During excitation with 488-nm light, no significant change occurs with the low-energy band (λ_{max} = 481 nm). However, the absorbance of the high-energy band (λ_{max} = 326 nm) slightly increases during the 5340 s of irradiation. The upper limit for the quantum yield for solutions of $FcSiMe_2$ in hexane was determined to be 10^{-3}. The ϕ_{dis} data in Table 4 show the solvent dependence of the photochemical process.

Photochemical mechanism of dimethylsila[1]ferrocenophane

As earlier discussed, Tanabe, Vandermeulen et al. observed that irradiation into the lowest-energy absorption band of $FcSiMe_2$ is necessary for polymerization.[28] This was rationalized by the theoretical work performed on [1]ferrocenophanes and by the experimental work performed on DFc.[18] Theoretical calculations on [1]ferrocenophanes showed that the increase in α of a [1]ferrocenophane is accompanied by weakening of the Fe-Cp bond.[19,20,21] Moreover, Mizuta, Imamura et al. reported that upon irradiation, ROP of phosphorus- bridged [1]ferrocenophanes in THF proceeds through Fe-Cp bond

Figure 18

(a) UV-vis spectral changes arising from the 488-nm irradiation of $FcSiMe_2$ in THF. Spectra were acquired in a 1-cm pathlength quartz cell initially and after 1320 seconds of irradiation. After irradiation, the solution was filtered in a 25 mm syringe filter with a 0.2 μm polypropylene membrane. The arrows indicate the direction of spectral changes as irradiation proceeds.

(b) UV-vis spectral changes arising from the 488-nm irradiation of $FcSiMe_2$ in hexane. Spectra were acquired in a 1-cm pathlength quartz cell initially and after 5340 seconds of irradiation. The arrow indicates the direction of spectral changes as irradiation proceeds.

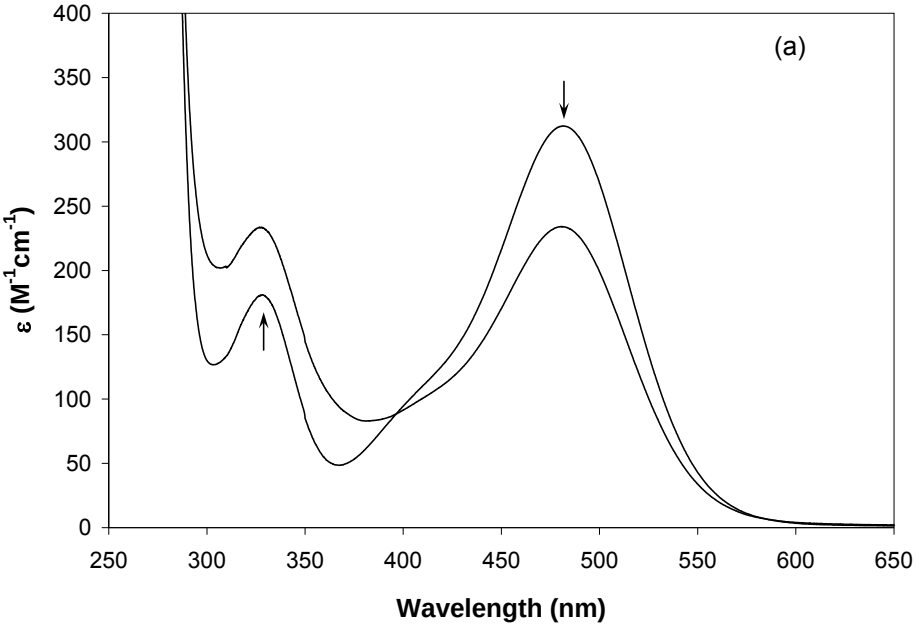
(a)
ε (M-1cm-1)
Wavelength (nm)
400
350
300
250
200
150
100
50
0
250
300
350
400
450
500
550
600
650

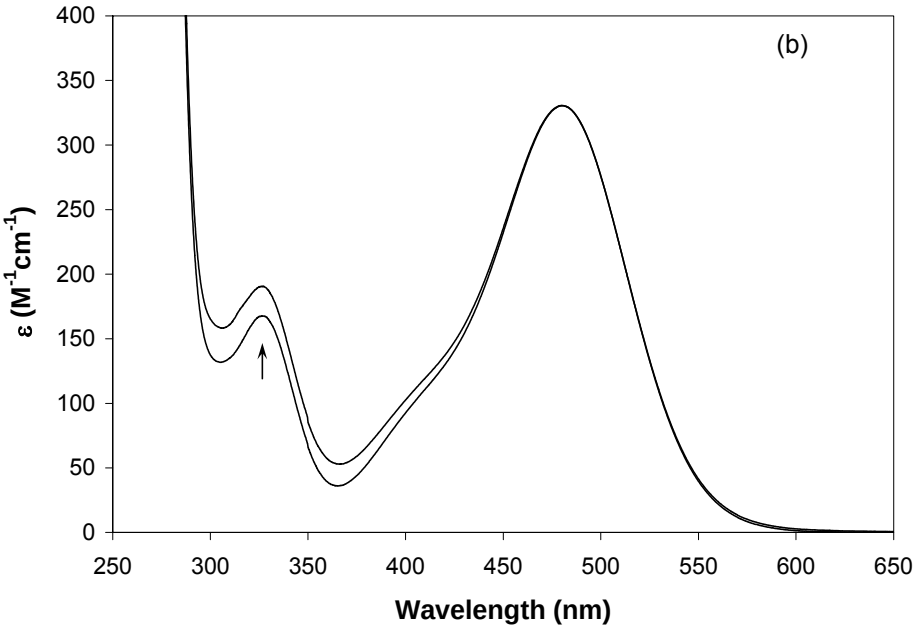
(b)
ε (M-1cm-1)
Wavelength (nm)
400
350
300
250
200
150
100
50
0
250
300
350
400
450
500
550
600
650

cleavage[57,58] (Equation 14). Therefore, we expect that photoexcitation of $FcSiMe_2$ is

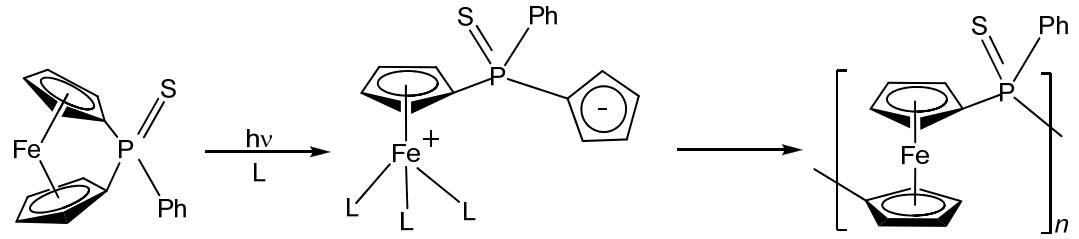

(14)

expected to selectively weaken the Fe-Cp bond, resulting in the attack of the iron center by solvent molecules, similar to what is observed upon irradiation of DFc in solution.

^{1}H NMR spectroscopy was employed to identify the products formed upon photolysis of $FcSiMe_2$ at 488 nm in methanol-d_4 and in acetonitrile-d_3. ^{1}H NMR data collected in this study along with those from other research groups are summarized in Table 5. As shown in the table, most of our band assignments agree with the data reported in the literature for the formation of tautomers of dimethylbis(cyclopentadienyl)silane, abbreviated in Table 5 and from now on as Me_2SiCp_2.

The ^{1}H NMR spectrum of 7.74 mM $FcSiMe_2$ (Batch 2a) in methanol-d_4 irradiated exhaustively at 488-nm is shown in Figure 19a. The initial $FcSiMe_2$ completely reacted to form photoproducts as a result of Fe-Cp bond cleavage that we estimate occurs at least 95% of the time. Within the time frame it took to prepare the irradiated sample for ^{1}H NMR analysis (approximately 2 h), the initial $FcSiMe_2$ in the thermal analogue reacted at least 40% to form the monosubstituted ferrocene derivative. In the filtered, irradiated sample, no production of the monosubstituted thermal product ensued via photochemically-induced bond breaking at the strained C-Si$(CH_3)_2$-C bridge. The ^{1}H

Table 5. Chemical shifts (ppm) in ^{1}H NMR spectra of Me_2SiCp_2

In CD_3OD (Me_2SiCp_2)[a]	In CD_3OD (Me_2SiCp_2)[b]	In CD_3CN (Me_2SiCp_2)[a]	(Me_2SiCp_2)[c]	(Me_2SiCp_2)[d]	Band Assignment[c, d]	Tautomers[c]
6.44-6.97	6.43-6.88	6.48-6.90	6.83	6.69		II-VI
			6.47	6.62	Unsaturated ring protons	I-III
			6.47	6.51		I-III
				6.46		
3.51		3.47	3.35	3.46	Saturated ring protons at the head of the bridge	I-III
3.41				3.37		
2.93-3.05	3.03	2.97-3.07	2.90	2.82-2.97	Saturated ring protons	II-VI
	2.93			2.27-2.39		
0.31- (-0.21)	0.31- (-0.21)	0.41	0.53	2.25		III-VI
		0.070-0.16	0.32	0.58	Methyl protons $Si(CH_3)_2$	II
		-0.22	0.25	0.45		III-VI
			-0.010	0.080 - (-0.047)		I

a. This study; excitation wavelength is 488 nm.

b. This study; excitation wavelength is 313 nm.

c. From Koepf and Klouras, Chimika Chromika, 1982, 11, 31-36.

d. From Cadenas et al., Revista de la Facultad de Ingenieria de la U.C.V., 2004, 19 (1), 79-88.

Figure 19

^{1}H NMR spectral changes resulting from (a) the 488-nm photolysis of 7.74 mM $FcSiMe_2$ in methanol-d_4 after exhaustive irradiation where * designates the residual protonated solvent resonances at 3.31 and 4.85 ppm; (b) the 313-nm photolysis of 8.36 mM $FcSiMe_2$ in methanol-d_4 after irradiation for 1.5 h; and (c) the photolysis of 11.34 mM $FcSiMe_2$ in acetonitrile-d_3 after irradiation for 3 h, where * designates the residual protonated solvent resonance at 1.94 ppm and ** designates HOD at 2.13 ppm. After irradiation, all solutions were filtered in a 25 mm syringe filter with a 0.2 μm polypropylene membrane.

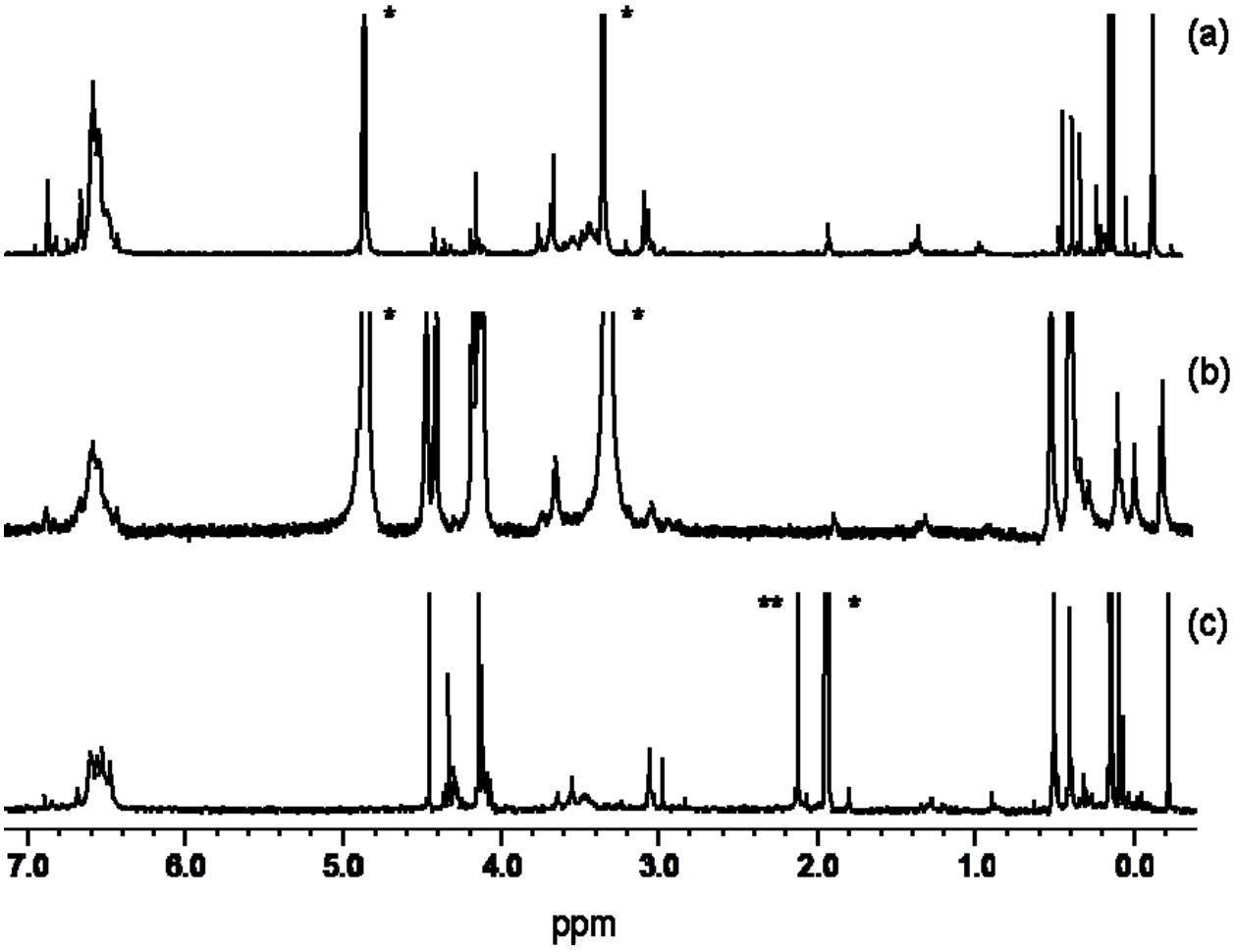
(a)
(b)
(c)
*
**
7.0
6.0
5.0
4.0
3.0
2.0
1.0
0.0
ppm

resonances that occur between 6.44 and 6.97 ppm indicate the presence of unsaturated ring protons.[59] A pair of new resonances at 3.51 and 3.40 ppm indicates the presence of saturated ring protons at the head of the bridge of the free ligand species, Me_2SiCp_2.[59,60] The ^1H resonances that occur between 2.93 and 3.05 ppm indicate the presence of saturated ring protons.[59] The $SiCH_3$ resonances in our work appear in the spectrum between -0.21 and 0.31 ppm and vary the most from the literature data. The tautomers of Me_2SiCp_2 that correspond to each band assignment are shown in Figure 20 and listed in Table 5.

The ^1H NMR spectrum of 8.36 mM $FcSiMe_2$ in methanol-d_4 irradiated at 313 nm is shown in Figure 19b. Approximately 80% of the initial $FcSiMe_2$ reacts in 1.5 h to form photoproducts. We cannot conclusively claim that the photoproducts result from Fe-Cp bond cleavage exclusively because of band broadening in the signal peaks that made it difficult to identify the products. The band broadening is most likely due to the presence of the monosubstituted derivative of ferrocene produced thermally. Most of the chemical shifts correlating to the free ligand species, Me_2SiCp_2, produced by Fe-Cp bond cleavage agree with the data obtained at 488 nm. This agreement, along with the UV-vis spectral agreement, verifies that irradiation of $FcSiMe_2$ solutions in methanol at 488 and 313 nm follow the same photochemical pathway.

The ^1H NMR spectrum of 11.34 mM $FcSiMe_2$ in acetonitrile-d_3 irradiated at 488 nm is shown in Figure 19c. Approximately 78% of the initial $FcSiMe_2$ reacts in 3 h to form photoproducts. The photoproducts result from Fe-Cp bond cleavage rather than *ipso*-Cp-Si bond breaking because there is no conclusive indication of the formation of a monosubstituted derivative of ferrocene. Most of the chemical shifts correlating to the

Figure 20

The six possible tautomers of the free species, Me_2SiCp_2, generated photochemically in solution via Fe-Cp bond cleavage of $FcSiMe_2$. Reproduced from Ref. (59). Copyright 1982 Chimika Chromika.

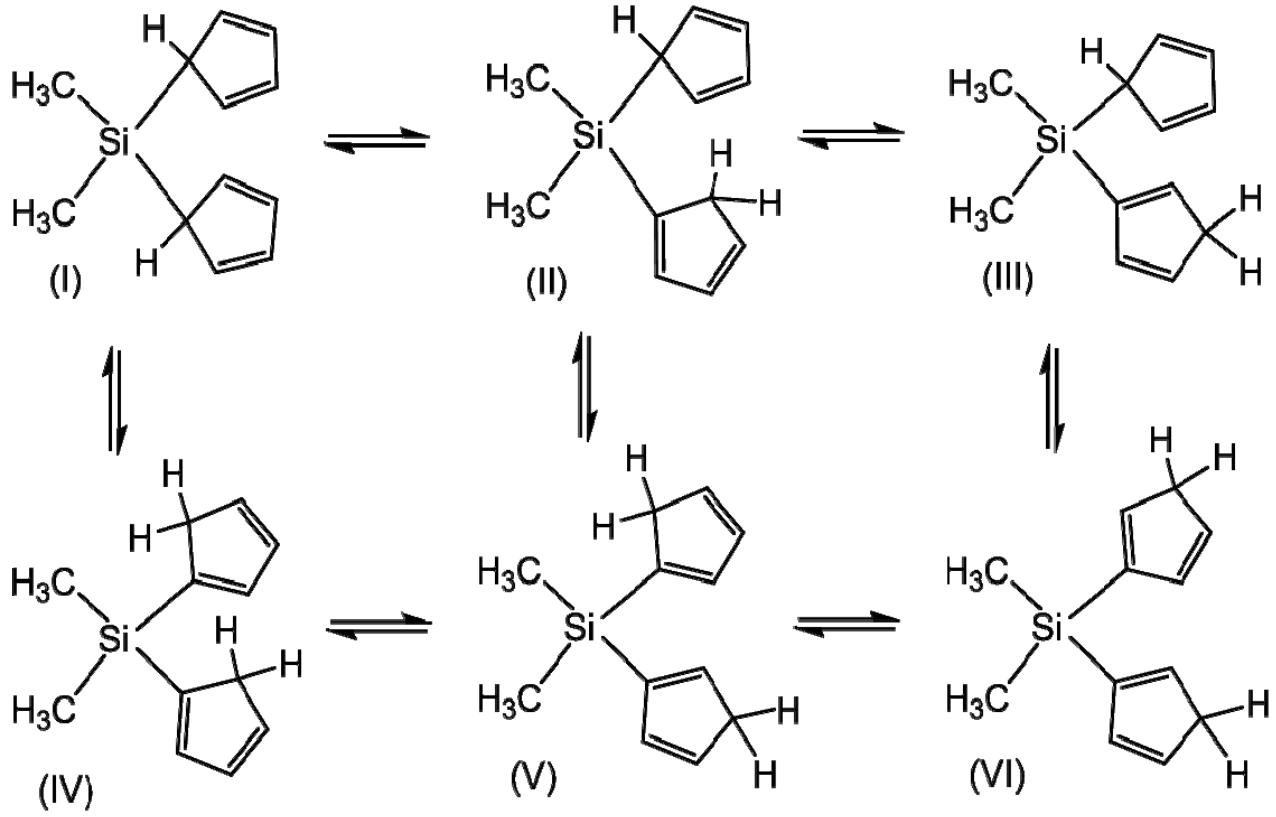
H
H3C
Si
H3C
H
(I)
(II)
(III)
(IV)
(V)
(VI)

free ligand species, Me_2SiCp_2, produced by Fe-Cp bond cleavage agree with the literature data in Table 5. With this collection of ^1H NMR evidence, we conclude that irradiation of $FcSiMe_2$ in solution generates photoproducts mainly via Fe-Cp bond cleavage as depicted in Equation 15. We propose that during irradiation, the Fe-Cp

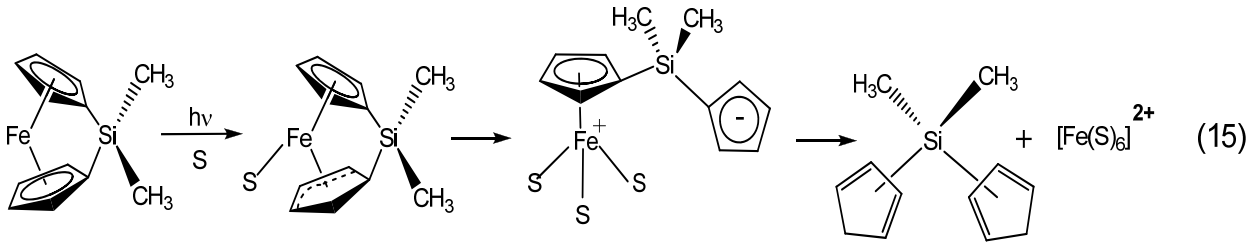

(15)

bond in the strained molecule weakens. This allows solvent to coordinate to the metal center to first form the η^5, η^3 ring-slipped intermediate that later yields the silyl-substituted, dangling cyclopentadienide anion and finally the free ligand product detected by proton NMR.

CHAPTER 5

SPECTROSCOPY AND PHOTOCHEMISTRY OF DIPHENYLSILA[1]FERROCENOPHANE

Electronic Structure

To examine the effect of varying the substituents on the bridging silicon atom on the excited state behavior of [1]ferrocenophanes, we expanded the study to diphenylsila[1]ferrocenophane ($FcSiPh_2$). This compound has been previously characterized by X-ray crystallography.[61] The molecular structure of $FcSiPh_2$ is comparable to that of $FcSiMe_2$. The tilt angle, α, between the Cp ligands in $FcSiPh_2$ is 19.1^o, which is slightly less than the corresponding value in $FcSiMe_2$.[51] A smaller deviation of δ (refer to Figure 11) from 180^o exists in $FcSiPh_2$, where the value is 167.3^o compared to 164.74^o in $FcSiMe_2$.[51] Less distortion in $FcSiPh_2$ is also apparent in the angle θ, where the value is 99.2^o compared to 95.7^o in $FcSiMe_2$.[51] In contrast, the value for β in $FcSiPh_2$ (40.0^o) is significantly more than that in $FcSiMe_2$ (37.0^o).[51] The effects of these distortions appear in the electronic absorption spectrum of $FcSiPh_2$ (Figure 21). Compared to Fc, band 3a in the absorption spectrum is more intense and shifted to longer wavelengths while band 1a is more intense but is obscured by the absorption of the phenyl groups. Applying the same analysis from Figure 13 used earlier for $FcSiMe_2$, the energy difference between the HOMOs and the LUMOs decreases significantly as α

Figure 21

Electronic absorption spectrum of Fc and $FcSiPh_2$ in room-temperature methanol.

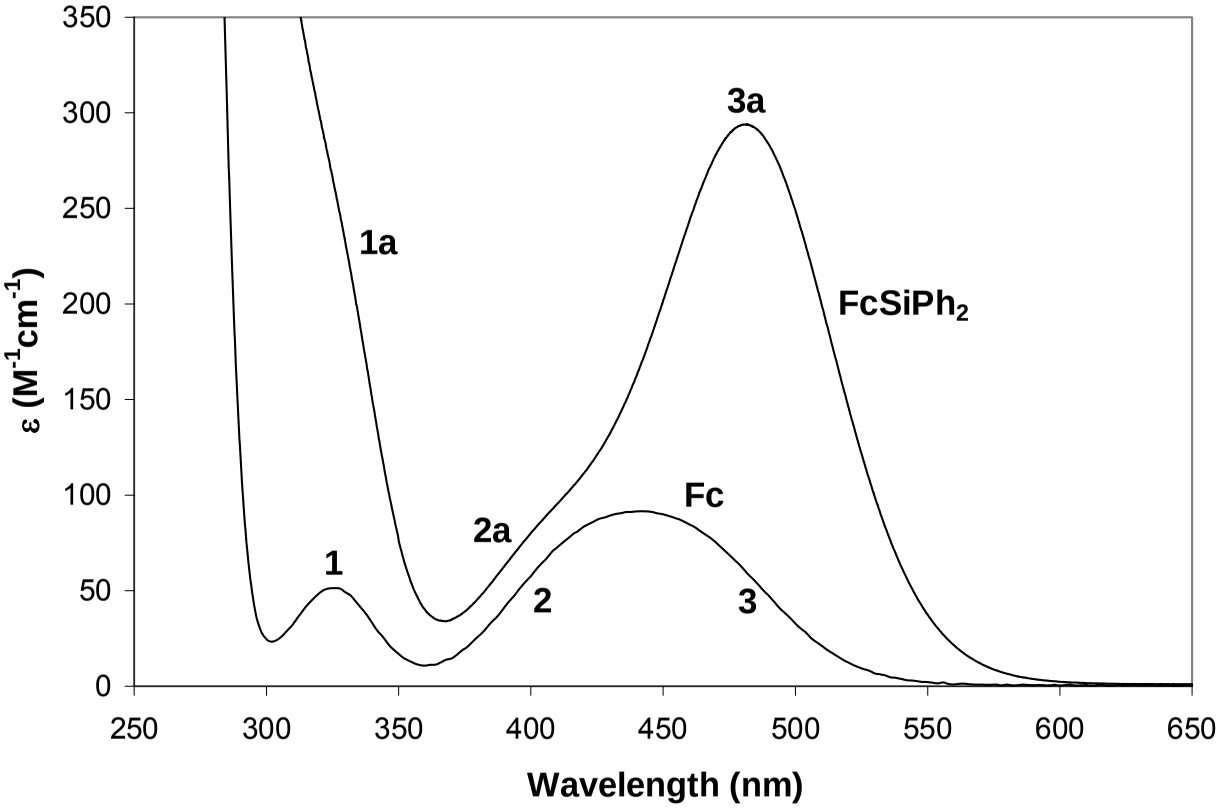
350
300
250
200
150
100
50
0
ε (M-1cm-1)
250
300
350
400
450
500
550
600
650
Wavelength (nm)
1a
3a
FcSiPh2
2a
Fc
1
2
3

increases. This reduction in energy difference causes band 3 of Fc to shift to longer wavelengths in [1]ferrocenophanes, while the lowered symmetry relaxes the Laporte rule forbidding ligand field transitions, resulting in the intensification of bands 1 and 3.[21]

To determine if increasing α introduces a degree of MLCT character into the low-energy excited states of $FcSiPh_2$, we recorded electronic absorption spectra of $FcSiPh_2$ in different solvents. Table 6 shows that the wavelength maxima (λ_{max}) for neither band 1a (in Figure 21) nor band 3a (in Figure 21) shift when the solvent polarity is varied. Therefore, we can conclude that the tilting inherent in $FcSiPh_2$ does not produce significant MLCT in the low-energy excited states of $FcSiPh_2$ and that the distortions in the complex are mainly responsible for the behavior observed in the absorption spectrum.

Thermal chemistry of diphenylsila[1]ferrocenophane

Fischer, Kinney et al. monitored the room-temperature thermal reactions of $FcSiMe_2$ and $FcSiPh_2$ in deuterated methanol with ^1H NMR and UV-vis absorption techniques.[53] Unlike $FcSiMe_2$, where reaction occurs as indicated in Equation 13, these workers reported that $FcSiPh_2$ appeared to be thermally inert. We monitored the progress of the thermal reaction of $FcSiPh_2$ in methanol-d_4 with ^1H NMR over a period of approximately 24 days. Since $FcSiPh_2$ is only slightly soluble in methanol, sonication was used to dissolve the compound. Table 7 summarizes the initial and final ^1H NMR data for the reaction. The ^1H NMR spectral changes in methanol-d_4 reveal that the reaction occurs thermally according to Equation 16. At the time the final ^1H NMR data

Table 6. Electronic Absorption Spectral Data for $FcSiPh_2$[a]

	λ_{max}, nm (ε, $M^{-1}cm^{-1}$)[b]	
Solvent (ε_r, DN^N)[c]	**Band 1a**	**Band 3a**
Hexane (1.9, 0)	308 (shoulder) (337)	481 (292)
Benzene (2.3, < 0.01)	315 (shoulder) (409)	482 (311)
THF (7.6, 0.52)	(shoulder)	482 (301)
Methanol (32.7, 0.77)	(shoulder)	482 (294)
Acetonitrile (35.9, 0.36)	(shoulder)	481 (306)

a. Data recorded at room temperature.

b. ε is extinction coefficient.

c. ε_r is dielectric constant; DN^N is normalized donor number; From Adams, et al., Chemistry in Alternative Reaction Media, 2004, 17.

Table 7. Thermal ^{1}H NMR Spectral Data for $FcSiPh_2$ in CD_3OD[a]

^{1}H NMR[b, c]	
Initial	**Later[d]**
7.92 (m, 4)	7.93 (m, 4)
	7.65 (m, 4)
7.46 (m, 6)	7.46 - 7.47 (m, 6)
	7.41 - 7.44 (m, 6)
4.56 (t, 4)	4.57 (t, 4)
	4.46 (t, 2)
	4.19 (t, 2)
4.11 (t, 4)	4.12 (t, 4)
	4.04 (s, 4)

a. Performed under Ar at 25 ± 0.5 °C.
b. ^{1}H NMR are δ ppm units relative to solvent.
c. In parentheses, s = singlet; t = triplet; m = multiplet and numbers are the relative integrations.
d. After approximately 24 days.

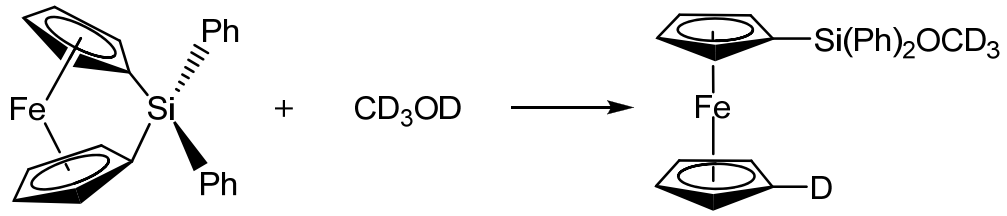

(16)

had been recorded for the thermal reaction, 50% of the initial $FcSiPh_2$ had reacted to form a product similar to the one observed in Equation 13. Most of the data in this study agree with the data reported in Chapter 4 that support attack of the –OD group on the strained C-$Si(Ph)_2$-C bridge to yield a simple, monosubstituted derivative of ferrocene, albeit at a much longer time period. In Figure 22, the later spectral data reveal the formation of three new resonances at 4.46, 4.19, and 4.04 ppm corresponding to Cp ring protons on the ring-opened product. Also in the later spectrum, a range of new resonances between 7.41 and 7.44 ppm and a new resonance at 7.65 ppm suggest the presence of phenyl ring protons on the ring-opened product. New resonances at 7.38, 7.40, and 7.45 ppm are unaccounted for.

Figure 23 shows the changes in the electronic absorption spectrum that occur over 7 days when $FcSiPh_2$ reacts thermally with methanol at room temperature. As time progresses, the lowest-energy band loses intensity and shifts to higher energy, which indicates the formation of the monosubstituted ferrocene, [Fe(η^5-C_5H_4D)(η^5-$C_5H_4Si(OCD_3)(Ph_2)$]. As previously discussed, the lowest-energy visible absorption band of $FcSiPh_2$ is redshifted compared to that of Fc. Upon hydrolysis with methanol, the absorption maximum of the lowest-energy band begins to shift to higher energy. The redshifted absorption maximum in $FcSiPh_2$ compared to Fc is thus due to the fact that

Figure 22

(a) Initial ^{1}H NMR spectrum of a saturated solution of $FcSiPh_2$ in CD_3OD. The * designates the residual protonated solvent resonance at 4.85 ppm.

(b) Later ^{1}H NMR spectrum resulting from the thermal reaction of a saturated solution of $FcSiPh_2$ in CD_3OD. The * designates the residual protonated solvent resonance at 4.85 ppm.

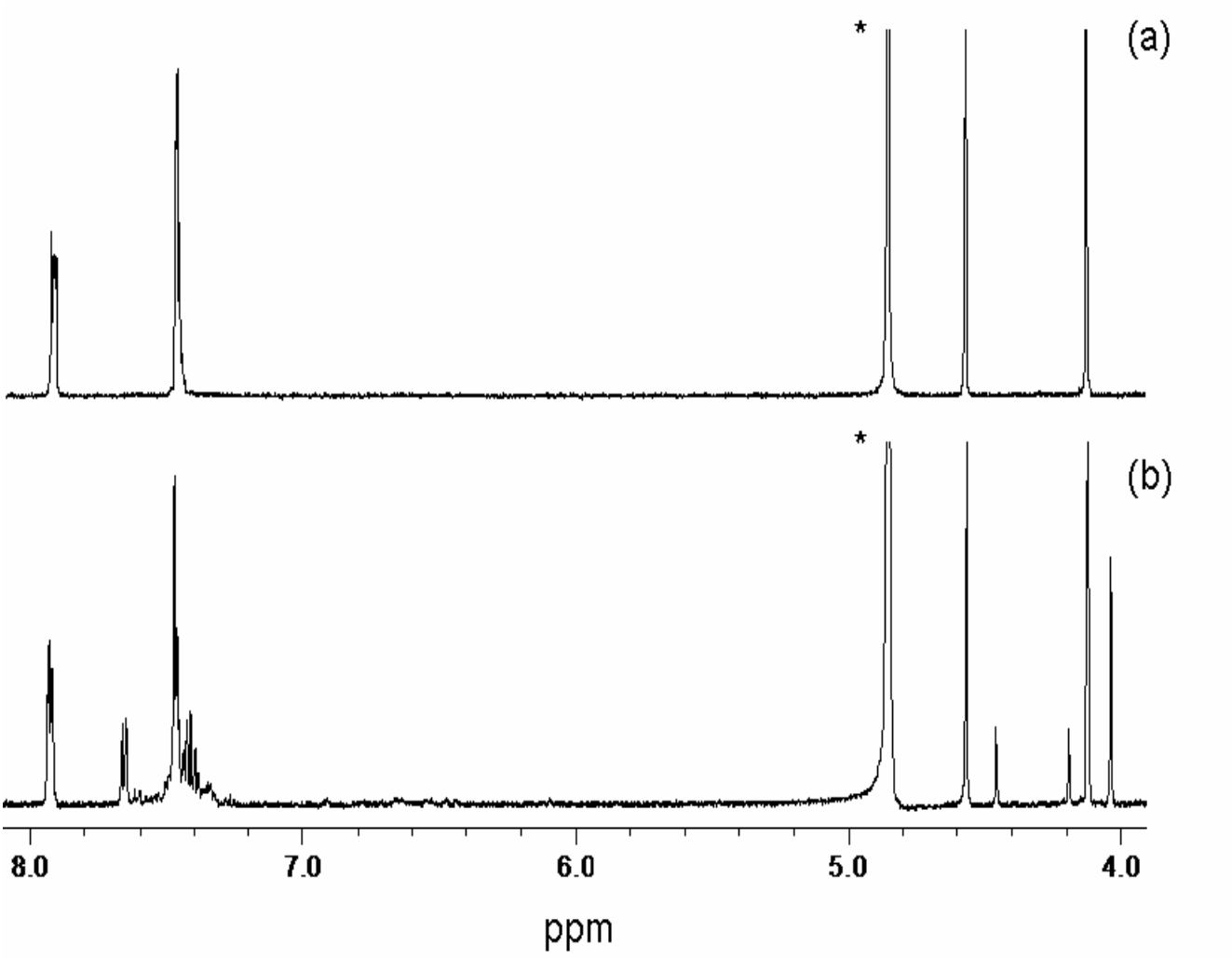
*
(a)
*
(b)
8.0
7.0
6.0
5.0
4.0
ppm

Figure 23

UV-vis spectral changes arising from the thermal reaction of 655 μM $FcSiPh_2$ in room-temperature methanol. The arrows indicate the direction of spectral changes as the reaction proceeds thermally.

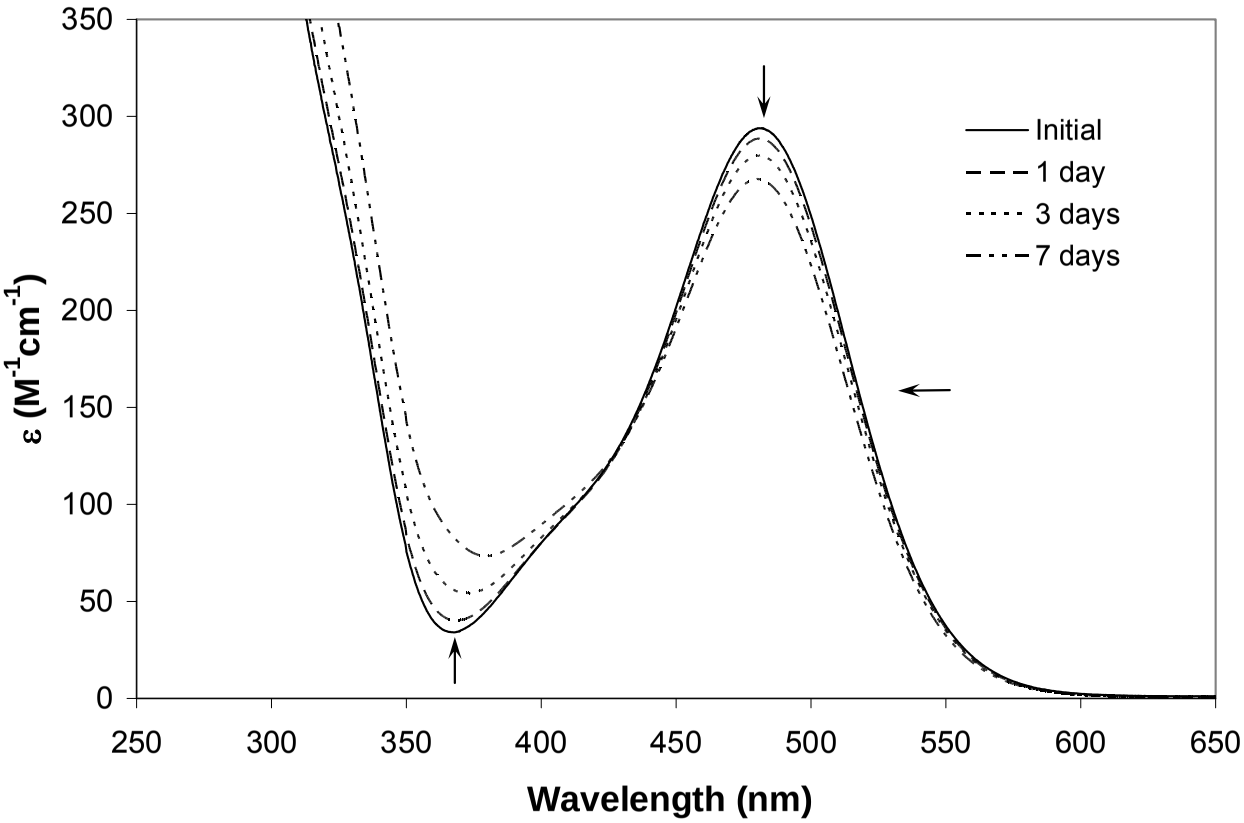
350
300
250
200
150
100
50
0
ε (M-1cm-1)
250
300
350
400
450
500
550
600
650
Wavelength (nm)
Initial
1 day
3 days
7 days

the Cp rings are not parallel owing to the bridging $SiPh_2$ group.[54,55] Both the starting compound and the monosubstituted derivative of ferrocene were detected by Fourier transform mass spectrometry (FT-MS). Figure 24 shows a portion of the mass spectrum of the 655 μM $FcSiPh_2$ solution in methanol after 7 days of reaction. The spectrum shows one signal for $FcSiPh_2$ at m/z = 366.0512 (theoretical monoisotopic mass = 366.0527) and one signal for $[Fe(\eta^5\text{-}C_5H_5)(\eta^5\text{-}C_5H_4Si(OCH_3)(Ph_2)]$ at m/z = 398.0780 (theoretical monoisotopic mass = 398.0789).

$FcSiPh_2$, unlike its dimethyl counterpart, is air and moisture stable. It is soluble in toluene, benzene, THF, and common chlorinated organic solvents. It is only slightly soluble in methanol, acetonitrile, and hexane. Whereas the compound is thermally stable in solutions of methanol, benzene, and hexane, it gradually decomposes in acetonitrile and THF. Figure 25 shows this thermal behavior in acetonitrile and THF. In both cases, the absorbance of the highest-energy band increases over time. Ultimately, a precipitate forms as the decomposition product falls out of solution. A proton NMR spectrum of a filtered acetonitrile solution showed only weak, obscure peaks.

Photochemistry of diphenylsila[1]ferrocenophane

Figure 26a shows representative spectral changes during 488-nm photolysis of $FcSiPh_2$ in room-temperature methanol for the purpose of calculating ϕ_{dis}. During the time intervals of excitation with 488-nm light, a steady bleaching of the low-energy band (λ_{max} = 481 nm) of $FcSiPh_2$ is accompanied by a sharp absorbance increase in the ultraviolet region. Equation 12 was applied to determine that approximately 35% of the initial $FcSiPh_2$ reacted in 80 s. As presented in Table 8, a quantum yield of 0.85 was determined for the 704 μM $FcSiPh_2$ solution in methanol, indicating that photoreaction

Figure 24

A portion of the mass spectrum of a solution of $FcSiPh_2$ and the monosubstituted ferrocene, $[Fe(\eta^5\text{-}C_5H_5)(\eta^5\text{-}C_5H_4Si(OCH_3)(Ph_2)]$, in room-temperature methanol.

Relative Intensity
0.000
0.002
0.004
0.006
0.008
0.010
0.012
360
380
400
m/z
FcSiPh2
366.0512
[Fe(η5-C5H5)(η5-C5H4Si(OCH3)(Ph2)]
398.0780

Figure 25

UV-vis spectral changes arising from the thermal reaction of (a) 3.00 mM $FcSiPh_2$ in room-temperature, spectral grade acetonitrile and (b) 4.48 mM $FcSiPh_2$ in room-temperature THF. The arrows indicate the direction of spectral changes as the reaction proceeds thermally.

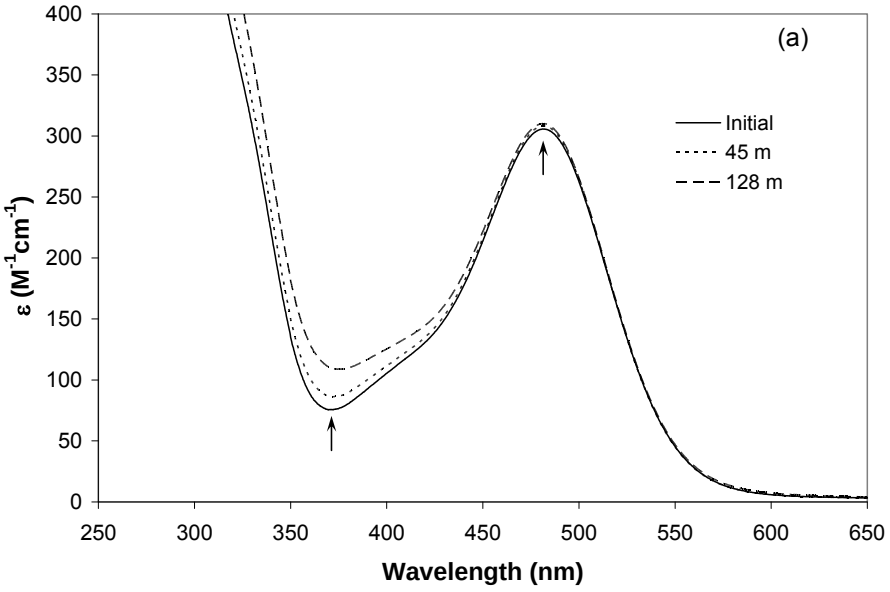
(a)
Initial
45 m
128 m
ε (M-1cm-1)
Wavelength (nm)
400
350
300
250
200
150
100
50
0
250
300
350
400
450
500
550
600
650

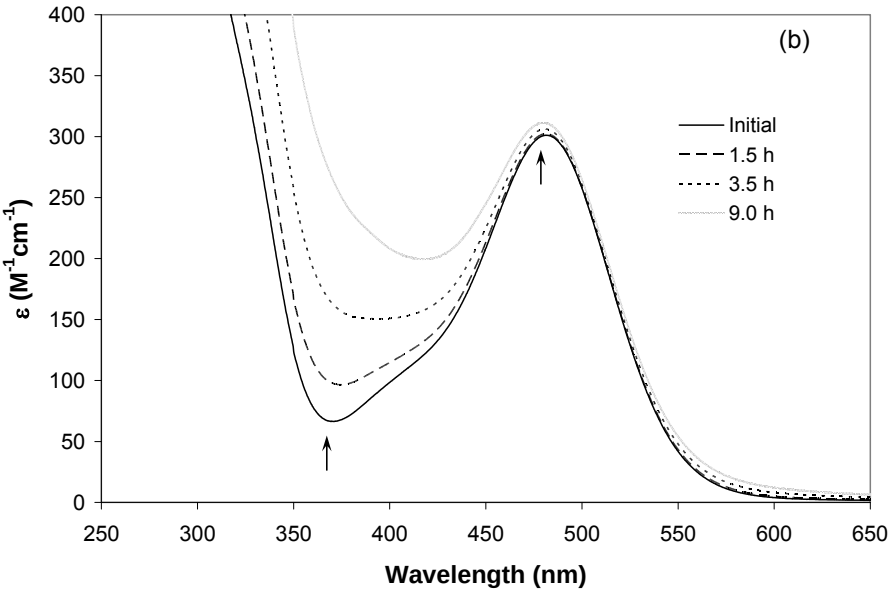
(b)
Initial
1.5 h
3.5 h
9.0 h
ε (M-1cm-1)
Wavelength (nm)
400
350
300
250
200
150
100
50
0
250
300
350
400
450
500
550
600
650

Figure 26

(a) UV-vis spectral changes arising from the 488-nm irradiation of 704 μM $FcSiPh_2$ in non-deaerated room-temperature methanol. Spectra were acquired in a 10-cm pathlength quartz cell after 0, 20, 40, 60, and 80 seconds of irradiation. The arrows indicate the direction of spectral changes as irradiation proceeds.

(b) UV-vis spectral changes arising from the 313-nm irradiation of 360 μM $FcSiPh_2$ in non-deaerated room-temperature methanol. Spectra were acquired in a 10-cm pathlength quartz cell after 0, 270, and 540 seconds of irradiation. The arrows indicate the direction of spectral changes as irradiation proceeds.

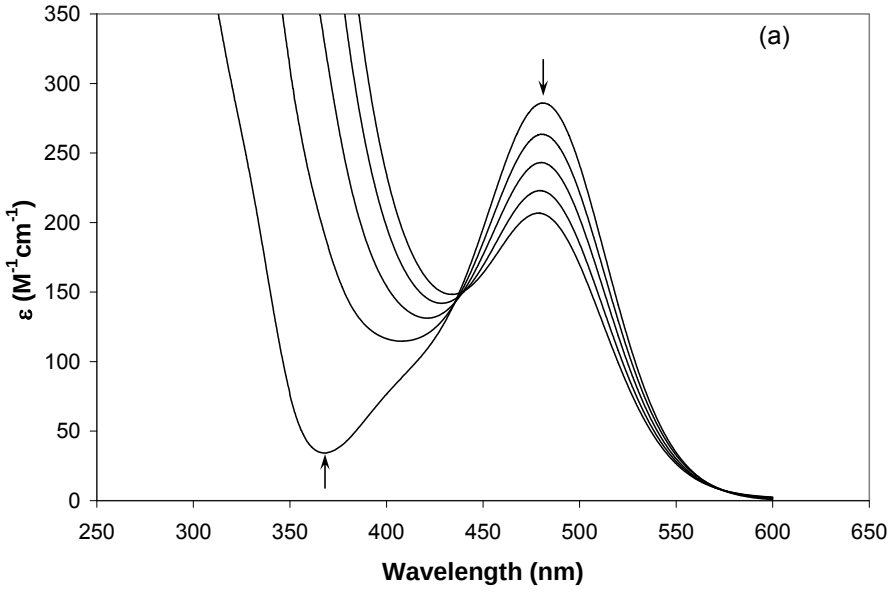
(a)
ε (M-1cm-1)
Wavelength (nm)
0
50
100
150
200
250
300
350
250
300
350
400
450
500
550
600
650

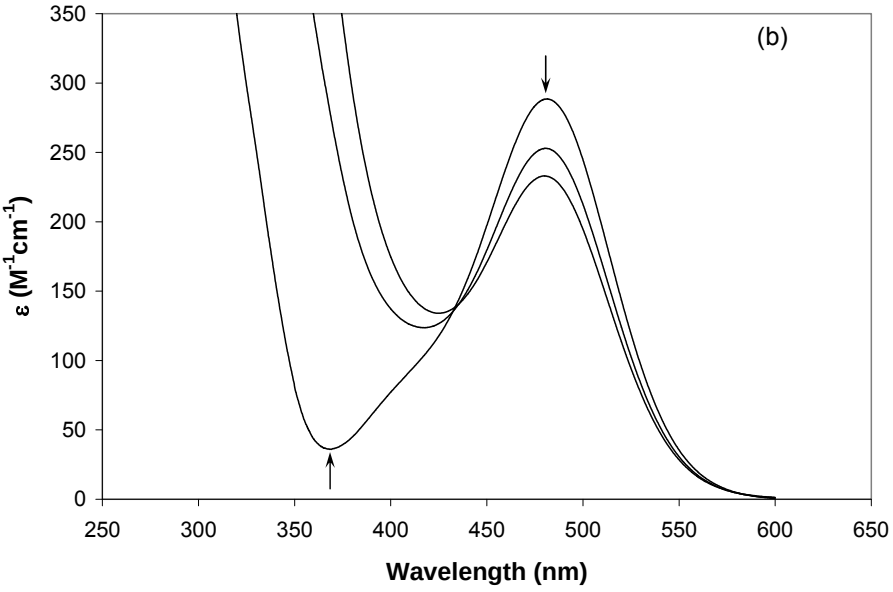
(b)
ε (M-1cm-1)
Wavelength (nm)
0
50
100
150
200
250
300
350
250
300
350
400
450
500
550
600
650

Table 8. Disappearance Quantum Yield (ϕ_{dis}) Data for $FcSiPh_2$

Solvent (# of Runs)[a]	λ_{excit} (nm)	ϕ_{dis}
Hexane (1)	488	$< 10^{-2}$
Benzene (1)	488	$< 10^{-2}$
Methanol (4)	488	0.86 ± 0.02
Methanol (3)[b]	313	0.54 ± 0.02
THF (3)	488	0.03 ± 0.01
THF (2)[c]	488	0.26 ± 0.01

a. Temperature is 23 ± 1 °C, unless noted otherwise.
b. Fraction of light absorbed at 313 nm is approximate owing to competitive absorption by photoproduct(s).
c. Temperature is 4 ± 1 °C.

occurs with very high efficiency. Figure 26a also shows an isosbestic point at 437 nm, indicating that secondary photolysis is negligible. The spectral changes that occur during photolysis in this system are similar to those observed during the photolysis of solutions of $FcSiMe_2$ in methanol.

Figure 26b shows representative spectral changes during 313-nm photolysis of $FcSiPh_2$ in room-temperature methanol. Due to competing absorption by the photoproducts with the starting material at λ_{excit} = 313 nm, the fraction of light absorbed by the starting material was calculated by the method described previously in Chapter 2. Then Equation 12 was applied to determine that approximately 24% of the initial $FcSiPh_2$ reacted in 540 s. Compared to 488-nm irradiation, 313-nm irradiation near the middle of band 1a results in a 37% decline of ϕ_{dis} (refer to Table 8). This result supports the earlier discussion in Chapter 4 that the photoreaction is wavelength dependent.

Figure 27 shows spectral changes during photolysis of $FcSiPh_2$ in room-temperature and low-temperature THF for the purpose of calculating ϕ_{dis}. During excitation with 488-nm light in both experiments, the absorbance of the low-energy band (λ_{max} = 481 nm) of $FcSiPh_2$ decreases. For the low-temperature experiment, approximately 79% of the initial $FcSiPh_2$ reacted in 120 s as the solution lost homogeneity and formed a precipitate. A quantum yield of 0.25 was determined for the 3.71 mM $FcSiPh_2$ solution in THF. The data for the room-temperature experiment was scaled from a different experiment to fit the low-temperature data in Figure 27. In that experiment, approximately 64% of the initial $FcSiPh_2$ reacted in 600 s as the solution lost homogeneity and formed a precipitate. A quantum yield of 0.034 was determined for the 3.88 mM $FcSiPh_2$ solution in THF.

Figure 27

UV-vis spectral changes arising from the room- and low-temperature 488-nm irradiation of $FcSiPh_2$ in THF. Spectra were acquired in a 1-cm pathlength quartz cell. After irradiation, the solution was filtered in a 25 mm syringe filter with a 0.2 μm polypropylene membrane. The arrows indicate the direction of spectral changes as irradiation proceeds.

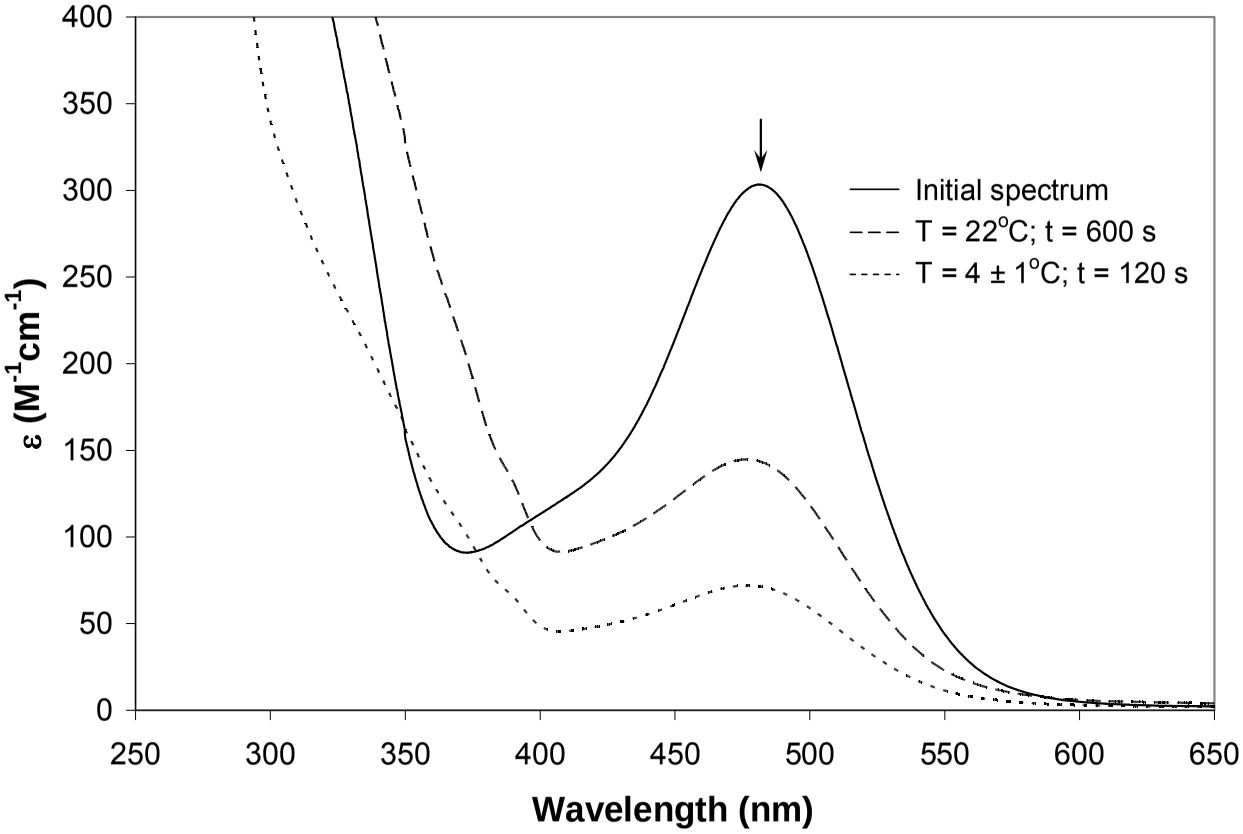
400
350
300
250
200
150
100
50
0
ε (M-1cm-1)
250
300
350
400
450
500
550
600
650
Wavelength (nm)
Initial spectrum
T = 22°C; t = 600 s
T = 4 ± 1°C; t = 120 s

Compared to room-temperature 488-nm irradiation, low-temperature 488-nm irradiation of $FcSiPh_2$ solutions in THF results in an impressive 767% rise of ϕ_{dis} (refer to Table 8). These observations lend support to the temperature-dependent studies discussed in Chapter 4. This study is also consistent with the work reported by Ieong, Chan et al. that a combination of low temperature (5°C) and UV light are required to achieve high reaction conversions of $FcSiPh_2$ with $[Fe(CO)_5]$ or $[Co_2(CO)_8]$ in THF.[31] In benzene and hexane, $FcSiPh_2$ is essentially photoinert. If it is assumed that 3% reaction is the minimum that can be detected experimentally upon irradiation of $FcSiPh_2$ in these solvents, then ϕ_{dis} would be $< 10^{-2}$. Over time, as solutions of $FcSiPh_2$ in these solvents undergo photolysis at 488 nm, the absorbance of the highest-energy band increases slightly, while the lowest-energy band remains stable. The ϕ_{dis} data in Table 8 show the solvent dependence of the photochemical process.

Photochemical mechanism of diphenylsila[1]ferrocenophane

^1H NMR spectroscopy and FT-MS were employed to identify the products formed upon photolysis of $FcSiPh_2$ in benzene-d_6, methanol-d_4, and acetonitrile-d_3. The ^1H NMR spectra of 7.58 mM $FcSiPh_2$ in benzene-d_6 irradiated for 0 and 2 h at 488-nm are shown in Figure 28. After 2 h of irradiation, no spectral differences were recorded. Thus, no decomposition of the initial compound took place, and we conclude that $FcSiPh_2$ is photoinert in benzene.

The ^1H NMR spectrum of a saturated solution of $FcSiPh_2$ in methanol-d_4 irradiated for 30 m at 488 nm is shown in Figure 29a. The initial $FcSiPh_2$ completely reacted to form photoproducts attributed to Fe-Cp bond cleavage that we estimate occurs at least 95% of the time. No evidence of either the starting compound or the

Figure 28

(a) Initial ^{1}H NMR spectrum of 7.58 mM $FcSiPh_2$ in C_6D_6. The * designates the residual protonated solvent resonance at 7.16 ppm. The ** designates the chemical shift of HOD at 0.38 ppm.

(b) ^{1}H NMR spectrum resulting from the 488-nm irradiation of 7.58 mM $FcSiPh_2$ in C_6D_6 for 2 h.

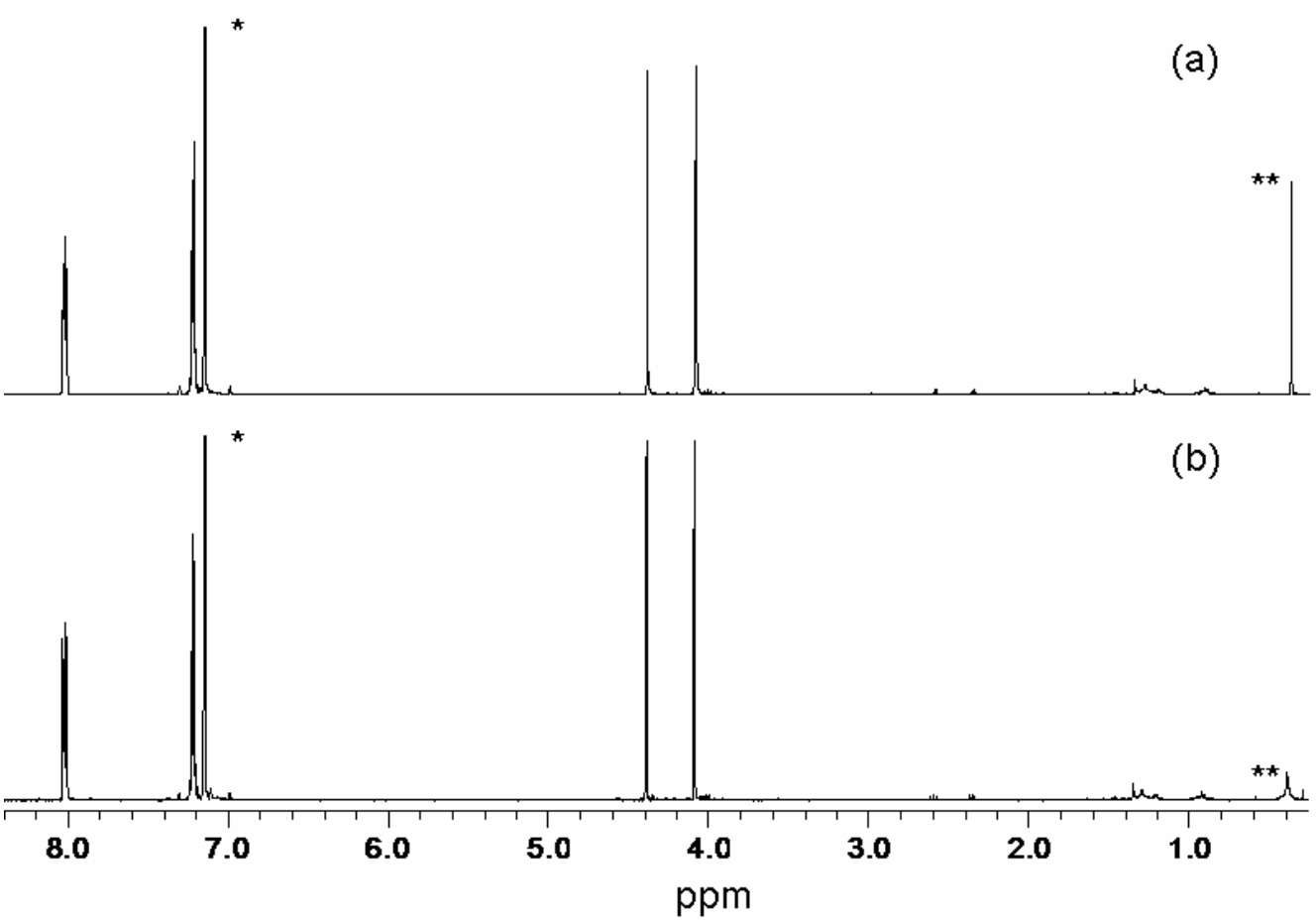
*
(a)
**
*
(b)
**
8.0
7.0
6.0
5.0
4.0
3.0
2.0
1.0
ppm

Figure 29

^{1}H NMR spectral changes resulting from (a) the 488-nm photolysis of ≤ 5.62 mM $FcSiPh_2$ in methanol-d_4 after irradiation for 30 m, where * designates the residual protonated solvent resonances at 3.31 and 4.85 ppm; (b) the 313-nm photolysis of 2.73 mM $FcSiPh_2$ in methanol-d_4 after irradiation for 2 h, where ^ designates TMS; and (c) the photolysis of 5.62 mM $FcSiPh_2$ in acetonitrile-d_3 after irradiation for 60 m, where * designates the residual protonated solvent resonance at 1.94 ppm and ** designates HOD at 2.13 ppm. After irradiation, all solutions were filtered in a 25 mm syringe filter with a 0.2 μm polypropylene membrane.

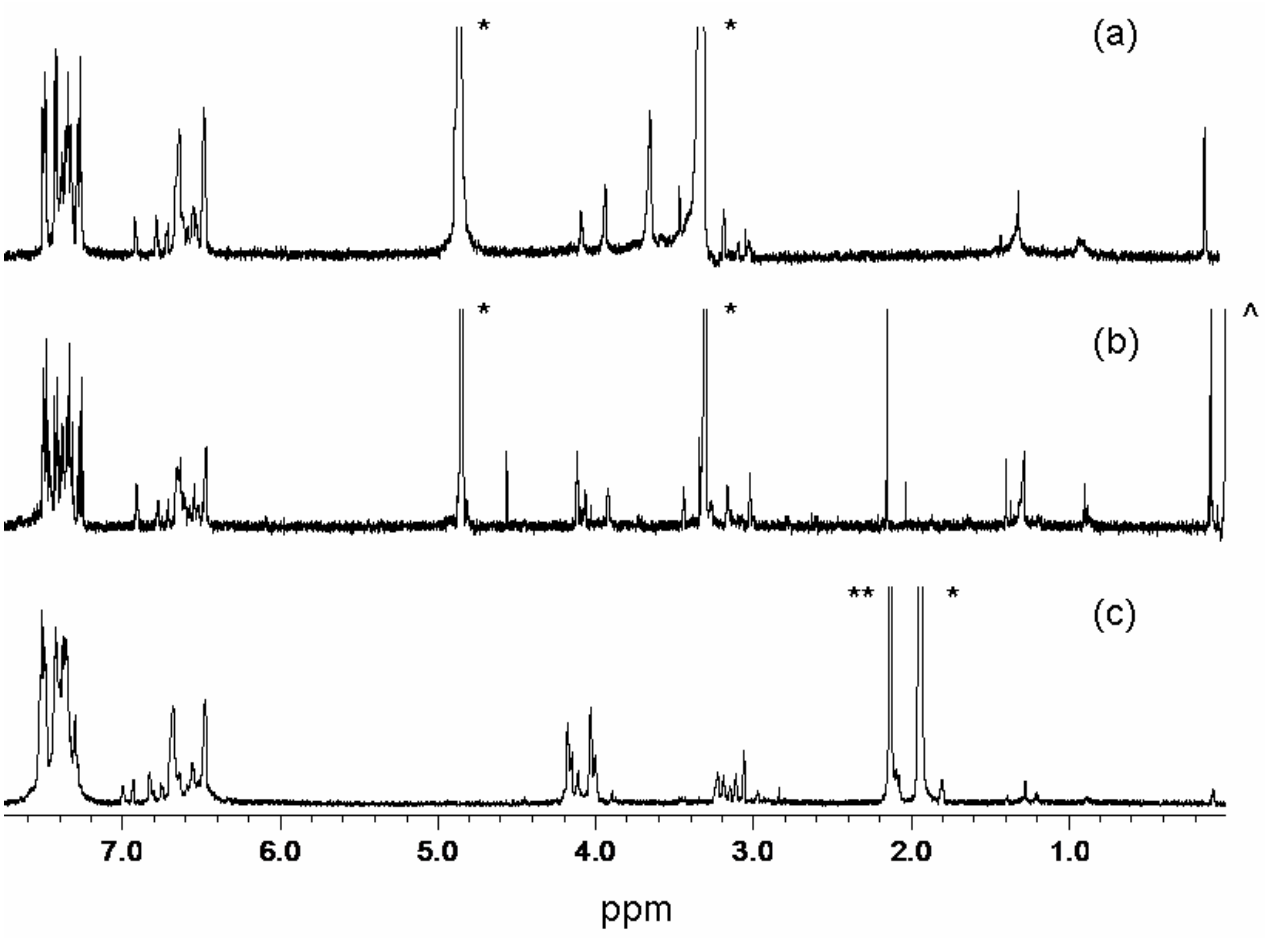
(a)
(b)
(c)
*
*
*
*
**
*
^
7.0
6.0
5.0
4.0
3.0
2.0
1.0
ppm

thermal, monosubstituted product (refer to Equation 16) is present. In the filtered, irradiated sample, the ^{1}H resonances that occur between 6.48 and 6.91 ppm indicate the presence of unsaturated Cp ring protons.[59] A range of new resonances between 7.25 and 7.50 ppm suggest the presence of unsaturated phenyl ring protons. The ^{1}H resonances that occur between 3.00 and 3.08 ppm indicate the presence of saturated Cp ring protons.[59] New resonances at 3.92 and 4.07 ppm are unaccounted for. These data support the formation of diphenylbis(cyclopentadienyl)silane, abbreviated from now on as Ph_2SiCp_2. The peaks at 0.10, 0.90, 1.29, 1.40, 3.17, 3.45, and 3.63 ppm are also found in the initial thermal sample and are assumed to be impurities.

The ^{1}H NMR spectrum of 2.73 mM $FcSiPh_2$ in methanol-d_4 irradiated at 313 nm is shown in Figure 29b. Most of the chemical shifts agree with the data obtained at 488 nm. This agreement, along with the UV-vis spectral agreement, verifies that irradiation of $FcSiPh_2$ solutions in methanol at 488 and 313 nm follow the same photochemical pathway. In the filtered, irradiated sample, the ^{1}H resonances that occur between 6.47 and 6.91 ppm indicate the presence of unsaturated Cp ring protons.[59] A range of new resonances between 7.25 and 7.50 ppm indicates the presence of unsaturated phenyl ring protons. The ^{1}H resonance that occurs at 3.02 ppm indicates the presence of saturated Cp ring protons.[59] A new resonance at 3.34 ppm (not found in the spectrum of the sample irradiated at 488 nm) suggests the presence of saturated Cp ring protons at the head of the bridge of the free ligand species, Ph_2SiCp_2.[59,60] New resonances at 3.27, 4.03, 4.07, 4.09, and 7.93 ppm are unaccounted for. The peaks at 4.12 and 4.56 ppm indicate the presence of starting material, since it did not all react during the

irradiation time period. The peaks at 0.10, 0.90, 1.29, 1.40, 2.15, 3.16, and 3.44 ppm are assumed to be impurities.

The ^{1}H NMR spectrum of 5.62 mM $FcSiPh_2$ in acetonitrile-d_3 irradiated at 488 nm is shown in Figure 29c. All of the initial $FcSiPh_2$ reacts in 60 m to form photoproducts. The photoproducts result from Fe-Cp bond cleavage rather than *ipso*-Cp-Si bond breaking because there is no conclusive indication of the formation of a monosubstituted derivative of ferrocene. In the filtered, irradiated sample, the ^{1}H resonances that occur between 6.48 and 7.00 ppm indicate the presence of unsaturated Cp ring protons.[59] A range of new resonances between 7.30 and 7.51 ppm indicates the presence of unsaturated phenyl ring protons. The ^{1}H resonance that occurs at 3.02 ppm indicates the presence of saturated Cp ring protons.[59] New resonances between 2.84 and 3.23 ppm (not found in the irradiated solutions in methanol-d_4) suggest the presence of saturated Cp ring protons.[59] The peaks between 4.00 and 4.17 ppm suggest some remnant of the starting material. But if that were the case, then we would have observed a triplet at 4.56 ppm indicating the presence of Cp ring protons on the starting material. ^{1}H NMR data collected in this study are summarized in Table 9.

We used FT-MS to reinforce our proposal of the formation of Ph_2SiCp_2 upon irradiation of $FcSiPh_2$ solutions in methanol-d_4 and acetonitrile-d_3 at 488 nm. Figure 30a shows a portion of the mass spectrum of a 672 μM $FcSiPh_2$ solution in methanol after 20 m of irradiation at 488 nm. The spectrum shows one signal for the proposed free ligand species, Ph_2SiCp_2, at m/z = 312.1324 (theoretical monoisotopic mass = 312.1334). Figure 30b shows a portion of the mass spectrum of a 650 μM $FcSiPh_2$

Table 9. Chemical shifts (ppm) in ^{1}H NMR spectra of irradiated solutions of $FcSiPh_2$

In CD_3OD (Ph_2SiCp_2)[a]	In CD_3OD (Ph_2SiCp_2)[b]	In CD_3CN (Ph_2SiCp_2)[a]	(Me_2SiCp_2)[c]	(Me_2SiCp_2)[d]	Band Assignment[c, d]	Band Assignment[e]
	7.93					
7.25-7.50	7.25-7.50	7.30-7.51				Unsaturated phenyl ring protons
6.48-6.91	6.47-6.91	6.48-7.00	6.47, 6.83	6.46, 6.51, 6.62, 6.69	Unsaturated Cp ring protons	
3.92, 4.07	3.92, 4.03, 4.07, 4.09					
	3.34		3.35	3.37, 3.46	Saturated Cp ring protons at the head of the bridge	
3.00, 3.03, 3.08	3.02	2.98, 3.06, 3.11, 3.15, 3.19, 3.23	2.90	2.82-2.97 2.27-2.39	Saturated Cp ring protons	

a. This study; excitation wavelength is 488 nm.

b. This study; excitation wavelength is 313 nm.

c. From Koepf and Klouras, Chimika Chromika, 1982, 11, 31-36.

d. From Cadenas et al., Revista de la Facultad de Ingenieria de la U.C.V., 2004, 19 (1), 79-88.

e. From this study.

Figure 30

A portion of the mass spectrum of a filtered solution of $FcSiPh_2$ irradiated at 488 nm in (a) room-temperature methanol and in (b) room-temperature acetonitrile.

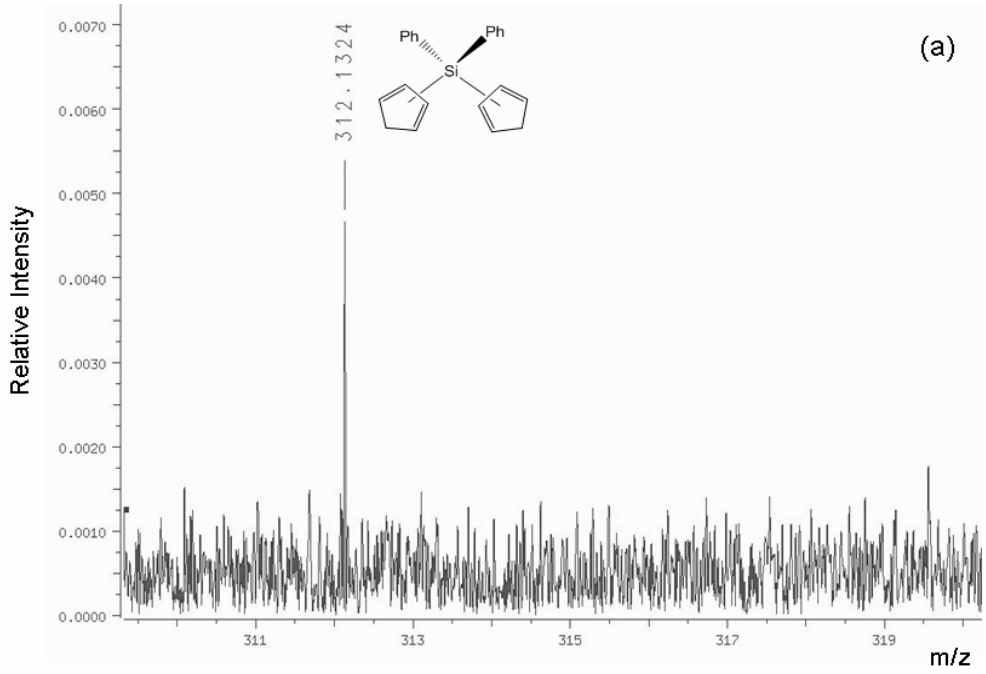
(a)
312.1324
Ph
Ph
Si
Relative Intensity
0.0070
0.0060
0.0050
0.0040
0.0030
0.0020
0.0010
0.0000
311
313
315
317
319
m/z

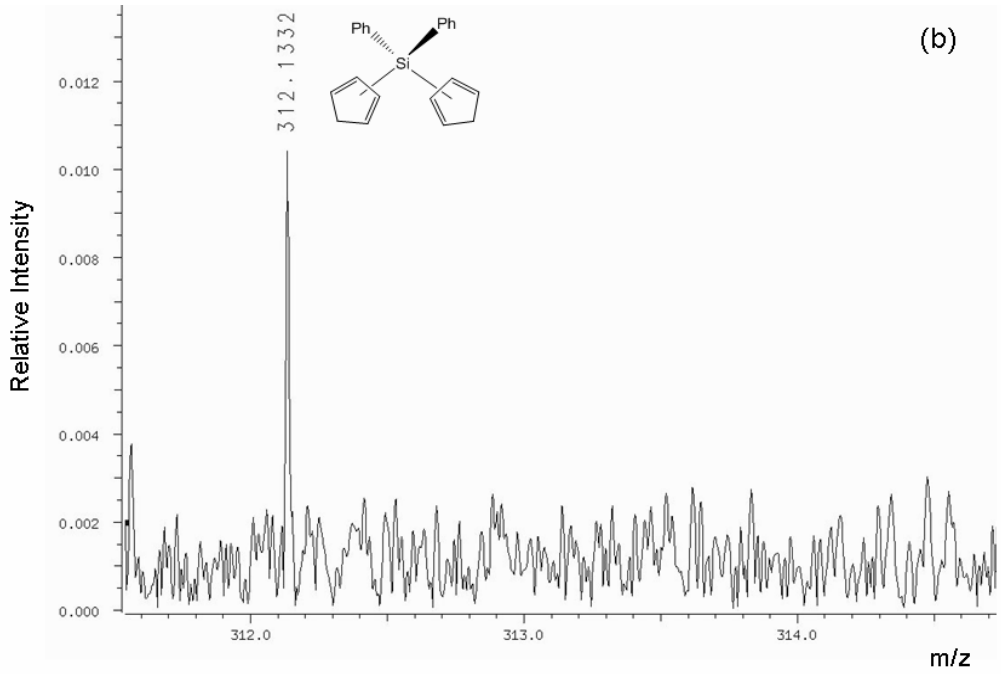
(b)
312.1332
Ph
Ph
Si
Relative Intensity
0.012
0.010
0.008
0.006
0.004
0.002
0.000
312.0
313.0
314.0
m/z

solution in acetonitrile after 30 m of irradiation at 488 nm. The spectrum shows one signal for the proposed free ligand species, Ph_2SiCp_2, at m/z = 312.1332 (theoretical monoisotopic mass = 312.1334).

With this collection of ^1H NMR and FT-MS evidence, along with the evidence of Fe-Cp bond cleavage provided in Chapter 4 for $FcSiMe_2$, we conclude that irradiation of $FcSiPh_2$ in solution generates photoproducts mainly via Fe-Cp bond cleavage as depicted in Equation 17. We propose that during irradiation, the Fe-Cp bond in the

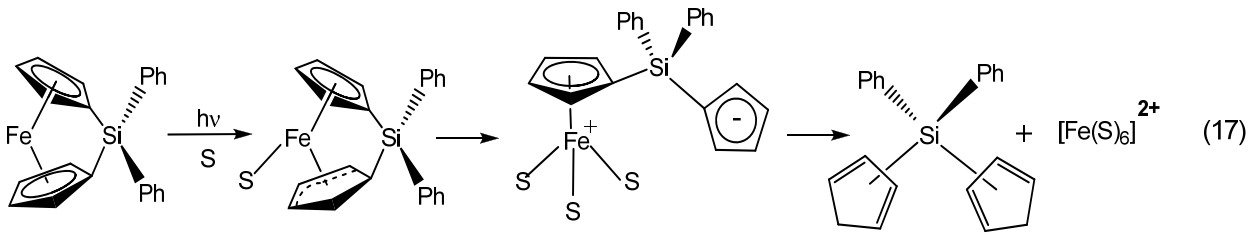

(17)

strained molecule weakens. This allows solvent to coordinate to the metal center to first form the η^5, η^3 ring-slipped intermediate that later yields the silyl-substituted, dangling cyclopentadienide anion and finally the free ligand product detected by proton NMR and mass spectrometry.

CHAPTER 6

GROUP TRANSFER POLYMERIZATION OF METHYL METHACRYLATE

Thermal group transfer polymerization (GTP) of methyl methacrylate (MMA) solutions in THF occurs in high yields at 50^{o}C when using methyl trimethylsilyl dimethylketene acetal (MTS) as the initiator and tetrabutylammonium thiocyanate as the nucleophilic catalyst. Figure 31 shows the time versus % polymerization plots for 1.5 M MMA GTP systems. The initiator to catalyst ratio was 30, except where indicated. In experiments where acetonitrile was used as the reference, we measured the decrease in the intensity of the vinyl peak of MMA at 1624 cm^{-1} and referenced it to the triple bond peak of acetonitrile at 2250 cm^{-1} using FT-IR spectroscopy. Figure 31 shows that the rate of polymerization is slower in the GTP systems containing acetonitrile versus the systems containing pure THF at both 23^{o}C and 50^{o}C. Bandermann et al. suggested that in acetonitrile, MMA reacts with the catalyst to produce a series of specific products and decreases the amount of catalyst available for polymerization.[62,63] They also found that acetonitrile undergoes an anion catalyzed reaction with MTS to silylate the solvent and produce Me_3SiCH_2R via an exchange of a proton for the trimethylsilyl group from MTS (R = catalyst). They presumed that this reaction, with the silyl ketene acetal of the propagating chain, was a major cause of termination.[64]

We observed polymerization of MMA after irradiating solutions of DFc in 1,2-dimethoxyethane (glyme) with 488-nm light. Glyme replaced THF as the solvent because it has a slightly higher donor number and dielectric constant. The initiator used

Figure 31

The thermal GTP of 1.5 M MMA in pure THF and in THF : acetonitrile mixtures (5-3/8:1) at room- (23^{o}C) and high-temperature (50^{o}C). The initiator to catalyst ratio was 30. The * designates that the initiator to catalyst ratio was 27.4.

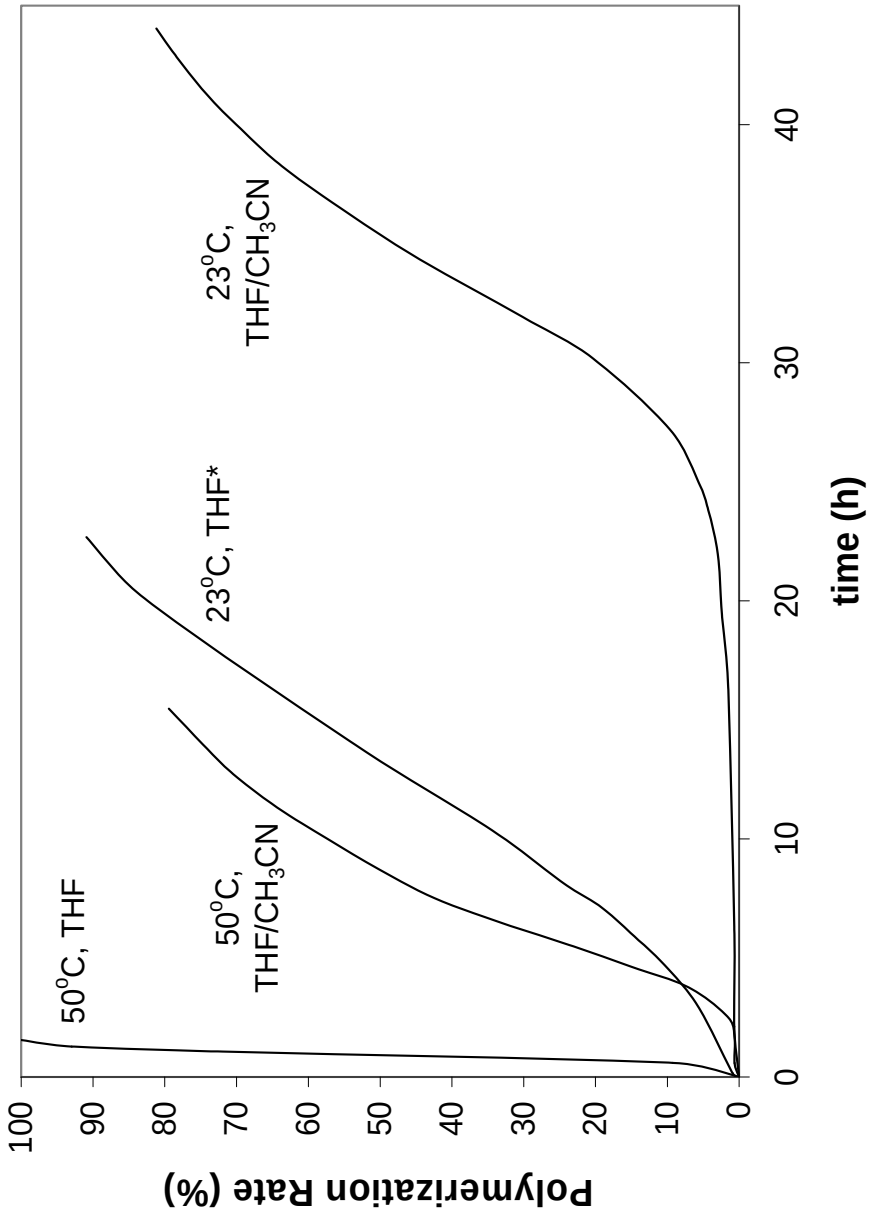
Polymerization Rate (%)
time (h)
50°C, THF
50°C, THF/CH3CN
23°C, THF*
23°C, THF/CH3CN
0
10
20
30
40
50
60
70
80
90
100
0
10
20
30
40

was MTS and the nucleophilic catalyst used was DFc. The initiator to catalyst ratio was 5, and the system temperature was 75^{o}C. The solution was irradiated for 5 m at 488 nm before heating. Percent polymerization was calculated from measuring the decrease in the intensity of the vinyl peak of MMA at 1624 cm^{-1} as the reaction proceeded using FT-IR spectroscopy. Figure 32 shows that when compared to a dark sample, the photolyzed sample undergoes no significant polymerization rate increase. One possible reason for poor photoreactivity is the solvent dependency of the photochemical process. In the photochemical GTP using glyme as the solvent, we speculate that a low quantum efficiency of DFc in glyme is responsible for no significant increase in the polymerization rate. Another possible reason for poor reactivity is the lack of a large, unreactive counterion. In the accepted dissociative mechanism of GTP, the large ions may work better by slowing down the rate of backbiting termination and formation of ketenes from the ester enolate ends.[65] In addition, the large counterions would foster complex formation of the enolate polymer ends with silyl ketene acetal ends.[40]

Having observed the significant temperature dependence on the photochemical reactivity of the silicon-bridged [1]ferrocenophanes, one might propose to use either $FcSiMe_2$ or $FcSiPh_2$ as a catalyst in a photochemical GTP system. Lowering the temperature from room temperature to approximately 5^{o}C increases the quantum efficiency of $FcSiPh_2$ by 767% in THF, a common solvent used in GTP. However, as discussed previously in Chapter 1, operating temperatures in the 50-80^{o}C range are required for a commercially viable process for controlled polymerization.

Figure 32

The photochemical GTP of 1.5 M MMA in glyme compared with a dark, control reaction. In both reactions, the initiator to catalyst ratio was 5, and the temperature was maintained at 75^{o}C.

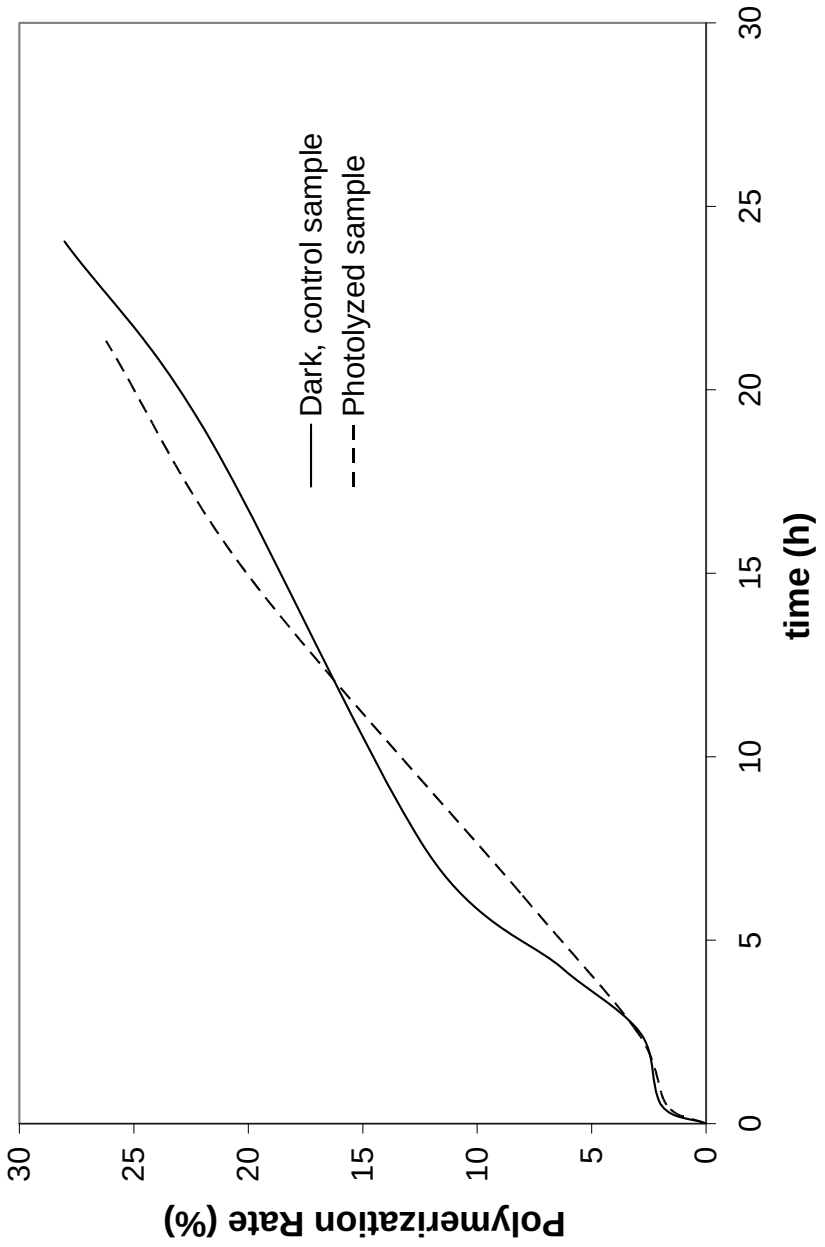
Polymerization Rate (%)
0
5
10
15
20
25
30
time (h)
0
5
10
15
20
25
30
Dark, control sample
Photolyzed sample

CHAPTER 7

CONCLUSIONS

Work reported here continues an interesting study on photoreactive ferrocene derivatives which find use in many areas. The [1]ferrocenophanes exhibit electronic properties similar to the benzoyl-substituted ferrocenes reported on previously. Present research on 1,1'-dibenzoylferrocene (DFc) and silicon-bridged [1]ferrocenophanes ($FcSiR_2$, where R = Me or Ph) has revealed several interesting characteristics.

The disappearance quantum yield of DFc is neither wavelength nor temperature dependent. This behavior suggests that the initially populated Franck-Condon excited state undergoes very rapid electronic and vibrational relaxation to yield a common thermally equilibrated excited (thexi) state of DFc.[7] Fe-Cp bond cleavage then occurs from this thexi state directly or from a close-lying reactive state reached by thermal upconversion.[50] Increasing solution temperature does not influence the excited state reactivity.

Tests for charge separation clearly show that Cp ring tilting induced by a bridging atom does not introduce significant metal-to-ligand charge transfer (MLCT) character into the low-energy excited states of silicon-bridged [1]ferrocenophanes ($FcSiR_2$, where R = Me or Ph). The inherent strain in these compounds facilitates metal-ring bond cleavage. Mass spectrometry, proton NMR, and UV-vis spectroscopy provide evidence that photoreaction proceeds via Fe-Cp bond cleavage at least 95% of the time. Based on this evidence, we have suggested that the photoinduced loss of the free ligand, $R_2(\eta$-

$C_5H_4)_2Si$ (R_2SiCp_2, where R = Me or Ph), proceeds via the formation of a η^5, η^3 ring-slipped intermediate and then a dangling silyl-substituted cyclopentadienide anion, similar to what Mizuta, Imamura et al. reported upon irradiation of a phosphorus-bridged [1]ferrocenophane.

$FcSiR_2$ are essentially photoinert in poorly coordinating solvents such as hexane and benzene. In more a strongly coordinating solvent like methanol, the photochemistry becomes more interesting. Irradiation at 488 nm into the low-energy absorption band of these complexes induces metal-ring bond cleavage with very efficient quantum yields (> 0.85). However, in the same solvent, irradiation at 313 nm into the high-energy absorption band reduces the quantum yield by almost 50%. Figure 33 shows that there are two possible explanations for this solvent dependence in solutions of $FcSiR_2$. In the first case, irradiation into the highest-energy excited state may result in either reaction from the excited state or vibrational relaxation to the ground state. In the second case, irradiation into the highest-energy excited state may result in either internal conversion (and then reaction) from the lowest-energy excited state or vibrational relaxation to the ground state. Currently, our data cannot distinguish between these two possibilities.

In both acetonitrile and THF, where metal-ring cleavage is not as efficient, we observe temperature dependence. Lowering the temperature of solutions of $FcSiMe_2$ in acetonitrile from room temperature to 5^oC improves the quantum yield by approximately 70%. Lowering the temperature of solutions of $FcSiPh_2$ in THF from room temperature to 5^oC also improves the quantum yield, but by almost 770%. After observing faster polymerization rates upon irradiating solutions of $FcSiMe_2$ in the presence of $Na[C_5H_5]$ at 5^oC, Tanabe, Vandermeulen, et al. proposed that deactivation of the photoexcited

Figure 33

Two possible scenarios to explain the wavelength dependence of solutions of silicon-bridged [1]ferrocenophanes. ES refers to the excited state and GS refers to the ground state.

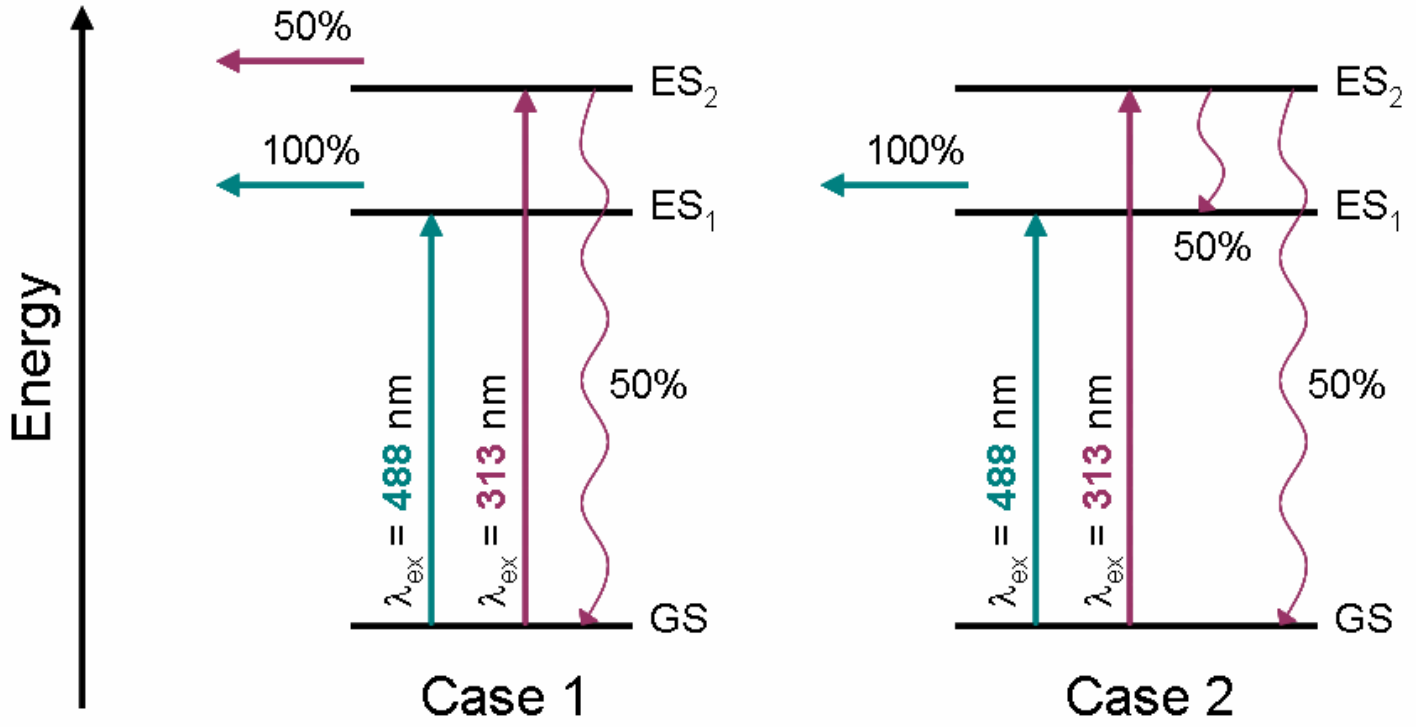
Energy
50%
100%
ES2
ES1
GS
λex = 488 nm
λex = 313 nm
50%
Case 1
100%
ES2
ES1
50%
GS
λex = 488 nm
λex = 313 nm
50%
Case 2

monomer is faster at higher temperatures than at 5^{o}C, whereas monomer excitation is independent of temperature.[28] Our quantum yield data provide the first direct evidence that this behavior indeed involves the electronically excited [1]ferrocenophane.

Future work could concentrate on the effect a different bridging atom would have on the excited-state reactivity of [1]ferrocenophanes. Rulkens, Gates et al. have studied the structures of [1]thia- and [1]selenaferrocenophanes and determined that the lowest-energy absorption bands of the [1]ferrocenophanes become increasingly redshifted as the tilt angle increases.[21] Studying the photochemistry of these complexes would allow us to determine whether increasing angle strain results in enhanced photoreactivity. [2]Ferrocenophanes with two silicon atoms in the bridge are substantially less strained than their silicon-bridged [1]ferrocenophane counterparts.[66] These [2]ferrocenophanes appear to be resistant to thermal ROP.[51] However, it has not yet been determined if they could undergo photolytic ROP. It would also be interesting to compare the photochemical properties of [1]ferrocenophanes with [2]ferrocenophanes that have analogous tilt angles. Here again the goal is to find whether a correlation exists between angle strain and photoreactivity, or if other factors such as metal-ring bond energy play an important role.

Although the reaction of 1,1'-dilithioferrocene with dichlorodimethylsilane is known to lead to the dimethylsila[1]ferrocenophane, the corresponding reaction of 1,1'-dilithioruthenocene does not give the mononuclear [1]ruthenocenophane.[67] However, a dinuclear [2]ruthenocenophane with a tilt angle of 29.6^{o} was synthesized by reacting $Li_2[C_5H_4CH_2]_2$ with the Ru^{II} complex *cis*-$[RuCl_2(dmso)_4]$ (dmso = dimethylsulfoxide).[66] Studies of the photochemistry of this 4d transition metal complex are underway in our

laboratory, and the results will be compared with the present work on 3d metallocenophanes. Such comparisons of the excited state reactivities of 3d and 4d metallocenophanes have not been reported previously.

REFERENCES

(1) Butler, I. S.; Harrod, J. F. *Inorganic Chemistry: Principles and Applications*; Benjamin-Cummings Pub Co: Redwood City, CA, 1989.

(2) Schlögl, K. *Topics in Stereochemistry*; Wiley-Interscience: New York, 1967; Vol. 1.

(3) Long, N. J. *Metallocenes: An Introduction to Sandwich Complexes*; Blackwell Science, 1998.

(4) Yamaguchi, Y.; Kutal, C. *Inorganic Chemistry* **1999**, *38*, 4861-4867.

(5) Sohn, Y. S.; Hendrick.Dn; Gray, H. B. *Journal of the American Chemical Society* **1971**, *93*, 3603-&.

(6) Warren, K. D. *Struct. Bond. (Berlin)* **1976**, *27*, 45.

(7) Yamaguchi, Y.; Ding, W.; Sanderson, C. T.; Borden, M. L.; Morgan, M. J.; Kutal, C. *Coordination Chemistry Reviews* **2007**, *251*, 515-524.

(8) Tarr, A. M.; Wiles, D. M. *Canadian Journal of Chemistry* **1968**, *46*, 2725-&.

(9) Brand, J. C. D.; Snedden, W. *Transactions of the Faraday Society* **1957**, *53*, 894-900.

(10) Sanderson, C. T.; Palmer, B. J.; Morgan, A.; Murphy, M.; Dluhy, R. A.; Mize, T.; Amster, I. J.; Kutal, C. *Macromolecules* **2002**, *35*, 9648-9652.

(11) Sinclair, J.; Subramanian, S.; Johnson, M. K.; Kutal, C. *Inorganic Chemistry* **2008**, In press.

(12) Ding, W.; Sanderson, C. T.; Conover, R. C.; Johnson, M. K.; Amster, I. J.; Kutal, C. *Inorganic Chemistry* **2003**, *42*, 1532-1537.

(13) Treadway, J. A.; Loeb, B.; Lopez, R.; Anderson, P. A.; Keene, F. R.; Meyer, T. J. *Inorganic Chemistry* **1996**, *35*, 2242-2246.

(14) Spiro, T. G.; Czernuszewicz, R. S. *Physical Methods in Bioinorganic Chemistry: Spectroscopy and Magnetism*; University Science Books: Sausalito, CA, 2000.

(15) Osborne, A. G.; Whiteley, R. H. *Journal of Organometallic Chemistry* **1975**, *101*, C27-C28.

(16) Barr, T. H.; Watts, W. E. *Tetrahedron* **1968**, *24*, 6111-&.

(17) Herbert, D. E.; Mayer, U. F. J.; Manners, I. *Angewandte Chemie-International Edition* **2007**, *46*, 5060-5081.

(18) Ieong, N. S.; Manners, I.; Elsevier Science Sa: 2008, p 802-807.

(19) Barlow, S.; Drewitt, M. J.; Dijkstra, T.; Green, J. C.; O'Hare, D.; Whittingham, C.; Wynn, H. H.; Gates, D. P.; Manners, I.; Nelson, J. M.; Pudelski, J. K. *Organometallics* **1998**, *17*, 2113-2120.

(20) Berenbaum, A.; Braunschweig, H.; Dirk, R.; Englert, U.; Green, J. C.; Jakle, F.; Lough, A. J.; Manners, I. *Journal of the American Chemical Society* **2000**, *122*, 5765-5774.

(21) Rulkens, R.; Gates, D. P.; Balaishis, D.; Pudelski, J. K.; McIntosh, D. F.; Lough, A. J.; Manners, I. *Journal of the American Chemical Society* **1997**, *119*, 10976-10986.

(22) Foucher, D. A.; Tang, B. Z.; Manners, I. *Journal of the American Chemical Society* **1992**, *114*, 6246-6248.

(23) Pudelski, J. K.; Manners, I. *Journal of the American Chemical Society* **1995**, *117*, 7265-7266.

(24) Ni, Y. Z.; Rulkens, R.; Manners, I. *Journal of the American Chemical Society* **1996**, *118*, 4102-4114.

(25) GomezElipe, P.; Macdonald, P. M.; Manners, I. *Angewandte Chemie-International Edition in English* **1997**, *36*, 762-764.

(26) Temple, K.; Jakle, F.; Sheridan, J. B.; Manners, I. *Journal of the American Chemical Society* **2001**, *123*, 1355-1364.

(27) Tanabe, M.; Manners, I. *J. Am. Chem. Soc.* **2004**, *126*, 11434.

(28) Tanabe, M.; Vandermeulen, G. W. M.; Chan, W. Y.; Cyr, P. W.; Vanderark, L.; Rider, D. A.; Manners, I. *Nature Mater.* **2006**, *5*, 467.

(29) Rider, D. A.; Manners, I. *Polymer Reviews* **2007**, *47*, 165-195.

(30) Arnaud, C. H. In *Chemical & Engineering News* 2008; Vol. 86, p 57-59.

(31) Ieong, N. S.; Chan, W. Y.; Lough, A. J.; Haddow, M. R.; Manners, I. *Chemistry-a European Journal* **2008**, *14*, 1253-1263.

(32) Kutal, C. *Coordination Chemistry Reviews* **2001**, *211*, 353-368.

(33) Kutal, C.; Yamaguchi, Y.; Ding, W.; Sanderson, C. T.; Li, X.; Gamble, G.; Amster, I. J. In *ACS Symposium Series, No. 847*; Belfield, K. D., Crivello, J. V., Eds.; American Chemical Society: Washington, DC 2003.

(34) Geoffrey, G. L.; Wrighton, M. S. In *Organometallic Photochemistry*; Academic Press: New York, 1979.

(35) Kutal, C.; Grutsch, P. A.; Yang, D. B. *Macromolecules* **1991**, *24*, 6872-6873.

(36) Yamaguchi, Y.; Kutal, C. *Macromolecules* **2000**, *33*, 1152.

(37) Sanderson, C. T.; Quinlan, J. A.; Conover, R. C.; Johnson, M. K.; Murphy, M.; Dluhy, R. A.; Kutal, C. *Inorganic Chemistry* **2005**, *44*, 3283-3289.

(38) Yamaguchi, Y.; Palmer, B. J.; Kutal, C.; Wakamatsu, T.; Yang, D. B. *Macromolecules* **1998**, *31*, 5155-5157.

(39) Webster, O. W.; Hertler, W. R.; Sogah, D. Y.; Farnham, W. B.; Rajanbabu, T. V. *Journal of the American Chemical Society* **1983**, *105*, 5706-5708.

(40) Webster, O. W. In *New Synthetic Methods*; Springer-Verlag Berlin: Berlin, 2004; Vol. 167, p 1-34.

(41) Quirk, R. P.; Kim, J. S. *Journal of Physical Organic Chemistry* **1995**, *8*, 242-248.

(42) Mai, P. M.; Muller, A. H. E. *Makromolekulare Chemie-Rapid Communications* **1987**, *8*, 99-107.

(43) Sitz, H.-D.; Bandermann, F. *NATO ASI Series C, Math. Phys. Sci.* **1987**, *215*, 41-47.

(44) Jolly, W. L. *The Synthesis and Characterization of Inorganic Compounds*; Prentice-Hall, Inc.: Englewood Cliffs, N.J., 1970.

(45) Jakle, F. http://newark.rutgers.edu/~jsheridn/chem448/ExptF.pdf, 2006.

(46) Wrighton, M. S.; Palazzotto, M. C.; Bocarsly, A. B.; Bolts, J. M.; Fischer, A. B.; Nadjo, L. *Journal of the American Chemical Society* **1978**, *100*, 7264-7271.

(47) Hatchard, C. G.; Parker, C. A. *Proceedings of the Royal Society of London Series a-Mathematical and Physical Sciences* **1956**, *235*, 518-536.

(48) Parker, C. A. *Proceedings of the Royal Society of London Series a-Mathematical and Physical Sciences* **1953**, *220*, 104-116.

(49) Wegner, E. E.; Adamson, A. W. *Journal of the American Chemical Society* **1966**, *88*, 394-&.

(50) Vlcek, A. *Coordination Chemistry Reviews* **1998**, *177*, 219-256.

(51) Finckh, W.; Tang, B. Z.; Foucher, D. A.; Zamble, D. B.; Ziembinski, R.; Lough, A.; Manners, I. *Organometallics* **1993**, *12*, 823-829.

(52) Pudelski, J. K.; Rulkens, R.; Foucher, D. A.; Lough, A. J.; Macdonald, P. M.; Manners, I. *Macromolecules* **1995**, *28*, 7301-7308.

(53) Fischer, A. B.; Kinney, J. B.; Staley, R. H.; Wrighton, M. S. *Journal of the American Chemical Society* **1979**, *101*, 6501-6506.

(54) Bark, T. H.; Watts, W. E. *J. Organomet. Chem.* **1968**, *15*, 177.

(55) Evans, H. S.; Osborne, A. G.; Whiteley, R. H. *Helv. Chim. Acta* **1976**, *59*, 2402.

(56) Penczek, S.; Kubisa, P.; Szymanski, R. *Makromolekulare Chemie-Rapid Communications* **1991**, *12*, 77-80.

(57) Mizuta, T.; Imamura, Y.; Miyoshi, K. *Journal of the American Chemical Society* **2003**, *125*, 2068-2069.

(58) Mizuta, T.; Onishi, M.; Miyoshi, K. *Organometallics* **2000**, *19*, 5005-5009.

(59) Koepf, H.; Klouras, N. *Chimika Chronika* **1982**, *11*, 31-36.

(60) Cadenas, J.; D'Ornelas, L.; Jimenez, L. J.; Jimenez, J.; Mendez, B.; Machado, Y. R. *Revista de la Facultad de Ingenieria de la U.C.V.* **2004**, *19*, 79-88.

(61) Stoecklievans, H.; Osborne, A. G.; Whiteley, R. H. *Helvetica Chimica Acta* **1976**, *59*, 2402-2406.

(62) Bandermann, F.; Sitz, H.-D.; Speikamp, H.-D. *Polym. Prepr.* **1986**, *27*, 169.

(63) Sitz, H. D.; Speikamp, H. D.; Bandermann, F. *Makromolekulare Chemie-Macromolecular Chemistry and Physics* **1988**, *189*, 429-435.

(64) Eastmond, G. C.; Webster, O. W. *New Methods of Polymer Synthesis*, 1991.

(65) Seebach, D. *Angewandte Chemie-International Edition in English* **1988**, *100*, 1624.

(66) Nelson, J. M.; Lough, A. J.; Manners, I. *Angewandte Chemie-International Edition in English* **1994**, *33*, 989-991.

(67) Herberhold, M.; Bartl, T. *Zeitschrift Fur Naturforschung Section B-a Journal of Chemical Sciences* **1995**, *50*, 1692-1698.